Cavity QED with superconductors and its application to the Casimir effect

Harald Richard Haakh

Diploma thesis
Institute of Physics and Astronomy
University of Potsdam

Second corrected edition
June 2009

Supervisor and first assessor
PD Dr. Carsten Henkel

Second assessor
Prof. Dr. Martin Wilkens

This work has been accepted as a diploma thesis at the University of Potsdam, Germany in April 2009. The present version features some minor changes with respect to the original one, concerning mostly typographic errors, and does not contain the declaration of authorship.

Parts of this work have been presented at

- FRISNO-10, Ein Gedi (Israel), February 2009,
- DPG Frühlingstagung, Hamburg (Germany), March 2009.

Harald R. Haakh
Cavity QED with superconductors and its application to the Casimir effect
Diploma thesis, University of Potsdam, 2009. Second corrected edition.

Contact: haakh@uni-potsdam.de

Published online at the
Institutional Repository of the University of Potsdam:
URL http://opus.kobv.de/ubp/volltexte/2009/3256/
URN urn:nbn:de:kobv:517-opus-32564
[http://nbn-resolving.org/urn:nbn:de:kobv:517-opus-32564]

Zusammenfassung

Diese Diplomarbeit untersucht den Casimir-Effekt zwischen normal- und supraleitenden Platten über einen weiten Temperaturbereich, sowie die Casimir-Polder-Wechselwirkung zwischen einem Atom und einer solchen Oberfläche. Hierzu wurden vorwiegend numerische und asymptotische Rechnungen durchgeführt. Die optischen Eigenschaften der Oberflächen werden dann aus dielektrischen Funktionen oder optischen Leitfähigkeiten erhalten. Wichtige Modellen werden vorgestellt und insbesondere im Hinblick auf ihre analytischen und kausalen Eigenschaften untersucht.

Es wird vorgestellt, wie sich die Casimir-Energie zwischen zwei normalleitenden Platten berechnen lässt. Frühere Arbeiten über den in allen metallischen Kavitäten vorhandenen Beitrag von Oberflächenplasmonen zur Casimir-Wechselwirkung wurden zum ersten mal auf endliche Temperaturen erweitert. Für Supraleiter wird eine analytische Fortsetzung der BCS-Leitfähigkeiten zu rein imaginären Frequenzen, sowohl innerhalb wie außerhalb des *schmutzigen* Grenzfalles verschwindender mittlerer freier Weglänge vorgestellt. Es wird gezeigt, dass die aus dieser neuen Beschreibung erhaltene freie Casimir-Energie in bestimmten Bereichen der Materialparameter hervorragend mit der im Rahmen des Zwei-Fluid-Modells für den Supraleiter berechneten übereinstimmt. Die Casimir-Entropie einer supraleitenden Kavität erfüllt den Nernstschen Wärmesatz und weist einen charakteristischen Sprung beim Erreichen des supraleitenden Phasenübergangs auf. Diese Effekte treten ebenfalls in der magnetischen Casimir-Polder-Wechselwirkung eines Atoms mit einer supraleitenden Oberfläche auf.

Es wird ferner gezeigt, dass die magnetische Dipol-Wechselwirkung eines Atomes mit einem Metall sehr stark von den dissipativen Eigenschaften und insbesondere von den Oberflächenströmen abhängt. Dies führt zu einer starken Unterdrückung der magnetischen Casimir-Polder-Energie bei endlichen Temperaturen und Abständen oberhalb der thermischen Wellenlänge. Die Casimir-Polder-Entropie verletzt in einigen Modellen den Nernstschen Wärmesatz. Ähnliche Effekte werden für den Casimir-Effekt zwischen Platten kontrovers diskutiert. In den entsprechenden elektrischen Dipol-Wechselwirkungen tritt keiner dieser Effekte auf.

Die Ergebnisse dieser Arbeit legen nahe, das bekannte Plasma-Modells als Grenzfall eines Supraleiters bei niedrigen Temperaturen (bekannt als London-Theorie) zu betrachten, statt als Beschreibung eines normales Metalles. Supraleiter bieten die Möglichkeit, die Dissipation der Oberflächenströme in hohem Maße zu steuern. Dies könnte einen experimentellen Zugang zu den optischen Eigenschaften von Metallen bei niedrigen Frequenzen erlauben, die eng mit dem thermischen Casimir-Effekt verknüpft sind. Anders als in entsprechenden Mikrowellen-Experimenten sind hierbei die Energien und Impulse unabhängige Größen. Die Messung der Oberflächenwechselwirkung zwischen Atomen und Supraleitern ist mit den heute verfügbaren Atomfallen auf Mikrochips möglich und der magnetische Anteil der Wechselwirkung sollte spektroskopischen Techniken zugänglich sein.

Abstract

This thesis investigates the Casimir effect between plates made of normal and superconducting metals over a broad range of temperatures, as well as the Casimir-Polder interaction of an atom to such a surface. Numerical and asymptotical calculations have been the main tools in order to do so. The optical properties of the surfaces are described by dielectric functions or optical conductivities, which are reviewed for common models and have been analyzed with special weight on distributional properties and causality.

The calculation of the Casimir energy between two normally conducting plates (*cavity*) is reviewed and previous work on the contribution to the Casimir energy due to the surface plasmons, present in all metallic cavities, has been generalized to finite temperatures for the first time. In the field of superconductivity, a new analytical continuation of the BCS conductivity to to purely imaginary frequencies has been obtained both inside and outside the extremely *dirty* limit of vanishing mean free path. The Casimir free energy calculated from this description was shown to coincide well with the values obtained from the two fluid model of superconductivity in certain regimes of the material parameters. The Casimir entropy in a superconducting cavity fulfills the third law of thermodynamics and features a characteristic discontinuity at the phase transition temperature. These effects were equally encountered in the Casimir-Polder interaction of an atom with a superconducting wall.

The magnetic dipole coupling of an atom to a metal was shown to be highly sensible to dissipation and especially to the surface currents. This leads to a strong quenching of the magnetic Casimir-Polder energy at finite temperature. Violations of the third law of thermodynamics are encountered in special models, similar to phenomena in the Casimir-effect between two plates, that are debated controversely. None of these effects occurs in the analog electric dipole interaction.

The results of this work suggest to reestablish the well-known plasma model as the low temperature limit of a superconductor as in London theory rather than use it for the description of normal metals. Superconductors offer the opportunity to control the dissipation of surface currents to a great extent. This could be used to access experimentally the low frequency optical response of metals, which is strongly connected to the thermal Casimir-effect. Here, differently from corresponding microwave experiments, energy and momentum are independent quantities. A measurement of the total Casimir-Polder interaction of atoms with superconductors seems to be in reach in today's microchip-based atom-traps and the contribution due to magnetic coupling might be accessed by spectroscopic techniques.

Acknowledgments

I would like to thank my supervisor *PD Dr. Carsten Henkel* who would answer all questions at any time, share his outstanding knowledge of physics, literature and mathematical formalism and never failed to come back to the physically relevant and *Dr. Francesco Intravaia*, who has become a good friend, helped me with all technical and physics questions and has spend a good share of his time discussing with me.

Salvo Spagnolo's visit to potsdam initiated the work on the Casimir-Polder forces, which - thought first as a small complementary facet - has taken more and more space in this work ever since. Also I want to thank *Prof. Giuseppe Bimonte* and *Simen Ellingsen* for sharing their knowledge, research results and numerical tricks. The *German-Israeli science foundation* (GIF) has funded my participation in the FRISNO 10 symposium and made it possible for me to meet and discuss with *Dr. Daniel Rohrlich*, *Prof. Baruch Horovitz, Prof. Ron Folman and Dr. Valery Dikovsky*. During all my studies I was supported by the *German national academic foundation (Studienstiftung des deutschen Volkes)*.

I would also like to mention my friends and fellow students, who took part in the seminar we held on mondays and who had always an open ear and unbiased ideas on any physics problem.

The special people who have shared my life during this year, who have supported and accompanied me all the time, stopped me from working too much on the weekends and tolerated if I still did are *Ana Sanfrutos Cano* and my *family*.

Contents

Introduction

In 1911 H. Kammerlingh-Onnes discovered that mercury undergoes a phase-transition at a critical temperature of $4.2\,\mathrm{K}$, below which it loses its electric DC-resistance: it turns into a *superconductor* [Kammerlingh-Onnes 1911]. Similar behavior was then also found in other materials. Meißner and Ochsenfeld demonstrated in 1933 that the interior of a superconductor is free from magnetic fields and introduced the notion of an *ideal diamagnet* [Meißner and Ochsenfeld 1933].

A phenomenological description that contained these two important phenomena was proposed in 1935 by the brothers F. and H. London [London and London 1935]. Their model gives a very good description for a system at zero temperature, but could not account for thermal effects. An extension was introduced following work by C. Gorter and H. B. Casimir [Gorter and Casimir 1934]. In today's language, it is an interpolation between the London zero temperature model and the Drude model for normal conductors, which holds pretty good above the phase transition. In this so-called two fluid model, a superconducting (dissipationless) current and a normal current are added up, and the relative weight between the two is characterized by an temperature dependent *order parameter*.

A generalization of the London model was given by L. D. Landau and V. Ginzburg [Ginzburg and Landau 1950, Ginzburg 1955] in 1950, based on general properties of arbitrary phase-transitions and was applied with great success to obtain a macroscopic description of superconductivity including the rich phenomenology of vortex dynamics. The fundamental concept of both London and Ginzburg-Landau theory is a macroscopic wave function, whose absolute square is identified with the order parameter. Thus superconductivity is understood as a macroscopic manifestation of the charge carrier's quantum nature.

Even so, the early phenomenological descriptions did not start from the basis of quantum mechanics. A very successful quantum-mechanical description of superconductivity was found by J. Bardeen, L. Cooper and J. R. Schrieffer [Bardeen *et al.* 1957]. They based their calculation an attractive interaction of electrons through virtual photons and found a ground state separated from the excitations by a temperature-dependent gap, the opening of which occurs at the superconducting transision. The connection of BCS theory to the macroscopic theories was later found by L. Gorkov [Gorkov 1959]. Today, classical superconductors have found wide use in technology and the BCS-type of superconductivity is well understood and covered in many textbooks, e.g. [Rickayzen 1965, Schrieffer 1999, Ketterson and Song 1999, Tinkham 2004].

It was the dawn of a new era when in 1986 J. G. Bednorz and K. A. Müller [Bednorz and Müller 1986] discovered materials that have extremely high critical temperatures in the order up to $100\,\mathrm{K}$. Typically high-T_c materials are made of layered structures of either cuprates $\mathrm{CuO_2}$ and a non-metallic elements or of iron and a pnictogen such as arsenic or phosphorous. For a review, see e.g. [Basov and Timusk 2005]. The physical mechanisms at work in any of these systems are still not completely understood and are a hot topic as well in experimental physics as in solid state theory.

While superconductivity was initially discovered in the laboratory, the discovery of vacuum interactions was triggered by a rather theoretical work. The concept of attractive *dispersion forces* between atoms or molecules was proposed by van-der-Waals [Van der Waals 1873] in 1873 in order to explain the non-ideal behavior of gases. He depicted the interaction as due to the interaction of fluctuation-induced dipoles with its mirror-charges. A first quantitative calculation [London 1930] was done by F. London[1]. In 1948 a QED description of the interaction between an atom and a perfectly reflecting surface, including the effects of retardation, was given by H. B. Casimir and D. Polder [Casimir and Polder 1948]. In honor of these researchers, vacuum effects are known today interchangeably under the names *van-der-Waals forces, London dispersion forces* or *Casimir-Polder forces*.

Casimir's and Polder's work on the atom-surface interaction led immediately to Casimir's prediction of the vacuum interaction between plates [Casimir 1948]. He found an attractive interaction acting on perfectly reflecting plates, which was then traced back to zero-point fluctuations of the electromagnetic vacuum in a bounded system.

[1] Looking at the names in this short historical outline, it is quite amazing to notice that many of the physicists working on superconductivity – like Landau, Lifshitz, London and Casimir, to name just a few – have also had an impact on the field of vacuum energy or vice versa.

Hence, vacuum interaction occurs not only between microscopic objects like atoms or molecules, but also between macroscopic objects. A seminal contribution to the theoretical understanding of these interactions was made by Lifshitz, when he derived a general formula for the Casimir-force between dielectrics which allowed for to include the effects of dispersion and dissipation [Lifshitz 1956].

First measurements were performed by Sparnaay in 1957 [Sparnaay 1957] but the results were rather indecisive, due to the big uncertainty of the data. Recently, thanks to advancing nanotechnology and quantum optics, interest in the vacuum-induced effects has been risen once again and it it has become possible to measure the electromagnetic Casimir force between two bodies to a very high precision [Lamoreaux 1997, Mohideen and Roy 1998, Harris *et al.* 2000, Chen *et al.* 2005, Chan *et al.* 2001, Iannuzzi *et al.* 2004, Lisanti *et al.* 2005, Decca *et al.* 2005, Bressi *et al.* 2002]. Theory has made great steps towards a thorough understanding as well, but new questions have come up, too, and controversial discussions keep being led [Milton 2004]. In nanotechnology one big problem is a phenomenon known as *stiction* [Chan *et al.* 2001, Buks and Roukes 2001], which is the jamming of small devices (known as *micro-electromechanic systems MEMS*) due to attractive forces. One of the goals of ongoing research is to find regimes of material parameters, e.g. in metamaterials, where the vacuum interaction is repulsive and could thus help to prevent these effects. On the other hand, switchable Casimir-forces could also be used to control small devices.

Casimir-Polder forces, too, are nowadays frequently seen in magnetic traps implemented on microchips (*atom chips*, e.g. [Fortagh and Zimmermann 2007]). Such setups allow to manipulate few or single atoms or even exotic states of matter like Bose-Einstein condensates near solid surfaces. The most simple scheme of an atom chip is drawn in fig. 0.1. It consists of a current-carrying wire that produces a constant magnetic field, and an external homogeneous bias field. The superposition of the two magnetic fields has a minimum which can be adjusted at a certain trapping height above the chip-surface. The right panel in fig. 0.1 shows the trapping potential ($\sim |\mathbf{B}|$) and its gradient, which is proportional to the force exerted on a static magnetic dipole moment. The potential minimum above the wire can thus be used to trap atoms in states with a dipole moment.

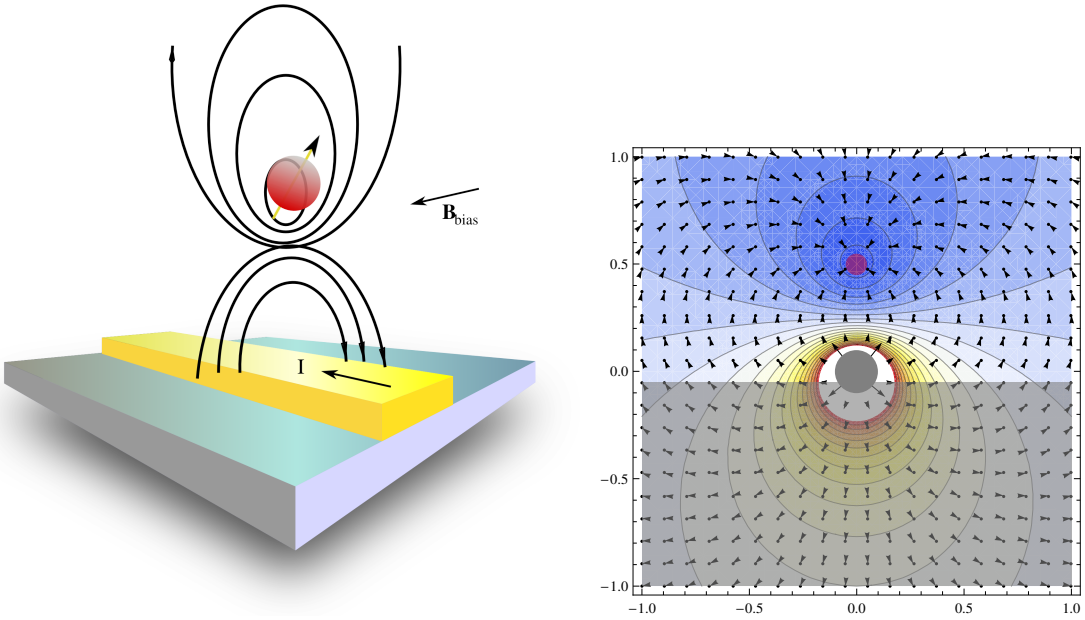

Figure 0.1: *Left: General setup for a magnetic line guide trap made of a wire on a chip surface placed in a homogeneous bias field. The field minimum is located above the wire (red) and can be used to trap electrically neutral atoms. Right: Magnetic trapping potential* $\sim |\mathbf{B}|$ *(color coded) and its gradient (arrows).*

Often the atom-surface interaction leads to a deformation of the potential and undesired losses of atoms from the trap, but the deformation of an otherwise well-known potential can also be used to measure the Casimir-Polder effect (section 3.1.2, [Obrecht *et al.* 2007, Obrecht 2007, Landragin *et al.* 1996, Yuju *et al.* 2004]).

The topic of this thesis is the Casimir effect in superconducting cavities and the Casimir-Polder interaction of an atom with a superconducting surface. Thus, the investigation involves two fields of physics, where the quantum

world and the macroscopic world meet, and exciting phenomena can be expected to arise from the combination. *Dissipation* is a key concept in this context, and it is exactly the possibility to switch off dissipation in superconducting materials below the critical temperature, that makes the vacuum interaction with such surfaces highly interesting:

- Superconductors provide physical systems that realize the plasma-model (London theory), which stands at the very center of this discussion about the role of dissipation in the Casimir effect [Milton 2004], and it has been proposed, that measurements of the Casimir-effect in a superconducting cavity might lead to a better understanding of the low frequency current response of metals [Bimonte *et al.* 2005b].
- Also the interaction between an atom and a superconducting surface may become relevant in the next generation of atom chips. Recently it has become interesting to use superconducting materials for the trapping wires, because it allows to reduce the magnetic noise [Dikovsky *et al.* 2009]. In normal metals this noise is connected to the dissipation (i.e. finite conductivity) and induces spin-flips of the trapped atoms, leading to their loss from the trap [Henkel *et al.* 1999, Henkel 2005, Hohenester *et al.* 2007, Skagerstam *et al.* 2006]. For the operation of these traps, an exact knowledge of the Casimir-Polder-potential is highly desirable.

This thesis is organized as follows.

In the *first chapter*, the electrodynamics and optics of the most relevant models for metals and superconductors are reviewed. Special attention is paid to the causal and analytical properties of optical response functions, which provide valuable tools like Kramers-Kronig relations and sum rules. The distributional properties are very important in the light of the discussions led over the low-frequency behavior of the plasma and Drude model. The analytic continuation of optical response functions to purely imaginary frequencies is introduced for later use. An important original result of this work shows how this can be done for the optical conductivity in the BCS model both inside and outside the extremely anomalous limit. Finally, the reflectivities of the different models (that will be the key ingredients for the calculation of the Casimir- and Casimir-Polder interactions) are compared and the effects of the collective mode in superconductors are discussed.

The *second chapter* covers the Casimir effect between conducting and superconducting half-spaces at both zero and finite temperature. The relevant thermodynamic potential from which all further quantities such as the entropy, Casimir pressure, specific heat etc. can be obtained, is the free energy per unit area. The scenario of perfectly reflecting walls is introduced as a first example, and shows already many of the effects that occur also in more realistic settings. An original calculation yields the thermal correction to the Casimir free energy from the surface plasmons. These give the dominating contribution to the Casimir interaction between metals at small distances, and the thermal effects found here will be recovered in other models. A numerical toolbox for calculations of the Casimir free energy has been developed and is applied to the different materials. The asymptotic behavior of the Casimir free energy and entropy is calculated in different distance and temperature regimes and recover negative entropies and a violation of the third law of thermodynamics, that have been discussed strongly during the last years. The origin and validity of this law is discussed in the context of a Casimir setup, and it is shown, that no thermal anomalies occur in the Casimir interaction between superconductors. The interaction between superconductors close to the critical temperature is investigated and is found to feature a characteristic entropy minimum and a discontinuity of the entropy at the critical temperature. An surprising result is, that the predictions obtained in the BCS and two fluid model coincide with great accuracy (at least in certain regimes of the material parameters). In these regimes it is therefore legitimate to use the two fluid model rather than the numerically and less convenient BCS model, which is valuable for future numerical work.

In the *third chapter*, the techniques developed earlier are adapted and applied to the Casimir-Polder effect between atoms and a conducting surface. The interaction energies due to electric and magnetic dipole-coupling are calculated and compared. Again the asymptotic behavior is calculated within different regimes and new effects are found in the magnetic case, where the interaction turns out to be highly sensitive to surface currents and the dissipative effects in the medium. Therefore, the contribution due to the magnetic coupling with a surface depends strongly on the material properties and differs strongly between the different models. It is shown, that thermal anomalies – similar to the ones known from the Casimir-interaction between plates – reappear in the special case of a perfect crystal, where the dissipation vanishes as $T \to 0$. Previous calculations had considered thermal effects only for the electric dipole contribution, where the above phenomena do not occur. Finally, the magnetic interaction of atom with a superconductor is calculated. Exactly as in the case of two plates there is an entropy discontinuity and a strong change of the Casimir-Polder free energy at the critical temperature.

In the end, the main results of this work are summarized briefly, and an outlook is given on connected topics, that might be the subject of future research.

1 Electrodynamics of superconductors

1.1 Electrodynamics of solids

1.1.1 Basic equations of electrodynamics

This chapter reviews some topics from the theory of electrodynamics and optics that will used in later parts of this work. The fundamental relations of electrodynamics are the macroscopic Maxwell equations, which in the frame of the *système international* (SI) are given by

$$\begin{aligned} \nabla \cdot \mathbf{B} = 0 \qquad & \nabla \cdot \mathbf{D} = \rho \\ \nabla \times \mathbf{H} = \mathbf{j} + \dot{\mathbf{D}} \quad & \nabla \times \mathbf{E} = -\dot{\mathbf{B}} \,. \end{aligned} \tag{1.1}$$

The connection between the electric and magnetic fields $\mathbf{E}$ and $\mathbf{H}$ and the dielectric displacement and the magnetic induction $\mathbf{D}, \mathbf{B}$ in a medium featuring electrical or magnetic polarization $\mathbf{P}$ or $\mathbf{M}$ is given by the material equations

$$\begin{aligned} \mathbf{B} \quad &= \mu_0(\mathbf{H} + \mathbf{M}) \quad &= \mu \mathbf{H} \\ \mathbf{D} \quad &= \epsilon_0 \mathbf{E} + \mathbf{P} \quad &= \epsilon \mathbf{E} \,, \end{aligned} \tag{1.2}$$

where the last identities hold only for linear media. More generally, permeabilities and permittivities μ, ϵ are tensor-valued and depend on the orientation of the medium. In addition, the responses for transverse and longitudinal field components do not generally coincide [Dressel and Grüner 2002]. The consideration of these properties is beyond the scope of this thesis, and – unless stated differently – all media will be considered linear, isotropic, homogeneous and local, which allows to use scalar quantities rather then tensors.

To obtain a complete system of equations, it is necessary to introduce one more relation which connects fields and currents. The simplest version is Ohm's law, given by the linearity

$$\mathbf{j} = \sigma \mathbf{E} \,, \tag{1.3}$$

where σ is the electrical DC conductivity. Later, more general relations including some nonlocal effects will be introduced for superconductors and for normal metals, from which Ohm's law is recovered in the local limit.

The continuity and wave-equation of electrodynamics follow directly from Maxwell's equations

$$\nabla \cdot \mathbf{J} + \frac{\partial}{\partial t}\rho = 0 \tag{1.4}$$

$$\left(\Delta - \frac{n^2}{c^2}\frac{\partial^2}{\partial t^2}\right)\mathbf{E} = \nabla(\nabla \cdot \mathbf{E}) + \mu \frac{\partial}{\partial t}\mathbf{j} \tag{1.5}$$

$$\left(\Delta - \frac{n^2}{c^2}\frac{\partial^2}{\partial t^2}\right)\mathbf{B} = -\mu \nabla \times \mathbf{j}.$$

Here $c = 1/\sqrt{\epsilon_0 \mu_0}$ is the speed of light in vacuum and the index of refraction is

$$n = c\sqrt{\epsilon \mu} \,. \tag{1.6}$$

1.1.2 Harmonic analysis

Harmonic time and spatial dependences are common in electrodynamics, so that it is convenient to express quantities in the Fourier representation. Different conventions for the sign of the frequencies are possible. In this text, the inverse and direct Fourier transforms connecting frequency and time domain are given by

$$\begin{aligned} f(\omega) &= \mathcal{F}^{-1} f(t) &:= \frac{1}{2\pi}\int_{-\infty}^{\infty} f(t)\exp(i\omega t)dt \\ \Leftrightarrow f(t) &= \mathcal{F} f(\omega) &= \int_{-\infty}^{\infty} f(\omega)\exp(-i\omega t)d\omega\ . \end{aligned} \tag{1.7}$$

Where no confusion can occur, the same symbol will be used for functions in both the time and the frequency domain ($f(t), f(\omega)$). If a spatial decomposition is performed, too, the sign convention is positive for outgoing waves

$$\begin{aligned} f(\mathbf{k},\omega) &= \mathcal{F}^{-1} f(\mathbf{r},t) &:= \frac{1}{(2\pi)^4}\int_{-\infty}^{\infty} f(\mathbf{r},t)\exp(-i\mathbf{k}\cdot\mathbf{r}+i\omega t)\ dt\ d\mathbf{r} \\ \Leftrightarrow f(\mathbf{r},t) &= \mathcal{F} f(\mathbf{k},\omega) &= \int_{-\infty}^{\infty} f(\omega)\exp(i\mathbf{k}\cdot\mathbf{r}-i\omega t)\ d\omega\ d\mathbf{k}\ . \end{aligned} \tag{1.8}$$

According to the well-known theorems of Fourier analysis one can replace differential operators $\nabla \rightarrow i\mathbf{k}$ and $\partial_t \rightarrow -i\omega$ by wave vectors and frequencies respectively in the frequency domain.

1.1.3 Electromagnetic waves in media

In a medium, there are not only *free charges* and *conductive currents*, but also *polarization charges* and *bound currents* due to the polarizability of the matter. In a static field, the two kinds have very distinct characteristics, but when the fields are not constant in time, it is no longer possible to clearly distinguish between conducting and displacement currents

$$\begin{aligned} \nabla\times\mathbf{H} &= \mathbf{j}+\dot{\mathbf{D}} \\ &= \underbrace{(\sigma-\epsilon_0\epsilon_r i\omega)}_{:=\sigma(\omega)}\mathbf{E} \\ &= \underbrace{(\epsilon_r+\frac{i\sigma}{\epsilon_0\omega})}_{:=\epsilon(\omega)}(-i\omega)\epsilon_0\mathbf{D}\ . \end{aligned} \tag{1.9}$$

It is then useful to define complex dielectric functions or complex conductivities and act, as if only one kind of currents were present. Throughout this text, the backgrounds are assumed to be non-polarizable $\epsilon_r = 1$, and the media under consideration are non-magnetic $\mu_r = 1$.

The relation between complex conductivity and dielectric function is given by

$$\epsilon(\omega) = 1+\frac{i\sigma}{\omega\epsilon_0}, \tag{1.10}$$

which can also be decomposed into real and imaginary parts denoted by primed and double primed quantities

$$\epsilon = \epsilon' + i\epsilon'', \qquad \sigma = \sigma' + i\sigma'', \qquad n = n' + in''$$

$$\begin{aligned} \epsilon' &= 1-\tfrac{\sigma''}{\epsilon_0\omega}, & \epsilon'' &= \frac{\sigma'}{\epsilon_0\omega} \\ \sigma' &= \epsilon''\epsilon_0\omega, & \sigma'' &= (1-\epsilon')\epsilon_0\omega\ . \end{aligned}$$

The real and imaginary parts are not independent of each other but are connected by *causality relations* or as they are sometimes called *dispersion relations* and which will be discussed in section 1.2.1.

Now, plugging a monochromatic wave ansatz

$$\mathbf{E}_{vac}(\mathbf{r},t) \quad = \quad \mathbf{E}(\mathbf{k},\omega)\exp(i\mathbf{k}\cdot\mathbf{r}-i\omega t) \tag{1.11}$$

into Ampere's law in the presence of matter (1.5) gives the *dispersion relation* that relates wave vectors and frequencies

$$\mathbf{k}(\omega) = \frac{\omega}{c}\sqrt{\epsilon'\mu' + \frac{i\mu'\sigma'}{\epsilon_0\omega}} =: \frac{\omega}{c}n(\omega)\ . \tag{1.12}$$

The last step defines the complex index of refraction, which could have been obtained as well by just plugging in the complex dielectric function into (1.6). Of course the descriptions through $n(\omega), \epsilon(\omega)$ and $\sigma(\omega)$ are totally equivalent.

Using the dispersion relation (1.12), one can express the field inside the medium in terms of the wave vector in free space.

$$\mathbf{E}_{matter}(\mathbf{r},t) \quad = \quad \mathbf{E}(\mathbf{k}_{vac},\omega)\exp(in'\mathbf{k}_{vac}\cdot\mathbf{r}-i\omega t)\exp(-n''\mathbf{k}_{vac}\cdot\mathbf{r})\ , \tag{1.13}$$

Obviously, the wave therefore damped during its propagation. Furthermore, a realistic wave packet contains several frequencies and will disperse since $n = n(\omega)$ is a function of frequency. So, absorption is due to the imaginary part of the index of refraction, while its real part leads to dispersion. As for the other complex response functions there are causality relations connecting the real to the imaginary parts and hence dispersion to dissipation.

1.1.4 Fields at boundaries

Each incoming wave traveling along a direction $\mathbf{k}$ can be decomposed into two polarizations

- s- or TE-polarization: electric field perpendicular to the plane of incidence,
- p- or TM-polarization: electric field parallel to the plane of incidence.

When incidence is normal to the plane, TE- and TM-modes coincide, and in free space in the absence of boundary conditions, all modes are both transverse electric and magnetic (TEM).

Let $\mathbf{k}_\perp$ be the wave vector in normal direction and $\mathbf{k}$ the orthogonal complement. The dispersion relation using definitions (1.10, 1.6) becomes

$$\mathbf{k}^2 + \mathbf{k}_\perp^2 = \epsilon\frac{\omega^2}{c^2}\ , \tag{1.14}$$

and it is quite useful to introduce a longitudinal wave number

$$\kappa \quad = \quad -ik_\perp = \sqrt{k^2 - \epsilon(\omega)\frac{\omega^2}{c^2}}\ . \tag{1.15}$$

The root must be chosen so that $\mathrm{Re}\,\sqrt{\cdot} > 0$, which implies that fields are damped along their propagation.

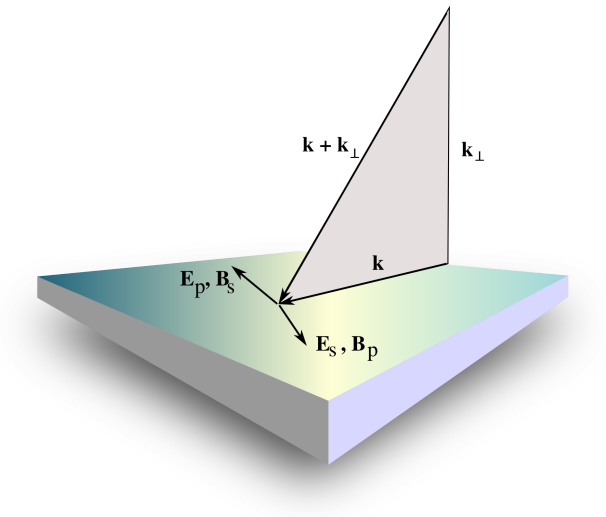

Figure 1.1: *Decomposition of an incoming wave.*

Maxwell's equation require the continuity of the normal components of $\mathbf{B}$ and the tangential components $\mathbf{E}$ across boundaries. From these follow the laws of reflection and refraction, and the general form of Fresnel's equations [Jackson 2002, Dressel and Grüner 2002]. The reflectivity for a wave of polarization $i \in \{TE, TM\}$ crossing from medium 1 to medium 2 can be expressed in terms of permittivities or impedances

$$r^i \quad = \quad \frac{Z_1^i - Z_2^i}{Z_1^i + Z_2^i}, \tag{1.16}$$

$$Z^{TE} = Z_0\frac{\kappa_2}{\kappa_1}\ , \qquad Z^{TM} \quad = \quad Z_0\frac{\epsilon_2(\omega)\kappa_1}{\epsilon_1(\omega)\kappa_2}, \qquad Z_0 = \sqrt{\frac{\mu_0}{\epsilon_0}} \approx 377\,\Omega\ . \tag{1.17}$$

Usually one medium will be the vacuum, where $\epsilon = 1$. In this case the reflectivities take the following form

$$r^{TE} = \frac{\sqrt{k^2 - \frac{\omega^2}{c^2}} - \sqrt{k^2 - \epsilon(\omega)\frac{\omega^2}{c^2}}}{\sqrt{k^2 - \frac{\omega^2}{c^2}} + \sqrt{k^2 - \epsilon(\omega)\frac{\omega^2}{c^2}}}, \qquad r^{TM} = \frac{\epsilon(\omega)\sqrt{k^2 - \frac{\omega^2}{c^2}} - \sqrt{k^2 - \epsilon(\omega)\frac{\omega^2}{c^2}}}{\epsilon(\omega)\sqrt{k^2 - \frac{\omega^2}{c^2}} + \sqrt{k^2 - \epsilon(\omega)\frac{\omega^2}{c^2}}}. \tag{1.18}$$

All information on the surface optics can be compiled in an *impedance tensor* [Jackson 2002, Landau and Lifshitz 1974, Ford and Weber 1984], which describes the resistance to a wave crossing a medium or an interface. Assuming only diagonal components, i.e. no mixing between the field components,

$$Z_p := \frac{E_p}{\int_0^\infty j_p dz} = \sqrt{\frac{\mu}{\epsilon}} \approx \frac{E_p}{H_p} \,. \tag{1.19}$$

The electric field is taken just outside the surface, while the current integral goes over the medium beyond. The second equality holds only, where - as in (1.16) - it is reasonable to introduce quantities $\mu(\omega), \epsilon(\omega)$. The last approximation gives the so-called Leontovich-impedance, that applies when the displacement current is negligible. Commonly the impedance is given as a scalar for perpendicular incidence [Dressel and Grüner 2002], where TE and TM coincide .

1.1.5 Electric conductivity

The first successful description of dissipative electronic transport phenomena in a metal was given by Drude. Even though the basic assumptions of Drude's original model are really simple, the result can be recovered from quantum-mechanical descriptions, which starting from the Boltzmann-equations and Fermi's golden rule lead to Kubo's equation and give asymptotically identical expressions [Dressel and Grüner 2002].

The basic equation is obtained in the *relaxation time approach*, where just a general *rate of dissipation* $\gamma = 1/\tau$ due to a mechanism not further defined is assumed, but where the conduction electrons are otherwise considered as free particles accelerated by the external electric field.

$$\dot{\mathbf{v}}_n \quad = \quad -\frac{\mathbf{v}_n}{\tau} - \frac{e}{m}\mathbf{E} \,. \tag{1.20}$$

The equations of motions have to be read as referring to the expectation value of a kinematic momentum operator $\mathbf{p}/m$.

Using harmonic time-dependence $\sim \exp(-i\omega t)$ and $\mathbf{j_i} = -n_i e_i \mathbf{v_i} \stackrel{!}{=} \sigma_i \mathbf{E}$ for the currents, the equation of motion yields the AC conductivity for a normal metal

$$\sigma_n(\omega) = \frac{n_n e^2 \tau}{m(1 - i\omega\tau)} =: \frac{\omega_p^2 \epsilon_0}{\gamma - i\omega} \,,$$

defining the *plasma frequency* ω_p (see below) and relations (1.10) give the dielectric function of the *Drude model*

$$\epsilon(\omega) = 1 - \frac{\omega_p^2}{\omega(\omega + i\gamma)} \,. \tag{1.21}$$

The poles and zeros of the dielectric function are connected to important phenomena.

- $\omega = 0$: This pole can be found from the continuity equation of electrodynamics. It must occur for a general conductivity just due to the conservation of charge.
- $\omega = -i\gamma$: Since γ is the dissipation rate of the relaxation time approach, this pole describes the relaxation of currents to the equilibrium.
- $\omega \approx \pm\omega_p - i\frac{\gamma}{2}$: A perturbation of the homogeneous charge distribution in the electron gas can excite collective oscillations known as plasma oscillations [Jackson 2002]. Without damping γ, the two modes of the system coincide at the *plasma frequency*

$$\omega_p = \sqrt{\frac{ne^2}{m_e \epsilon_0}} \,. \tag{1.22}$$

In the *high frequency limit* $\gamma \ll \omega_p < \omega$ of (1.21), all excitations or resonant effects become irrelevant and the response is dominated by inertia. The asymptotic function is well-known in solid state physics as the *plasma model*

$$\epsilon(\omega) = 1 - \frac{\omega_p^2}{\omega^2} \,. \tag{1.23}$$

In fact it is recovered as an asymptotic for any conducting system at high frequencies well above the resonant regime [Jackson 2002, Dressel and Grüner 2002]. Even so, it has often been used to describe metals also at low frequencies, where it is certainly not valid, e.g. [Geyer *et al.* 2007]. It can be argued though, that in this regime it rather approximates the optics of a superconductor and later in this thesis more support for this point will be given (sections 1.4.1, 1.7.3). For a first try at the superconducting case, it comes quite natural to set $\gamma \equiv 0$, and so the equation of motion becomes

$$\dot{\mathbf{v}}_s \quad = \quad -\frac{e^*}{m^*}\mathbf{E} \tag{1.24}$$

which gives exactly the plasma conductivity, which will turn out to be the fundamental result of London's theory of superconductivity (1.72).

The plasma model conductivity is purely imaginary and is given by

$$\sigma_s(\omega) \quad = \quad i\frac{n_s^* e^{*2}}{\omega m^*} = i\frac{\omega_p^2 \epsilon_0}{\omega} \,. \tag{1.25}$$

If instead of an identically vanishing relaxation $\gamma \equiv 0$ the limit $\gamma \to 0$ is taken, a causal distribution is obtained whose imaginary and real parts are connected by Kramers-Kronig relations (see 1.2.5) in contrast to the pure plasma model. The model is thus extended and reads

$$\sigma_s(\omega) \quad = \quad \omega_p^2 \epsilon_0 \frac{1}{\omega + i0^+} = \pi\omega_p^2\epsilon_0\,\delta(\omega) + i\omega_p^2\epsilon_0 \mathcal{P}\frac{1}{\omega}$$

or in terms of the dielectric function (*causal* or *distributional plasma model*)

$$\epsilon(\omega) = 1 - \frac{\omega_p^2}{\omega}\mathcal{P}\frac{1}{\omega} + i\pi\frac{\omega_p^2}{\omega}\delta(\omega) \,. \tag{1.26}$$

1.1.6 Temperature dependence of Drude's relaxation

The temperature dependence of Drude's relaxation parameter γ has strong impacts on the conductivity. Its finite value is due to scattering of the charge carriers, for instance in electron-electron interaction, electron-phonon scattering and the scattering at crystal imperfections, impurities or interfaces.

If different mechanisms occur, each one can be attributed a characteristic dissipation rate γ_i or equivalently a resistivity ϱ_i. The total resistivity is then given approximately by their sum, which is known as Matthiessen's rule

$$\varrho = \sum_i \varrho_i \,. \tag{1.27}$$

The interaction between the conduction electrons is relevant in semiconductors, but in common metals the most important interaction is between electrons and phonons, which is well described by the Bloch-Grüneisen-formula [Bloch 1930, Grüneisen 1933]. Electric conduction is a non-equilibrium process, but it is safe to assume that the phonon-gas is in a thermal equilibrium and follows Debye statistics. Details of the calculation can be found in [Ashcroft and Mermin 1987, Ziman 1972, Jones and March 1973]. The final result reads

$$\begin{aligned} \varrho_{BG}(T) \quad &= \quad \frac{C}{\Theta}\left(\frac{T}{\Theta}\right)^5 \int_0^{\Theta/T} du \frac{u^5}{(1-e^{-u})(e^u-1)} \\ &\overset{T\to 0}{\to} \quad \varrho_0 \left(\frac{T}{\Theta}\right)^5 , \qquad \varrho_0 = 124.431\frac{C}{\Theta} \end{aligned} \tag{1.28}$$

At low temperatures the dissipation rate follow asymptotically a T^5 power law, which works up to about 10% of the Debye temperature Θ, as is shown in fig. 1.2 for aluminum, together with reference data from data from [Lide 1995].

Numerically it can be necessary to use functions that show a similar qualitative behavior but do not request the numerical evaluation of integrals. An example is

$$\varrho(T) = \varrho_0 \left[1 - \exp\left(-(T/T_0)^\alpha\right)\right] \tag{1.29}$$

where the parameters ϱ_0, T_0, α must be chosen adequately. Drude's relaxation rate and the Bloch-Grüneisen-parameter are connected by

$$\gamma = \frac{1}{\tau} = \varrho_{BG}\epsilon_0\omega_p^2 \,. \tag{1.30}$$

The other important contribution to resistivity in normal metals is the one due to scattering at crystal imperfections, impurities and interfaces which does not depend on temperature. Only close to the melting point could thermally induced defects become relevant.

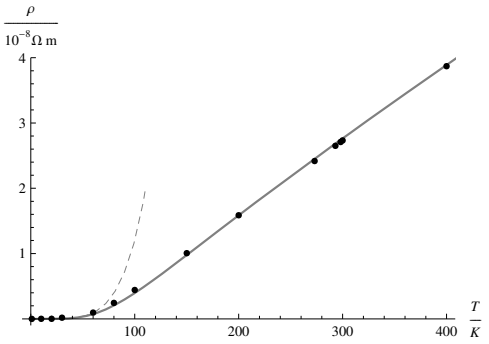

Figure 1.2: *Resistivity of aluminum and Bloch-Grüneisen-law and its low-temperature asymptotics. The result of the fit of ϱ_{BG} data from [Lide 1995] are $C = 7.5 \cdot 10^{11}\,\Omega\mathrm{mK}, \Theta = 429\,\mathrm{K}$, which is remarkably close to the reference value for aluminum $\Theta = 428K$.*

If there is a constant contribution to the relaxation rate due to material imperfections, it will dominate the resistivity at low temperatures. In the case of aluminum, an estimate for the plasma frequency gives $\omega_p \approx 2.4 \cdot 10^{16}\,\mathrm{Hz}$ and thus, using the resistivity at $T = 1\,\mathrm{K}$ from [Lide 1995] an order of $\gamma \approx 2 \cdot 10^{-7}\omega_p$. Presumably the measurements were done on extremely pure samples, so that typical values may be even higher.

This consideration motivates the distinction of two limiting cases of dissipative models:

- *Drude models* with a constant relaxation rate for impure metals.
- *Perfect crystals* for models of the Bloch-Grüneisen-type.

1.1.7 The skin effect

Normal skin effect

The last term in (1.13) leads to the attenuation of a wave in a dissipative medium over a characteristic length scale $\delta :=$ Im $1/k(\omega)$ given by the imaginary part of the wave-vector in the medium.

At low frequencies the current in a metal is dominated by conducting currents and the wave equation reduces to the diffusion equation

$$\Delta\mathbf{E} = \mu\sigma\dot{\mathbf{E}} \,, \tag{1.31}$$

which is solved by a diffusive wave $E \sim \exp(ikz - i\omega t)$, where

$$k = \pm\sqrt{i\mu\sigma\omega} \approx \pm(1+i)\sqrt{\frac{\mu\sigma\omega}{2}} \tag{1.32}$$

$$\Rightarrow \delta = \sqrt{\frac{2}{\mu\sigma\omega}} \,. \tag{1.33}$$

The approximation is valid at small enough frequencies. From the form of the wave equation it is clear, that identical relations hold also for a magnetic field. The final result is, that a time-dependent electromagnetic field can penetrate only a short distance into a metal. This is known as the *normal skin effect* [Jackson 2002].

It is easy to obtain a general expression for the impedance of a metal in the regime of the normal skin effect. A comparison of the low frequency approximation for the wave vector in a metal (1.33) with the dispersion relation gives the permittivity

$$\epsilon \approx \frac{i\sigma}{\omega\epsilon_0} \tag{1.34}$$

which can be plugged into (1.16 ff.) and yields the low frequency surface impedance

$$Z \approx Z_0(1-i)\sqrt{\frac{\omega\epsilon_0}{2\sigma}} \,, \tag{1.35}$$

Thus, the impedance of metals features a characteristic $\sqrt{\omega}$-behavior at low frequencies.

Anomalous skin effect

At low temperatures or high frequencies, the skin depth becomes smaller than the mean free path in the material $\delta \ll l \approx v_F\tau$, and the penetration depth is no longer described by the above expression but can become much larger. In this regime it is common to talk about the *anomalous skin effect*. Chambers gave a phenomenological description in terms of a nonlocal current-field relation

$$\mathbf{j}(\mathbf{r},\omega) = \frac{e^2N(E_F)v_F}{2\pi}\int d\mathbf{R}\frac{\mathbf{R}(\mathbf{R}\cdot\mathbf{E}(\mathbf{r}-\mathbf{R}))\exp(-R/l)}{R^4}\,, \tag{1.36}$$

where $N(E_F), v_F$ are the density of states and electron velocity at the Fermi edge. A similar analysis as in the previous case of the normal skin effect can be performed (e.g. [Dressel and Grüner 2002]) and gives a skin depth

$$\delta \sim \left(\frac{l}{\omega}\right)^{1/3}\,.$$

In the local limit, the field is assumed to vary on much larger scales than the mean free path l and can be taken out of the integral. In this case the current-field relation reduces to Ohm's law which leads to the normal skin effect

$$\mathbf{j}(\mathbf{r},\omega) \approx \mathbf{E}(\mathbf{r})\frac{e^2N(E_F)v_F}{2\pi}\int d\mathbf{R}\frac{\mathbf{RR}}{R^4}\exp(-R/l) \tag{1.37}$$

$$= \mathbf{E}(\mathbf{r})\frac{e^2N(E_F)v_F}{2\pi}\frac{4\pi l}{3} =: \sigma\mathbf{E}(\mathbf{r})\,. \tag{1.38}$$

1.2 Causality and optics

This section deals with the analytical properties of optical response functions, such as the conductivity, the dielectric functions or generally susceptibilities. All of these are complex functions and can be expressed in the time domain (hence the name *response function*) or equivalently in the frequency domain. The two representations are linked by Fourier transformations as introduced in section 1.1.2. In many calculations it is convenient to use a analytical continuation into the Gaussian plane of complex frequencies, where the analytical and distributional properties of the response functions become important, more so as these properties are closely connected to deep physical concepts such as causality and the link between dispersion and dissipation.

1.2.1 Causality and analytical properties

The first part of this work has introduced the basic quantities used to describe response of a material to an electromagnetic field. Among these were the electric conductivity, the index of refraction or the dielectric function. Most of the time, these functions have been expressed in the frequency domain, i.e. as the Fourier-transforms of a system's time-dependent response to a perturbation or excitation.

A general linear response function to a time dependent source h has the form

$$f(t) = \int_{-\infty}^{\infty} dt' g(t-t')h(t') = [g*h](t)\,, \tag{1.39}$$

where the last identity defines the convolution product. If the system is to be causal, the response must not precede an excitation, so

$$g(t) \stackrel{!}{=} g(t)\theta(t) \Leftrightarrow g(t<0) = 0\,. \tag{1.40}$$

Such functions are called *causal transforms*[1]. Now, if $g(-|t|)$ is expressed through its Fourier transform,

$$g(-|t|) = \int d\omega \exp(i\omega'|t|) \exp(-\omega''|t|) g(\omega) \ , \quad (1.41)$$

the integration path can be closed in the upper complex plane ($\mathrm{Im}\ \omega > 0$) as shown on the left of figure 1.3 because the integrand vanishes asymptotically, and since causality requires that integral must vanish for $t < 0$, there cannot be any poles in this region according to Cauchy's theorem (e.g. [Nussenzveig 1972, Landau and Lifshitz 1979]).

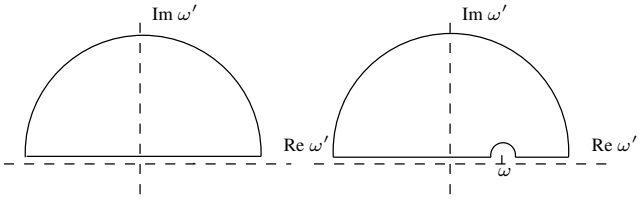

Figure 1.3: *Integration contours for causal functions.*

1.2.2 Causality relations

For causal and square-integrable analytic functions $g(\omega') \in \mathcal{L}^2$ on $\mathbb{R}$, $\frac{g(\omega')}{\omega'-\omega}$ has a single pole in the ω'-plane at real $\omega \neq 0$. Cauchy's theorem applied to the contour on the right in figure 1.3 gives

$$0 = \frac{1}{2\pi i} \oint \frac{g(\omega')}{\omega' - \omega} d\omega' \ . \quad (1.42)$$

As the integral along the large semi-circle vanishes due to the properties of g, the contribution from the pole must compensate the rest of integral along the real axis, which defines Cauchy's principle value (*valeur principale*) of the integral[2]

$$\begin{aligned} g(\omega) &= \frac{1}{\pi i} \mathcal{PV} \int_{-\infty}^{\infty} \frac{g(\omega')}{\omega' - \omega} d\omega' \quad (1.43) \\ &:= \lim_{\epsilon \to 0} \frac{1}{\pi i} \left[\int_{-\infty}^{-\epsilon} + \int_{\epsilon}^{\infty} \right] \frac{g(\omega')}{\omega' - \omega} d\omega' \ . \end{aligned}$$

If this is separated into real and imaginary part it becomes obvious that both are not independent but connected by Hilbert-Transforms known as *Plemelj's equations*, *causality relations* or *dispersion relations*

$$\mathrm{Re}\ g(\omega) = \frac{1}{\pi} \mathcal{PV} \int_{-\infty}^{\infty} \frac{\mathrm{Im}\ g(\omega')}{\omega' - \omega} d\omega' \quad (1.44)$$

$$\mathrm{Im}\ g(\omega) = -\frac{1}{\pi} \mathcal{PV} \int_{-\infty}^{\infty} \frac{\mathrm{Re}\ g(\omega')}{\omega' - \omega} d\omega' \ . \quad (1.45)$$

Besides, it can be shown that

$$\begin{aligned} g(\omega) &= \lim_{v \to 0} g(\omega + iv) \quad (1.46) \\ g(\omega + iv) &\in \mathcal{L}^2 \text{ for almost all } v > 0 \ . \end{aligned}$$

All these properties are connected by Titchmarsh's theorem: *All of the expressions (1.40), (1.44), (1.45) and (1.46) are equivalent for square-integrable and causal functions on* $\mathbb{R}$.

[1] Nussenzveig [Nussenzveig 1972] calls this *primitive causality* to distinguish it from the more general concept of *relativistic causality* which takes into account the retardation due to a signal's maximum velocity of propagation. In covariant notation, this requires

$$g(x_\mu) \stackrel{!}{=} g(x_\mu)\theta(x_\mu x^\mu)$$

. The primitive causality condition is thus the local limit of the relativistic one.

[2] How this is connected to distribution $\mathcal{P}1/\omega$, known as Cauchy's principal value of $1/\omega$ is discussed below. The definition is actually a generalization of the integral concept, and there is another even more general one:

If the divergences of an integral can be separated as the limit of a series R in terms of $\log\epsilon$ and $\frac{1}{\epsilon}$, then

$$\mathcal{PF} \int f := \int f - R\left(\log(\epsilon), \frac{1}{\epsilon}\right)$$

defines Hadamard's *part finie* (finite part) of the integral, which does coincide with Cauchy's principal value of the integral, whenever the latter exists. The identification of integrals with their *part finie* is considered good practice in quantum field theory, where divergent parts are absorbed into otherwise badly defined constants through a renormalization procedure.

Anyway, for the scope of this text, the principal value integral is powerful enough.

1.2.3 Basic theory of distributions

In many physical contexts, Titchmarsh's theorem does not apply because it applies only to square-integrable functions $g \in \mathcal{L}^2$. Also, response functions will often contain distributions like the Dirac δ-distribution, so that they are not even regular functions. The theory of distributions can of course not be fully covered here, but it is useful to sketch a few important elements, that will be used later and allow to find a more general form of Titchmarch's theorem. More complete introductions to the field can be found e.g. in [Vladimirov 1972,Gel'fand *et al.* 1962]. The topic of causal transforms has been treated thoroughly from the physicist's point of view by Nussenzveig [Nussenzveig 1972] and in a rigorous mathematical way by Beltrami and Wohlers [Beltrami and Wohlers 1966].

Distributions are linear functionals that act on a space of functions. The evaluation of a distribution is performed by means of the *inner product* with a test function, typically from a space of quickly decaying functions like e.g. $\mathcal{L}^2$. The inner product is is usually defined by

$$\langle \alpha, f \rangle \quad := \quad \int_{-\infty}^{\infty} \alpha(x) f(x) dx \; . \tag{1.47}$$

A distribution is called regular, if it can be replaced by an element of the function space itself. Then it has a well-defined value in any point of its support. In physics non-regular distributions are omnipresent. The most prominent one of which is Dirac's δ-distribution. It cannot be expressed through any regular function but it can be obtained as the limit of a family of functions. The δ-distribution is defined by its property to select a value of the test-function

$$\langle \delta, f \rangle \quad := \quad f(0) \tag{1.48}$$

The *distributional derivative* can be defined in terms of the inner product (1.47). Performing a partial integration and using the fast decay of the test functions

$$\Rightarrow \langle \alpha', f \rangle \quad := \quad -\langle \alpha, f' \rangle \; . \tag{1.49}$$

Every distribution (even the irregular ones) can be expressed as distributional derivatives of regular functions. The space of distributions that are the nth derivative (D_{t^n}) of a continuous regular functions is usually called

$$\mathcal{E}_0^{(n)} = \{ D_{t^n} f(t) : f(t) \in C^0 \} \; . \tag{1.50}$$

Another important space is made up by the (anti-)causal distributions

$$\mathcal{D}^{\pm} = \{ g_t \in \mathcal{E}_0^{(1)} : g_t = g_t \theta(\pm t) \} \; . \tag{1.51}$$

This includes the causal regular functions as defined by equation (1.40) as a special case. The elementary (anti-) causal distribution $\delta^{\pm}$ is obtained as the Fourier transform of the unit step function

$$\mathcal{F} \left[\delta^{\pm}(\omega) \right] = \theta(\mp t) \tag{1.52}$$

$$\delta^{\pm}(\omega) \quad = \tfrac{1}{2}\delta(\omega) \mp \tfrac{1}{2\pi i} \mathcal{P} \tfrac{1}{\omega} \quad = \lim_{\epsilon \to 0} \mp \frac{1}{2\pi i} \frac{1}{\omega \pm i\epsilon} \tag{1.53}$$

$$\delta(\omega) \quad = \delta^{+}(\omega) + \delta^{-}(\omega) \quad = \lim_{\epsilon \to 0} \frac{1}{\pi} \frac{\epsilon}{\omega^2 + \epsilon^2} \; . \tag{1.54}$$

The distribution $\mathcal{P}\frac{1}{\omega}$ is *defined* by means of Cauchy's principal value of the integral (1.43)

$$\langle \mathcal{P} \frac{1}{\omega}, f(\omega) \rangle \quad := \quad \mathcal{PV} \int_{-\infty}^{\infty} \frac{f(\omega)}{\omega} d\omega \; . \tag{1.55}$$

This clarifies the connection between the symbols $\mathcal{PV}$ for Cauchy's principal value of an integral and $\mathcal{P}$ as the notation for a special distribution, which cannot be generalized to arbitrary functions.A common equivalent representation of (1.53, 1.54), which has been used earlier in this text to introduce the causal plasma model, is known as Dirac's identity or Sochozky's formula

$$\lim_{\epsilon \to 0} \frac{1}{\omega \pm i\epsilon} = \mathcal{P} \frac{1}{\omega} \mp i\pi\delta(\omega) \; . \tag{1.56}$$

Finally, a surprising identity can be obtained from the convolution theorem of Fourier analysis

$$\mathcal{P} \frac{1}{\omega} * \mathcal{P} \frac{1}{\omega} = -\pi^2 \delta(\omega) \; . \tag{1.57}$$

1.2.4 Causality relations for distributions

In the case of causal distributions $g_\omega \in \mathcal{D}^+$ the analog to (1.43) is the fundamental theorem

$$g_\omega = -\frac{1}{i\pi} g_\omega * \mathcal{P}\frac{1}{\omega} \,. \tag{1.58}$$

The generalization of Plemenj's equations are thus

$$\text{Re } g_\omega = -\frac{1}{\pi} \text{ Im } g_\omega * \mathcal{P}\frac{1}{\omega} \tag{1.59}$$

$$\text{Im } g_\omega = \frac{1}{\pi} \text{ Re } g_\omega * \mathcal{P}\frac{1}{\omega} \,. \tag{1.60}$$

As in Titchmarsh's theorem, both equations are equivalent, since one is obtained from the other by a convolution with the distribution $\mathcal{P}\frac{1}{\omega}$ and (1.57).

An example for a causal distribution is the distributional plasma model introduced in (1.26). In the above notation, it becomes

$$\epsilon(\omega) = 1 - \frac{\omega_p^2}{\omega}\mathcal{P}\frac{1}{\omega} - i\pi\frac{\omega_p^2}{\omega}\delta(\omega) = 1 + \frac{2\pi\omega_p^2}{\omega}\delta^+(\omega) \,. \tag{1.61}$$

As a causal distribution it fulfills the distributional Plemenj's equations, which can be shown directly with help of (1.57).

Note that it is not possible to introduce only the δ-contribution without doing the replacement $\frac{1}{\omega} \to \mathcal{P}\frac{1}{\omega}$ at the same time. This step is often neglected, e.g. in [Dressel and Grüner 2002, Berlinsky *et al.* 1993], and is a common source of confusion, because the version of Plemenj's equations for functions will not give the desired results.

This stresses, that consistent causal response functions and causality relations are obtained only, if the distributional properties are taken into account completely.

1.2.5 Kramers-Kronig relations and sum rules

The Kramers-Kronig relations

Special examples of response functions introduced earlier are the

- *dielectric function* $\epsilon(\omega)$: response of the dielectric displacement to an electric field.
- *electric susceptibility* $\chi(\omega) = \epsilon(\omega) - 1 = i\frac{\sigma(\omega)}{\epsilon_0\omega}$: response of the dielectric polarization to an electric field.
- *electric conductivity* σ: current response to an applied field.

The responses must be causal, and so there should be Plemenj's equations. Unfortunately, dielectric functions have the limit $\epsilon(\infty) = 1$ and are hence not (square-)integrable. On the other hand the closely related susceptibility $\chi(\omega) = \epsilon(\omega) - 1$ fulfills all requirements and Kramers-Kronig relations can be introduced. The final result can then be expressed in terms of $\epsilon(\omega)$.

These causality relations for the dielectric functions were introduced independently by Kramers and Kronig [Kramers 1927, Kronig 1926] and are therefore known as *Kramers-Kronig (KK-) relations*.

$$\begin{aligned} \epsilon'(\omega) &= 1 + \frac{1}{\pi}\mathcal{PV}\int_{-\infty}^{\infty}\frac{\epsilon''(\omega')}{\omega'-\omega}d\omega' \\ \epsilon''(\omega) &= -\frac{1}{\pi}\mathcal{PV}\int_{-\infty}^{\infty}\frac{\epsilon'(\omega')-1}{\omega'-\omega}d\omega' \,. \end{aligned} \tag{1.62}$$

Since physical electric fields are real, $\epsilon(-\omega) = \epsilon^*(\omega)$ and $\sigma(-\omega) = \sigma^*(\omega)$. Using these properties, (1.44), (1.45) can be written in a symmetric form, which for the conductivity gives

$$\begin{aligned} \sigma'(\omega) &= \frac{2}{\pi}\mathcal{PV}\int_0^{\infty}\frac{\omega'\sigma''(\omega')}{\omega'^2-\omega^2}d\omega' \\ \sigma''(\omega) &= -\frac{2\omega}{\pi}\mathcal{PV}\int_0^{\infty}\frac{\sigma'(\omega')}{\omega'^2-\omega^2}d\omega' \,. \end{aligned} \tag{1.63}$$

Kramers-Kronig relations for conductors

Kramers-Kronig relations are unambiguous only up to a constant, which is usually fixed by a reference value at a fixed frequency. A first example for a subtraction scheme for dispersion relations was already given in the last section. Here, the quantity $\epsilon(\omega) - \epsilon(\infty)$ could have been used instead of the susceptibility with identical results.

Similarly, subtractions can be introduced in order to renormalize even UV- and IR-divergences. This leads to *generalized* or *higher order Kramers-Kronig relations*.

In conductors $\sigma'(0) \neq 0$, and $\epsilon''(0)$ features an IR-divergence, such that the first of (1.62) does not exist. The pole may be renormalized by simply subtracting it and the resulting function is analytic and fulfills Plemenj's equations. For conductors, the second of (1.62) is now replaced by

$$\epsilon''(\omega) - \frac{\sigma'(0)}{\epsilon_0 \omega} = -\frac{2\omega}{\pi} \mathcal{PV} \int_0^\infty \frac{\epsilon'(\omega') - 1}{\omega'^2 - \omega^2} d\omega' \, .$$

Kramers-Kronig relations for the plasma model

The formalism of subtraction from the last section can be applied to the singularity of the plasma model. Of course this means just subtracting the complete plasma model from the dielectric function and the resulting function is analytic *per definitionem*. This was done in in [Klimchitskaya *et al.* 2007] for a version of the plasma model featuring additional resonances. These resonances, which are Drude-like and do not create problems are everything that is left over after the subtraction. Higher order KK-relations similar to the ones given in [Landau and Lifshitz 1979] have then been recalculated by performing contour integrations explicitly. The interpretation needs some clarification in my point of view:

- The method of constructing an analytic function by subtraction of single terms, makes it possible to describe correctly mathematical properties of functions. Of course this does not guarantee the causality of the *original* function and does thus not prevent the problems created by non-causal functions.
- The authors of [Klimchitskaya *et al.* 2007] reject the introduction of a δ-contribution as it fulfills only one of the Kramers-Kronig relations. But it has been pointed out in section 1.2.4 that it is absolutely essential in this case to use the distributional Plemenj's equations (1.59, 1.60) rather than the functional KK-relations.

The oscillator strength sum rule

Sum rules are yet another consequence of causal properties of the optical response functions. It has been stated before that the plasma model is the general limit of dielectric functions at high frequencies, where absorption or excitation do not longer occur, but where the response is due to inertia. In this regime

$$\epsilon(\omega) \approx \epsilon'(\omega) \approx 1 - \frac{\omega_p^2}{\omega^2}. \tag{1.64}$$

Plugging this limit into the left hand side of the Kramers-Kronig relation and using $\omega \gg \omega'$ also in the denominator under the integral, gives what is known as the *oscillator sum rule*

$$\epsilon'(\omega) - 1 = \frac{2}{\pi} \mathcal{P} \int_0^\infty d\omega' \frac{\omega' \epsilon''(\omega')}{\omega'^2 - \omega^2} \approx -\frac{2}{\omega^2 \pi} \int_0^\infty d\omega \omega' \epsilon''(\omega') \tag{1.65}$$

$$\Rightarrow \int_0^\infty \omega' \epsilon''(\omega') d\omega' = \int_0^\infty \frac{\sigma'(\omega')}{\epsilon_0} d\omega' = \frac{\pi \omega_p^2}{2}. \tag{1.66}$$

Thus, the total dissipation of a system is connected to the plasma-frequency. Arguments of this type can be used to estimate parts of the spectral dissipation function if only a part is known. Is is obvious, that the sum rule (1.66) holds in the case of the Drude model.

The term *oscillator strength* stems from a semi-classical model of the matter of structure, introduced by Lorentz and based on the observation, that general dielectric functions can be well-fitted by a sum of Lorentz oscillators. The Drude model (with only one resonance frequency $\omega = 0$) is just the simplest scenario. Each of the oscillators is interpreted as an ensemble of harmonically bound electrons in the solid. In this picture, the relative weight of the

resonances is measured by the *oscillator strength* which is just proportional to the respective fraction of electrons. Since the total number of electrons must be conserved, the oscillator strengths must add up to 1, which is mirrored by the above sum rule. In quantum mechanics, the oscillator strength of the classical model can be linked directly to a transition matrix element.

Optics at imaginary frequencies

Optical response-functions such as the conductivity, dielectric function or (complex) index of refraction are causal functions or distributions and they allow generally for analytic continuation into the upper half of the complex frequency plane. A description of optical properties at purely imaginary frequencies is very desirable. As an example, frequency-integrations along the imaginary axis result in exclusively real-valued square-roots in Fresnel's formulas (1.16). Later in this work, when surface interactions are calculated, the use of imaginary frequencies will turn out to be very favorable for the evaluation of thermal corrections.

Often the analytic continuation can be obtained from the known response function at real frequencies by simply substituting $\omega = i\xi$, where $\xi \in \mathbb{R}$. This direct complexification is very simple, where the frequency dependence is explicitly known and no further complications, such as branch cuts due to multiple valued functions occur. Examples for dielectric functions that allow a direct evaluation at imaginary frequencies are the ones of the plasma and Drude model.

Where this is not possible - as in the BCS theory presented below - the Kramers-Kronig relations or the Cauchy formula respectively may be used to evaluate the response functions along the imaginary axis. Since the complete information is contained in either the real or the imaginary part of a response function, the analytical continuation can be done from either of them. After some algebra the corresponding KK-relations read

$$\sigma(i\xi) = \frac{2}{\pi}\int_0^\infty d\omega \frac{\omega\sigma''(\omega)}{\xi^2+\omega^2} \tag{1.67}$$

$$= \frac{2}{\pi}\xi\int_0^\infty d\omega \frac{\sigma'(\omega)}{\xi^2+\omega^2}\,. \tag{1.68}$$

If the analytic continuation is obtained by other means, such as the explicit evaluation along the imaginary axis, the above KK-relations are still very helpful to check the results.

1.3 Phenomena in superconductivity

The previous sections have dealt with the general electrodynamical and optical properties of conductors or metals. Superconductors are a special case and before some of the most important descriptions are presented, the most relevant phenomena occurring in these materials shall be presented. A historical overview on the discovery of superconductivity has already been given in the introduction.

Superconductors feature a phase transition at a critical temperature T_c, below which they expose two very characteristic macroscopic properties

- *Vanishing resistivity* $\sigma_0 \to \infty$: superconducting materials loose their electric DC-resistance below a critical temperature T_c in the order of magnitude of some Kelvin [Kammerlingh-Onnes 1911].
- *Meißner-Ochsenfeld effect* $\mathbf{B} \to 0$: The inside of superconductors is free of magnetic fields[3] [Meißner and Ochsenfeld 1933]

These two points alone - later the details and mechanisms will be discussed much more carefully - are sufficient to give rise to many optical, thermodynamical and electrical properties and must be reproduced by any theoretical description of the superconductors. In fact the great success of the London model described in the next section, which is still the standard description of a superconductor for many technical and engineering purposes, is due to the fact, that for the first time both effects could be recovered from one model.

[3] This is strictly true only for so-called type I superconductors in the Meißner-state. In section 1.5 it will turn out, that in some materials (type II superconductors) superconducting and normally conducting domains can coexist in a mixed phase.

Due to the vanishing conductivity a superconductor can carry huge persistent supercurrents that do not decay on any experimental time scale. The Meißner-Ochsenfeld effect (cf. section 1.4.2) can be understood as the consequence of surface supercurrents that will adapt to the external field and cancel it out in the interior of the superconductor. Note that supercurrents can be excited only in a multiply connected body, i.e. in superconducting rings or as a part of a circuit.

Superconductivity breaks down at certain critical thresholds of the temperature T_c, external fields H_c or the current j_c. These critical values can all be connected to a critical energy scale, e.g. $k_B T_c \sim \frac{\mu}{2} H_c^2(T=0)$, which was an important hint at the energy gap fundamental for the BCS description. At finite temperature, the value of the critical field was very early found to follow well a parabolic law [Shoenberg 1938]

$$H_c(T) \sim \left(1 - \frac{T^2}{T_c^2}\right) . \tag{1.69}$$

There is vast literature on superconductivity and solid state electrodynamics. Some relevant textbooks and monographes on superconductivity are [Landau and Lifshitz 1979, Tinkham 2004, Buckel 1977, Schrieffer 1999, Rickayzen 1965, Ketterson and Song 1999, Zhou 1991], whereas general solid state physics and optics are covered e.g. in [Landau and Lifshitz 1974, Dressel and Grüner 2002, Ashcroft and Mermin 1987, Jones and March 1973, Kittel 2002]. A classical review article on classical superconductors is [Tinkham 1974] and a concise review is also given in the introduction of [Basov and Timusk 2005] covering the new and exciting field of high T_c superconductors. Such materials were discovered in 1986 [Bednorz and Müller 1986] and cannot be covered in this text, which is limited to classical superconductors in the Meißner-state (cf. 1.5).

1.4 The two fluid model

1.4.1 The London's model

The London equations

A very successful early model of superconductivity was proposed in the 1930s by the brothers F. and H. London [London and London 1935]. They considered a fluid of superconducting charge-carriers of mass m^*, charge e^* and density $n_s^* = |\Psi|^2$ described by a macroscopic wave function

$$\Psi = \sqrt{n_s^*}\exp(i\varphi) . \tag{1.70}$$

The gauge-invariant current due to this wave function is

$$\mathbf{j}_s = \frac{e^*}{m^*}\langle\Psi| - i\hbar\overrightarrow{\mathcal{D}}|\Psi\rangle = \frac{n_s^* e^* \hbar}{m^*}(\nabla\varphi - \frac{e^*}{\hbar}\mathbf{A}) . \tag{1.71}$$

The London brothers assumed the order parameter to be rigid towards perturbations [4] so that $\langle\Psi| - i\hbar\nabla|\Psi\rangle \approx 0$, and obtained the celebrated gauge invariant London equations [London and London 1935]

$$\nabla \times \mathbf{j}_s = -\frac{{e^*}^2 n^*}{m^*}\mathbf{B} \tag{1.72}$$

$$\mathbf{E} = \frac{m^*}{{e^*}^2 n^*}\frac{d\mathbf{j}_s}{dt} =: \Lambda\frac{d\mathbf{j}_s}{dt} \tag{1.73}$$

The London equations are often given in terms of the vector potential

$$\mathbf{j}_s = -\epsilon_0\omega_p^2\mathbf{A} , \tag{1.74}$$

but one must keep in mind that this requires the proper transverse choice of gauge $\nabla\cdot\mathbf{A} = 0$, or the correct definition of the boundary conditions which will eventually lead to the subtraction of gauge-violating terms in any physical situation [Schrieffer 1999].

[4] Since $\nabla\cdot\mathbf{B} = 0$, the magnetic field is necessarily transverse and perturbations affect only transverse excitations. The order parameter is thus rigid only towards transverse perturbations [Schrieffer 1999] and it is the non-rigidity w.r.t. longitudinal excitations, that leads to corrections.

Superconductivity is clearly a quantum effect but interestingly the London equations do not depend on Planck's constant $\hbar$, which is the typical signature of "quantumness". Interestingly, it is the very assumption of phase rigidity, responsible for the special properties of a superconductor, that suppresses the only term in (1.71) that depends on $\hbar$. Hence, the only element of a quantum mechanical description left over in the London equations, is the interpretation of the density n_s^* of the charge carriers in terms of a wave-function.

When in the 1950s the pairing theory of superconductivity came up, the charge carriers were immediately interpreted as Cooper-pairs of electrons[5] of mass $m^* = 2m_e$, charge $|e^*| = 2|e|$ and density $n_s^* = \frac{n_s}{2} = |\Psi_0|^2$. A nice observation is, that the London equations are independent of the nature of the charge-carriers (single electrons or pairs within an one-particle picture as defined above), as is the specific charge e/m and the charge density $e \cdot n$, so that the stars can be dropped from the notation.

The quantity Λ appearing in the London equations is known as the *London-parameter* and is closely related to the plasma-frequency

$$\Lambda = \frac{1}{\epsilon_0 \omega_p^2}, \qquad \omega_p^2 = \frac{ne^2}{m\epsilon_0} \; .$$

Plasma model and impedance

In the frequency domain, the second London equation (1.72) becomes

$$\mathbf{E}(\omega) \quad = \quad -\frac{i\omega}{\epsilon_0 \omega_p^2} \mathbf{j}(\omega). \tag{1.75}$$

As in section 1.1.5 a complex conductivity or equivalently a dielectric function can be introduced to describe the current-field relation

$$\sigma(\omega) = \frac{i\omega_p^2 \epsilon_0}{\omega}, \qquad \epsilon(\omega) = 1 - \frac{\omega_p^2}{\omega^2} \; ,$$

which is just the plasma model (1.23) known from section 1.1.5. From this, equation (1.16 ff.) can be used to obtain the impedance of a superconductor, which grows linearly with frequency [Zhou 1991]

$$Z = Z_0 \sqrt{\frac{1}{\epsilon(\omega)}} = Z_0 \frac{\omega}{\omega_p} \; . \tag{1.76}$$

This power law differs from the one in (1.35) obtained for the normal metal which shows once again, that the plasma model should not be carelessly used to model normal metals especially at low frequencies.

Quantization of magnetic flux

An immediate consequence of the macroscopic wave-function ansatz is the quantization of the magnetic flux through a superconducting ring [Ashcroft and Mermin 1987]. Since the macroscopic wave-function must be single-valued, it must change by a multiple of 2π along the ring, and using that inside the bulk $\oint \mathbf{j} \cdot d\mathbf{l} = 0$

$$\Phi = \oint \mathbf{A} \cdot d\mathbf{l} = \frac{\hbar}{e^*} \oint \nabla\varphi \cdot d\mathbf{l} = \frac{\hbar}{e^*} \underbrace{\Delta\varphi}_{2\pi k} = k\Phi_0 \; , \tag{1.77}$$

where the quantum of flux is $\Phi_0 = \frac{h}{e^*}$. This is a measurable quantity and the experimental confirmation of the value $e^* = 2e$ contributed immensely to the acceptance of the pair-description of superconductivity. Anyhow, recently doubt has been raised on this value for high-T_c superconductors [Loder *et al.* 2008].

1.4.2 The Meißner-Ochsenfeld effect

In 1933 Meißner and Ochsenfeld discovered [Meißner and Ochsenfeld 1933], that the magnetic field is expulsed from the superconductor's interior while undergoing the superconducting transition. Together with the vanishing

[5] Actually, Cooper pairs are quasi-particles in a many-particle-theory, while the London theory deals with one-particle-states. The densities occurring e.g. in the BCS theory features therefore coherence effects, so that London-theory is but a first approximation, cf. 1.4.3, 1.6, [Landau and Lifshitz 1979, §144].

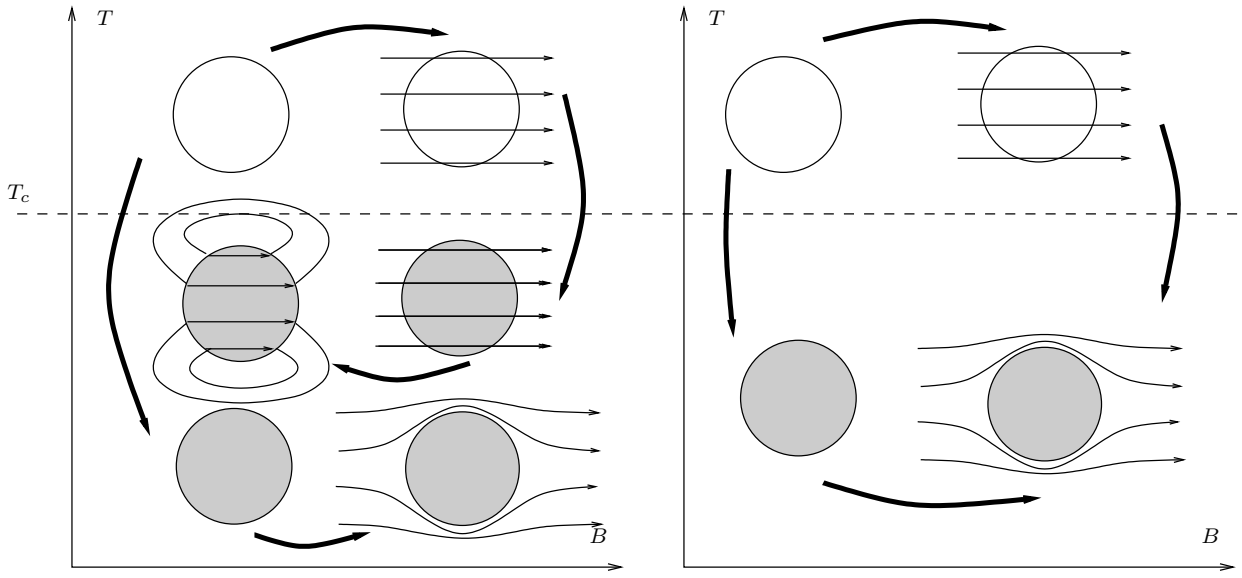

Figure 1.4: *Ideal conductor $\dot{\Phi} = 0$ (left). Superconductor $\Phi = \dot{\Phi} = 0$ (right). In thermodynamic equilibrium states the final state must not depend on the path chosen in $B - T$-plane.*

resistivity this is the reason, why superconductors have often been called both *ideal conductors* and *ideal diamagnets*. Both terms may be somewhat misleading and need some clarification [Tinkham 2004, Schrieffer 1999].

The term *ideal diamagnet* hints at a medium with a magnetic susceptibility $\chi_m = -1 = -\frac{|\mathbf{M}|}{|\mathbf{H}|}$ and thus $\mu_r = 1 + \chi_m = 0$, which produces the required property $\mathbf{H} \neq \mathbf{B} = 0$ on the interior.

Another way of looking at things is to leave magnetization completely out of the picture, but assume that *free* surface supercurrents arise in response to the external field and contribute to the discontinuity of $\mathbf{B}$ at the surface such as to shield the interior. The London theory (using $\mu_r = 1$) is formulated within this framework and it is certainly the more common point of view. But, since the description by a ideal diamagnet requires some kind of magnetic moments, connected to bound currents in the classical picture, both pictures cannot be well distinguished. Anyway it is clear now, that when talking about ideal diamagnets, materials are meant, that feature the Meißner-Ochsenfeld effect.

In an *ideal conductor*, characterized by zero resistivity, the electric field needed to produce a given current vanishes, and from Maxwell's equation follows that the magnetic field *freezes*, i.e. the magnetic flux is constant

$$\begin{aligned} \mathbf{E} &= \lim_{\sigma\to\infty} \frac{1}{\sigma}\mathbf{j} = 0 \\ \Rightarrow \int \nabla \times \mathbf{E} dA &= -\int \dot{\mathbf{B}} dA = -\dot{\Phi} = 0 \,. \end{aligned}$$

If superconductors and ideal conductors were identical, the magnetic flux would have to be conserved even when going through the superconducting transition. But in this case, the state of the material would depend on the path in $B - T$-space (fig. 1.4), which is not possible, if the superconductor is to be a thermodynamic equilibrium state and furthermore is in clear contradiction to the well-established Meißner-Ochsenfeld effect.

On the other hand, when the London equations are used as the current-field relation, and coordinates are chosen so that x points into the superconductor, the stationary solution reads

$$\begin{aligned} \Delta\mathbf{B} &= \frac{\mu_0}{\Lambda}\mathbf{B}, \qquad \Delta\mathbf{j} = \frac{\mu_0}{\Lambda}\mathbf{j} \\ \Rightarrow \mathbf{B}, \mathbf{j} &\sim \exp(-x/\lambda_L) \Rightarrow \lim_{x\to\infty} \mathbf{B} = 0 \,. \end{aligned} \tag{1.78}$$

Hence, not only is the flux constant but also vanishes inside the superconductor. This explanation of the Meißner-Ochsenfeld effect was a great success of the London theory. The scale, on which the field decays is known as the London penetration depth and coincides with the plasma wavelength

$$\lambda_L = (\omega_p^2 \epsilon_0 \mu_0)^{-1/2} = \frac{c}{\omega_p} = \lambda_p \,. \tag{1.79}$$

The London theory includes thus a stronger condition than just that of vanishing resistance. At the same time, the Meißner-Ochsenfeld effect is the solution to the thermodynamical conundrum arising from the ideal conducting case.

It must be stressed that London theory deals with stationary states and order parameters and does not give a description of *how* the field is expulsed from the bulk. Clearly the processes depicted above include an evolution in time. A dynamical description of the process is possible in a time-dependent generalization of Ginzburg-Landau theory (check section 1.5, [Tinkham 2004]) but is beyond the scope of this thesis.

1.4.3 Two fluid model and the Gorter-Casimir relation

The London theory works very well but only at very low temperatures. The two fluid model is an extension of the original theory and was constructed in analogy to Landau's theory of superfluidity [Landau and Lifshitz 1979, Soldati 2003]. In this model, the total current through the superconducting metal is described as a superposition of dissipative normal contribution and a superconducting non-dissipative current

$$\mathbf{j} \;=\; \mathbf{j}_n + \mathbf{j}_s, \qquad \mathbf{j}_n = \sigma \mathbf{E}\,. \tag{1.80}$$

As this description is based on a classical model, charge conservation requests that the total number of charge-carriers be constant, but they can still be distributed between the supercurrent and the normal current depending on temperature. The partial densities of charge carriers responsible are described by a temperature-dependent order parameter

$$\eta(T) = \frac{n_s}{n} = 1 - \frac{n_n}{n} \tag{1.81}$$

It seems reasonable to describe the superconducting current by a London type plasma model and the normal current by the Drude model. Hence, a first educated guess at the dielectric function of superconductors reads

$$\epsilon(\omega) = 1 - \frac{\omega_p^2}{\omega^2}\eta(T) - \frac{\omega_p^2}{\omega(\omega + i\gamma)}[1 - \eta(T)]\,. \tag{1.82}$$

At very low temperatures, the plasma model is a good description for the superconductor, so generally $\eta(0) = 1$, i.e. all electrons contribute to the superconducting current. On the other hand above the critical temperature T_c the material behaves as a normal conductor and $\eta(T > T_c) = 0$.

A specific form of the order parameter was proposed by Gorter and Casimir based on a somewhat artificial form of the free energy including a constant condensation energy for the superfluid [Gorter and Casimir 1934, Zhou 1991, Schrieffer 1999]

$$\mathcal{F} = \underbrace{-\sqrt{1-\eta(T)}\frac{a}{2}T^2}_{\text{normal current}} \underbrace{-\eta(T)b}_{\text{supercurrent}}\quad, \tag{1.83}$$

which when varied with respect to $\eta \sim n_s \sim |\Psi|^2$ gives the Gorter-Casimir order parameter

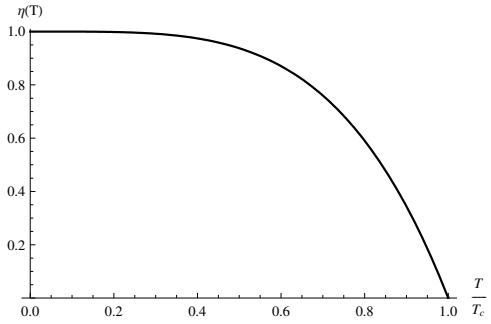

Figure 1.5: *The Gorter-Casimir order parameter* $\eta(T)$

$$\eta(T) \;=\; \left[1 - \left(\frac{T}{T_c}\right)^4\right]\theta(T_c - T) \tag{1.84}$$

$$\theta(x) \;=\; \begin{cases} 1 & x > 0 \\ 0 & x < 0 \end{cases}$$

Heaviside's unit-step function $\theta(x)$ is introduced to cut off the temperature dependence at the critical temperature. A jump of the specific heat occurs at the critical temperature, and if the difference between the two contributions is balanced to a critical field,

$$\frac{\mu \mathbf{H_c}^2}{2} = \mathcal{F}_n(T) - \mathcal{F}_s(T) \Rightarrow H_c(T) \sim \left(1 - \frac{T^2}{T_c^2}\,,\right)\,,$$

which recovers (1.69) and fits very well to the experimental data.

The Gorter-Casimir relation (fig. 1.5) gives the generally correct asymptotics of the superconducting gap at low temperatures, which is the analog to an order parameter obtained from microscopic BCS theory (cf. 1.6).

1.5 The Ginzburg-Landau model

1.5.1 The free energy approach

Another highly successful macroscopic description of superconductivity was given by Ginzburg and Landau (GL) [Ginzburg and Landau 1950, Ginzburg 1955]. This section will give only a brief overview over the fundamental concepts of this theory and show a few results that are important for the definition and understanding of the systems considered in the rest of this work, but it is not possible to give a complete introduction to this complex and rich theory. Extensive material can be found in references [Lifshitz *et al.* 1984, Tinkham 2004, Ketterson and Song 1999, Schrieffer 1999].

GL theory is based on general properties of the free energy per unit volume of a system near a phase transition, described through an order parameter. The theory can be seen as a generalization of the London model, and as in the earlier model, the order parameter is identified with a macroscopic wave-function but without the restriction of rigidity.[6].

Gorkov [Gorkov 1959] showed that the Ginzburg-Landau model can be derived asymptotically from BCS theory (section 1.6), and found thus a microscopic justification for the macroscopic description. It turned out, that $\Psi \sim \Delta(T)$ is closely connected to the superconducting gap $\Delta(T)$, which takes the role of an order parameter in BCS theory.

The potential in the Ginzburg-Landau ansatz can contain only contributions in even powers of the density $|\Psi|^2$, since a global phase must not show up in the physics. The free energy ansatz contains the normal free energy density f_n, a kinetic term and the first two orders of the Ginzburg-Landau potential $V(\Psi)$

$$f_s = f_n + \frac{\hbar}{2m^*}|\nabla\Psi|^2 + \underbrace{a|\Psi|^2 + \frac{b}{2}|\Psi|^4}_{V(\Psi)} \,. \qquad (1.85)$$

At the critical temperature T_c, the equilibrium state of the potential must change its stability. This happens if a spontaneous symmetry breaking at T_c introduced through the parameters a, b. Since GL theory holds only at temperatures close to T_c, the exact form of the ansatz is not very important, because any expression can be expanded in low order terms of the form

$$a = \alpha(T - T_c), \qquad \alpha > 0 \qquad (1.86)$$

$$b = \text{const.} \qquad (1.87)$$

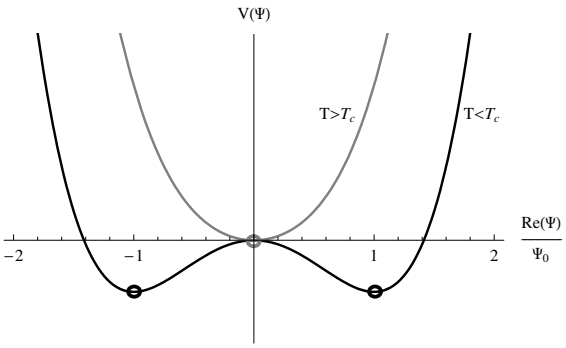

Figure 1.6: *Ginzburg-Landau potential $V(\Psi)$ in the normal state at $T > T_c$ (gray) and in the superconducting state with broken symmetry at $T < T_c$ (black). The respective stable equilibria are indicated by the circles. Note that the potential is invariant under rotations in the complex Ψ plane.*

Figure 1.6 shows the Ginzburg-Landau potential above and below T_c. Above the critical temperature, $\Psi = 0$ is the stable minimum corresponding to the normal state, but below T_c the potential takes a *Mexican hat* form with a stable minimum at a non-vanishing value of the order parameter and superconductivity sets in.

Without any external fields, for instance deep inside the bulk, where field are screened, Ψ does not depend on the spatial coordinates, i.e. $\nabla\Psi = 0$. The equilibrium value of the order parameter is given by

$$\frac{\partial F}{\partial|\Psi|^2} = 0 \Leftrightarrow |\Psi|^2 = \frac{|a|}{b} =: \Psi_0^2 \,. \qquad (1.88)$$

[6] Also in the microscopic BCS theory, where the gap between the ground and excited state takes the role of an order parameter, it is supposed to be spatially constant.

The superconducting phase transition is of second degree, thus it features a discontinuity in the heat capacity, yet entropy is continuous. The difference of free energy between normal and superconducting state can be connected to a thermodynamic critical value of the external field as in London theory,

$$\frac{\mu}{2}{\mathbf{H_c}}^2 = \frac{|a|^2}{2b} \,. \tag{1.89}$$

Yet another relation between a and b can be taken by analogy from London theory, stating that $\lambda^2 \sim 1/|\Psi|^2$, thus all parameters can be expressed by the measurable quantities critical field and penetration depth.

When an external field is present, minimal coupling must be introduced by replacing the derivative by its covariant equivalent. Minimizing the free energy with respect to the parameters of the system $\Psi, \Psi^*, \mathbf{A}$ yields the famous Ginzburg-Landau equations

$$\begin{aligned} 0 &= \frac{1}{2m^*}(-i\hbar\nabla\Psi - \frac{e^*}{\hbar}\mathbf{A})^2\Psi + a\Psi + b|\Psi|^2\Psi \\ \nabla\times\mathbf{B} &= \mu_0\mathbf{j} \\ \mathbf{j} &= \frac{-ie^*\hbar}{2m^*}[\Psi^*\nabla\Psi - \Psi\nabla\Psi^*] - \frac{e^*}{2m^*}|\Psi|^2\mathbf{A} \end{aligned} \tag{1.90}$$

In order to perform the variation, it is necessary to evaluate a surface-integral. It vanishes if no currents occur perpendicular to the superconductor surface

$$\mathbf{n}\cdot(-i\hbar\nabla - e^*\mathbf{A})\Psi \stackrel{!}{=} 0 \tag{1.91}$$

While this is certainly true at superconductor-vacuum interfaces, attention has to be paid at superconductor-metal interfaces, for instance where superconductors are part of a circuit.

1.5.2 Weak fields

An adimensional form of the Ginzburg-Landau equations can be obtained introducing the so-called *coherence length*

$$\xi = \sqrt{\frac{\hbar^2}{2m^*|a|}} \,, \tag{1.92}$$

and normalizing the wave function to its equilibrium value $f = \Psi/\Psi_0$. The coordinate x points into the superconductor. In the absence of external fields the first of the GL-equations (1.90) written in the adimensional form

$$\begin{aligned} 0 &= -\xi^2 f'' - f + f^3 \\ &= \frac{d}{dx}\left[-\frac{1}{2}f'^2\xi^2 - \frac{1}{2}f^2 + \frac{1}{4}f^4\right] \end{aligned} \tag{1.93}$$

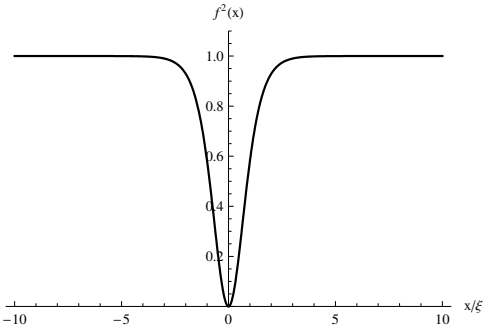

Figure 1.7: *The relaxation of the squared order parameter to its equilibrium value shows the typical vortex structure.*

Deep inside the material ($x \to \infty$), the system it is completely superconducting, i.e. $f' \to 0, f^2 \to 1$ and the term in brackets on the right hand side takes the value $-\frac{1}{4}$. Since this value is independent of x,

$$\xi^2 f'^2 = \frac{1}{2}(1-f^2)^2 \qquad \Rightarrow \qquad f(x) = \tanh\left(\frac{x}{\sqrt{2}\xi}\right) \,. \tag{1.94}$$

Thus, the coherence length describes the scale on which a perturbation of the wave function present at $x = 0$ decays inside the bulk. Fig. 1.7 shows the square of f^2, which as in the two fluid model can be interpreted as the density of the superconducting charge carriers. This function features the characteristic form of a vortex, in the center of which a single flux filament can penetrate the superconductor.

If the external field is non-vanishing but weak, the GL-equations (1.90) can be solved using an expansion of the order parameter in powers of the field. Using only the lowest order, i.e. the constant equilibrium value $\Psi = \sqrt{-\frac{a}{b}}$ from the field-free case, the dimensional form of the field equation yields

$$\Delta \mathbf{B} \quad = \quad \frac{e^{*2}}{m^* \epsilon_0} |\Psi|^2 \mathbf{B} \,, \tag{1.95}$$

which is solved by a field which decays exponentially on the length scale

$$\lambda_{GL}^{-2} = \frac{e^{*2} |\Psi|^2}{\epsilon_0 m^*} \,. \tag{1.96}$$

This is obviously the London-limit (1.79) and identifying $|\Psi|^2 = n_s \Rightarrow \lambda_{GL} \equiv \lambda_L$. In fact the order parameter's independence from the weak magnetic field at lowest order has reintroduced the rigidity, that had been explicitly present in the London model and which will be somewhat softened if leading or higher orders in the field are taken into account.

1.5.3 Type I and II superconductivity

The relation of the two typical length scales, the skin depth and the coherence length, is called the Ginzburg-Landau-parameter

$$\kappa = \frac{\lambda_{GL}}{\xi} \,. \tag{1.97}$$

It can be shown [Lifshitz *et al.* 1984] that this parameter is connected to the surface energy of a superconductor. Table 1.8 compiles the typical scales of a few superconducting elements [Buckel 1977, Kittel 2002]. The Ginzburg-Landau parameter is often used to distinguish two classes of superconducting materials with distinct properties.

- *Type I-superconductors* $\kappa < \frac{1}{\sqrt{2}} \approx 0.7$ have a positive surface energy. No domains are created and the order parameter is basically homogeneous in the bulk. Hence the system is in the Meissner-state, which breaks down rapidly above the critical temperature. Type I superconductors are the ones well-described by London theory or the two fluid model and BCS theory.

- *Type II-superconductors* $\kappa > \frac{1}{\sqrt{2}}$ have a negative surface energy. This favors the creation of domains and vortex structures and the order parameter can show strong spatial dependences. Superconductivity does not break down as rapidly as in type I-materials in strong external fields but instead undergoes a transition to a mixed (Shubnikov) state, where the superconductor is penetrated by flux filaments and beautiful vortex-structures are created.

The possibility to deal with the effects arising from the spatial dependence of the order parameter and describe type II superconductors is one great advantages of GL theory. It is interesting to mention, that there is also a time dependent extension of GL theory (*TDGL* [Gorkov and Eliashberg 1968], cf. [Tinkham 2004]), which makes it possible to look at fields not constant in time. For example, in such a theory it should be possible to determine the way in which the equilibrium state is reached and find a dynamical description of the Meißner-Ochsenfeld effect.

Element	T_c/K	κ	$\lambda_L/\,\mathrm{nm}$
Al	1.2	0.03	16
Sn	3.7	0.1	34
Pb	7.2	0.4	37
Nb	9.5	0.8	39

Figure 1.8: *Characteristic physical scales of superconducting elements.*

An optical description in terms of reflectivities or dielectric functions starting from GL theory is quite tricky, because it requires the evaluation of nonlinear systems of equations. To my knowledge there is no established formalism in which optical response functions can be obtained for general time dependent external fields. Nevertheless it might be possible to find reflectivities and transmittivities in a scattering approach. This is a possible topic of future work.

In the following chapters the optical response of superconductors will be described in the framework of BCS theory and the two-fluid model, where reflectivities can be calculated more readily. Of course this limits the description to type-I superconductors and hence throughout the rest of this work superconductors are always assumed to be in the Meißner-state.

1.6 BCS theory

1.6.1 The BCS approach

Bardeen, Cooper and Schriefer [Bardeen *et al.* 1957] introduced a microscopic theory of superconductivity based on Cooper's theory of correlated electron pairs. Following a proposal by Fröhlich in 1950, Cooper had shown, that the Fermi-sea is not stable with respect to the formation of two-particle states of electrons if these interact attractively. The interaction stated by BCS was attributed to the interchange of virtual phonons. This was backed by the discovery of the isotope effect [Tinkham 2004]: For different isotopes of the same superconducting element, the critical quantities are connected to the mass of the lattice atoms, which is a clear signature of the relevance of lattice vibrations:

$$T_c, H_c \sim M^{-1/2} \, .$$

Due to the Pauli principle, the only excitable electrons are those close to the Fermi surface, and the conservation of the total momentum leads to the highest probability for a correlation of electron pairs of opposite spin and momentum.

The BCS-Hamiltonian [Jones and March 1973, Nolting 1990, Ketterson and Song 1999, Tinkham 2004, Dressel and Grüner 2002, Henkel 2007] has therefore an attractive two-particle interaction term, where the coupling constant is set constant over a range close to E_F and the interaction acts only between momentum and spin states $|\mathbf{k}, +\rangle$ and $|-\mathbf{k}, -\rangle$

$$H = \sum_{\mathbf{k},\sigma} \frac{\hbar^2 \mathbf{k}^2}{2m} a^\dagger_{\mathbf{k},\sigma} a_{\mathbf{k},\sigma} - \frac{g}{V} \sum_{\mathbf{k},\mathbf{k}'} a^\dagger_{\mathbf{k}',+} a^\dagger_{-\mathbf{k}',-} \, a_{-\mathbf{k},-} a_{\mathbf{k},+} \tag{1.98}$$

In the grand canonical description the chemical potential can be fixed by a constant mean number of one particle-states $N = \sum_{\mathbf{k},\sigma} a^\dagger_{\mathbf{k},\sigma} a_{\mathbf{k},\sigma} \stackrel{!}{=} \bar{N}$ which is done by adding a Lagrange multiplier $-\mu N$. This is of course equivalent to introducing new variables which measure the energy from the Fermi level

$$\frac{\hbar^2 \mathbf{k}^2}{2m} \to \eta_{\mathbf{k}} = \frac{\hbar^2 \mathbf{k}^2}{2m} - \mu \approx \frac{\hbar^2 k_F}{m} \cdot (k - k_F) \, .$$

The last approximation holds close to the Fermi edge $\mu \approx E_F$ and assuming a spherical Fermi surface.

Now the Hamiltonian may be diagonalized through a canonical *Bogoliubov transformation*[7]. Creation and annihilation operators $a^\dagger_{\mathbf{k},\sigma}, a_{\mathbf{k},\sigma}$ are replaced by linear combinations

$$b_{\mathbf{k},-} = u_{\mathbf{k}} a_{\mathbf{k},-} + v_{\mathbf{k}} a^\dagger_{-\mathbf{k},+} \tag{1.99}$$

$$b_{\mathbf{k},+} = u_{\mathbf{k}} a_{\mathbf{k},+} - v_{\mathbf{k}} a^\dagger_{-\mathbf{k},-} \tag{1.100}$$

where the coherence factors

$$u^2_{\mathbf{k}} + v^2_{\mathbf{k}} = 1 \tag{1.101}$$

describe the probability of a pair state being occupied or not. The field operators fulfill fermionic anti-commutation rules

$$\left[b_{\mathbf{k},\sigma}, b^\dagger_{\mathbf{k}',\sigma'} \right]_+ = \delta_{\mathbf{k},\mathbf{k}'} \delta_{\sigma,\sigma'} \, . \tag{1.102}$$

The energy of the system in terms of the quasiparticle excitation number

$$n_{\mathbf{k},\sigma} = b^\dagger_{\mathbf{k},\sigma} b_{\mathbf{k},\sigma} = 1 - b_{\mathbf{k},\sigma} b^\dagger_{\mathbf{k},\sigma}$$

[7] This transformation has been proposed independently by Valentin and Bogoliubov. A first attempt at the pairing hypothesis by Cooper used the easiest of choice of two-particle-states

$$c^\dagger_{\mathbf{k}} = a^\dagger_{\mathbf{k},+} a^\dagger_{-\mathbf{k},-}, \qquad c_k = a_{-\mathbf{k},-} a_{\mathbf{k},+} \, .$$

The Fermi ground state cannot be expressed exactly through these operators that produce two-particle states, but it can be approximated by $\sum_{\mathbf{k},\sigma} \frac{\hbar^2 \mathbf{k}^2}{2m} a^\dagger_{\mathbf{k},\sigma} a_{\mathbf{k},\sigma} \to \sum_{\mathbf{k}} 2 \frac{\hbar^2 \mathbf{k}^2}{2m} c^\dagger_{\mathbf{k}} c_{\mathbf{k}}$ [Schrieffer 1999, Nolting 1990]. The particles created by the new operators are not physical (i.e. eigenstates under permutation), because they conform neither to bosonic nor fermionic commutation relation, but

$$[c_{\mathbf{k}}, c^\dagger_{\mathbf{k}'}] = \delta_{\mathbf{k},\mathbf{k}'} \left(1 - (a^\dagger_{\mathbf{k},+} a_{\mathbf{k},+} + a^\dagger_{-\mathbf{k},-} a_{-\mathbf{k},-}) \right), \qquad [c_{\mathbf{k}}, c_{\mathbf{k}'}] = [c^\dagger_{\mathbf{k}}, c^\dagger \mathbf{k}'] = 0 \, .$$

Nevertheless, the resulting spectrum and predictions are rather good.

reads

$$E = 2\sum_{\mathbf{k}} \eta_{\mathbf{k}} v_{\mathbf{k}}^2 + \sum_{\mathbf{k}} \eta_{\mathbf{k}} (u_{\mathbf{k}}^2 - v_{\mathbf{k}}^2)(n_{\mathbf{k},+} + n_{\mathbf{k},-}) - \underbrace{\frac{g}{V}\left(\sum_{\mathbf{k}} v_{\mathbf{k}} u_{\mathbf{k}} (1 - n_{\mathbf{k},+} + n_{\mathbf{k},-})\right)^2}_{=:\Delta^2} . \tag{1.103}$$

Variation of the energy with respect to $u_{\mathbf{k}}$, gives

$$2\eta_{\mathbf{k}} u_{\mathbf{k}} v_{\mathbf{k}} = \Delta(u_{\mathbf{k}}^2 - v_{\mathbf{k}}^2) \tag{1.104}$$

and using (1.101)

$$u_{\mathbf{k}}^2 = \frac{1}{2}\left(1 + \frac{\eta_{\mathbf{k}}}{\sqrt{\Delta^2 - \eta_{\mathbf{k}}}}\right), \qquad v_{\mathbf{k}}^2 = \frac{1}{2}\left(1 - \frac{\eta_{\mathbf{k}}}{\sqrt{\Delta^2 - \eta_{\mathbf{k}}}}\right) . \tag{1.105}$$

Thus the Hamiltonian is diagonalized, and its excitation spectrum can be obtained performing the variation of energy with respect to the quasiparticle number $n_{\mathbf{k}}$. Putting in the original expression for the canonical momentum, the spectrum is then given by

$$E(\mathbf{p}) = \sqrt{\Delta^2(T) + \left(\frac{\mathbf{p}^2}{2m} - \mu\right)^2} . \tag{1.106}$$

It features a ground state separated from the excitations by $\Delta(T)$. This gap - similar to the effects in Bose-Einstein condensates - is responsible for the special properties of the superconducting state. In order to break up a Cooper pair and create free conducting electrons, an energy of 2Δ must be provided.

If the expressions for $u_{\mathbf{k}}, v_{\mathbf{k}}$ and $E(\hbar\mathbf{k})$ are plugged into (1.103), one obtains an implicit equation for the temperature-dependent value of the gap (the so-called gap function). The resulting expression is known as a *self-consistency condition* and can be solved, assuming a fixed average number of quasi-particles. Following [Thouless 1960, Ashcroft and Mermin 1987, Jones and March 1973] this condition and its asymptotics can be written as follows

$$\frac{\Delta(T)}{\Delta(0)} = \tanh\left(\frac{T_c}{T}\frac{\Delta(T)}{\Delta(0)}\right) \tag{1.107}$$

$$\rightarrow \quad 1.74\sqrt{1 - \frac{T}{T_c}} \qquad \text{as } T \rightarrow T_c\,. \tag{1.108}$$

The normalized gap function $\Delta(T)/\Delta(0)$ is universal and agrees exquisitely with experimental data [Townsend and Sutton 1962].

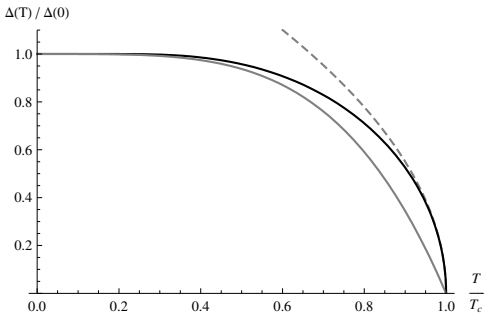

Figure 1.9: $\Delta(T)$ *Temperature dependence of the BCS gap* $\Delta(T)$ *(black) and its asymptote near* T_c *(dashed). The Gorter-Casimir parameter* $\eta(T)$ *(gray solid line) is shown for comparison.*

The numerical solution of the implicit equation (1.107) is shown in fig. 1.9 together with the Gorter-Casimir relation (1.84) which is the equivalent quantity in the two fluid model. The two quantities show good agreement only at low T.

1.6.2 Mattis-Bardeen theory

The macroscopic approach

The calculation of surface interactions in the following chapters requires knowledge of the optical response functions. In the framework of BCS theory the fundamental quantity is usually the optical conductivity. A first calculation valid at $T = 0$ was given already in the original paper by Bardeen, Cooper and Schrieffer [Bardeen *et al.* 1957]. An interesting result was, that the BCS conductivity calculated in the limit $T \rightarrow 0, \omega \rightarrow 0$ takes the form of the causal plasma model (1.26), including the $\delta-$peak at zero frequency [Berlinsky *et al.* 1993].

Shortly after, a generalization to finite temperature was given by Mattis and Bardeen (MB) [Mattis and Bardeen 1958] which agreed splendidly with Glover's und Tinkham's experimental data [Glover and Tinkham 1957]. Today,the optical description of BCS superconductors is commonly called *Mattis-Bardeen theory*. A general introduction may be found in [Schrieffer 1999] or [Dressel and Grüner 2002].

Mattis and Bardeen considered only what they called the *extremely anomalous limit* of a *dirty superconductor*, where the interaction between the external field and the response of the superconductor can be assumed totally local. More general expressions outside the extremely anomalous limit have been given by Zimmermann, Berlinsky and co-workers [Zimmermann *et al.* 1991,Berlinsky *et al.* 1993], but the interaction is still considered local. Closed analytical evaluations for the MB integral kernel including nonlocal effects where derived in [Pöpel 1989].

The fundamental equations in the original paper by Mattis and Bardeen are obtained from first order perturbation theory in the external field and lead a nonlocal formula for the current-field-relation

$$\mathbf{j}(\mathbf{r},\omega) = \frac{3\sigma_0}{(2\pi)^2 l}\int d\mathbf{R}\frac{\mathbf{R}(\mathbf{R}\cdot\mathbf{A}(\mathbf{r}+\mathbf{R}))}{R^4} I(\omega,R,T)\exp(-R/l) \tag{1.109}$$

$$I(\omega,R,T) = \int d\varepsilon \int d\varepsilon' \left[L(\omega,\varepsilon,\varepsilon') - \frac{f(\varepsilon)-f(\varepsilon')}{\varepsilon'-\varepsilon}\right]\cos\left(\frac{R}{\hbar v_F}(\varepsilon-\varepsilon')\right) \tag{1.110}$$

$$L(\omega,\varepsilon,\varepsilon') = -\frac{1}{2E}(1-2f(E))\left[\frac{E^2+E\hbar\omega+\Delta^2+\varepsilon\varepsilon'}{E'^2-(E+\hbar\omega)^2} + \frac{E^2-E\hbar\omega+\Delta^2+\varepsilon\varepsilon'}{E'^2-(E-\hbar\omega)^2}\right] \tag{1.111}$$

$$E = \sqrt{\varepsilon^2+\Delta^2} > 0\,, \tag{1.112}$$

where f is Fermi's function with energies measured from the Fermi energy, N_F is the density of states at the Fermi edge and $\Delta = \Delta(T)$ is the temperature dependent BCS gap. A finite value of the mean free path $l \approx v_F\tau$ is generally included in this description.

The response functions at the end of this calculation should describe macroscopic electrodynamics. This is consistent with the assumption that $\mathbf{A}$ vary slowly compared to the mean free path l. In this local limit the vector potential can be taken out of the integral. At a flat interface the tensor is diagonalized by TE and TM polarization vectors. No mixing occurs between the components of the vector potential, so that it can be taken out of the integral and the angular integral can be performed

$$\mathbf{j}(\mathbf{r},\omega) = \frac{e^2 N_F v_F}{2\pi^2\hbar}\frac{4\pi}{3}\mathbf{A}(\mathbf{r})\int_0^\infty dR I(\omega,R,T)\exp(-R/l) \tag{1.113}$$

In the frequency-representation, $\mathbf{A} = \mathbf{E}/i\omega$, so that the scalar complex conductivity be read off directly.

Following Mattis-Bardeen, the ε'-integral can be performed by contour-integration introducing a cut-off function, which allows to neglect the second term in (1.110), that does not depend on Δ. The integration path is determined by the representation of the cosine as a sum of two exponentials. In order to ensure causality, it is necessary to introduce a small shift from the real axis and to define the square roots appearing in the poles with a positive imaginary part and

$$\varepsilon = \sqrt{E^2-\Delta^2}, \qquad \varepsilon_\pm = \sqrt{(E\pm\hbar(\omega-i0))^2-\Delta^2}\,. \tag{1.114}$$

It is then sufficient to consider the first term in L, as the second may be obtained from the first one by substituting $\omega \to -\omega$ and complex conjugation, so that

$$L(\omega,\varepsilon,\varepsilon') = -\frac{1}{2E}(1-2f(E))\left[\frac{E^2+E\hbar\omega+\Delta^2+\varepsilon\varepsilon'}{(\varepsilon'-\varepsilon_+)(\varepsilon'+\varepsilon_+)} + (\omega\to-\omega)^*\right] \tag{1.115}$$

Note that in this form, L contains terms that are odd under the exchange $\varepsilon \leftrightarrow \varepsilon'$ and should vanish during the integration. Using the residue theorem for the ε'-integral and performing the substitution $\varepsilon \to E$ (and in a further

step $E \to E - \hbar\omega$ respectively), one obtains Mattis' and Bardeen's result

$$\begin{aligned} I(\omega,R,T) &= -\frac{i\pi}{2}\int_{\Delta}^{\infty} dE\,[1-2f(E)]\Big[(1-g_+)e^{-i\alpha(\varepsilon+\varepsilon_+)} - (1+g_+)e^{i\alpha(\varepsilon-\varepsilon_+)} \\ &\quad + (1+g_-)e^{i\alpha(\varepsilon+\varepsilon_-)} - (1-g_-)e^{-i\alpha(\varepsilon-\varepsilon_-)}\Big] \qquad (1.116) \\ &= -i\pi\int_{\Delta-\hbar\omega}^{\infty} dE\,[1-2f(E+\hbar\omega)]\,[g(E)\cos(\alpha\varepsilon_+) - i\sin(\alpha\varepsilon_+)]\exp(i\alpha\varepsilon) \\ &\quad + i\pi\int_{\Delta}^{\infty} dE\,[1-2f(E)]\,[g(E)\cos(\alpha\varepsilon) + i\sin(\alpha\varepsilon)]\exp(-i\alpha\varepsilon_+) \qquad (1.117) \\ g_+ &= g(E) = \frac{E^2+\Delta^2+\hbar\omega E}{\varepsilon\,\varepsilon_+}, \qquad g_- = \frac{E^2+\Delta^2-\hbar\omega E}{\varepsilon\,\varepsilon_-}\,, \end{aligned}$$

where $\alpha = R/\hbar v_F$.

It should be stressed that up to this point only the approximation of macroscopic (local) electrodynamics has been used. No assumptions whatsoever have been made as for the relaxation-processes.

The extremely anomalous limit

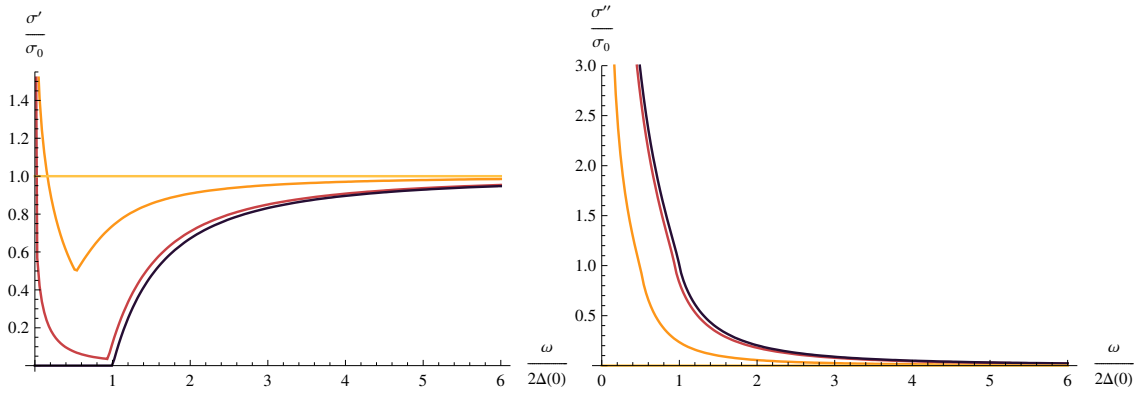

Figure 1.10: *Real and imaginary part (left, right) of the Mattis-Bardeen BCS conductivityat $T/T_c \in \{0.1, 0.5, 0.9, 1.1\}$ (black - yellow).* .

In their fundamental paper, Mattis and Bardeen considered the *extremely anomalous limit*, where the free path $l = v_F\gamma = v_F/\tau$ is much smaller than the range of correlation of electrons $\xi \approx \hbar v_F/\pi\Delta$ [Bardeen *et al.* 1957] connected to the energy gap Δ. Thus, it is the limit $\hbar\gamma \gg \Delta$ of an extremely *dirty superconductor*, where the interaction can be considered local and so that only values of $R \approx 0$ contribute.

Let us consider for a moment the extremely anomalous limit in a normal metal ($\Delta = 0$) at low frequencies $\omega \approx 0$. In this case, the integral kernel $I(\omega, 0, T) = -i\pi\hbar\omega$ [Mattis and Bardeen 1958], so that equations (1.113, 1.109) coincide with Chambers' formula given in section 1.1.7. Hence, the extremely anomalous limit in a normal metal recovers the DC conductivity of a Drude metal σ_0.

This observation allows to express the conductivity of a superconductor generally in units of this value σ_0

$$\frac{\sigma}{\sigma_0} = \int \frac{dR}{l} e^{-R/l}\frac{I(\omega,R,T)}{-i\pi\hbar\omega}\,, \qquad (1.118)$$

even outside the local limit, where I depends on R.

Returning to that limit, all trigonometric functions in (1.118) become trivial. In order to separate the real and imaginary part of the conductivity, the frequency-shifted part of the integral integral is cut into pieces

$$\int_{\Delta-\hbar\omega}^{\infty} = \int_{\Delta-\hbar\omega}^{-\Delta} + \int_{-\Delta}^{\Delta} + \int_{\Delta}^{\infty}\,. \qquad (1.119)$$

To get the real and imaginary part right, one must keep in mind that the root ε becomes imaginary in the interval $-\Delta < E < \Delta$, while ε_+ is real-valued over all the range considered. The integral over $[-\Delta, \Delta - \hbar\omega]$ can give a contribution depending on the values of Δ and ω

- If $\hbar\omega > 2\Delta$, the interval $E \in [\Delta - \hbar\omega, -\Delta]$ gives a real contribution that sets in at lower frequencies as the gap closes (fig. 1.10). This contribution is due to *direct absorption*, i.e. the breaking up of Cooper-pairs that cannot occur at lower energies. Of course, as real and imaginary part are connected through causality, the direct absorption edge has an effect on the imaginary part, too.
- If $\hbar\omega < 2\Delta$ no direct absorption takes place, and only the interval $E \in [\Delta - \hbar\omega, \Delta]$ gives an imaginary contribution.

The cancellation of some parts of the integrals can be expressed most elegantly, yielding the result of Mattis and Bardeen

$$\begin{aligned} \frac{\sigma'}{\sigma_0} &= \frac{2}{\hbar\omega}\int_{\Delta}^{\infty}\left[f(E) - f(E+\hbar\omega)\right] g(E) dE \qquad (1.120) \\ &\quad + \theta(\omega - 2\Delta)\frac{1}{\hbar\omega}\int_{\Delta-\hbar\omega}^{-\Delta}\left[1 - 2f(E+\hbar\omega)\right] g(E) dE \\ \frac{\sigma''}{\sigma_0} &= -\frac{1}{\hbar\omega}\int_{\max\{\Delta-\hbar\omega,-\Delta\}}^{\Delta}\left[1 - 2f(E+\hbar\omega)\right]\left(-ig(E)\right) dE\,. \qquad (1.121) \end{aligned}$$

The real and imaginary parts of the MB conductivity at different temperatures is shown in figure 1.10. Note that at $T > T_c$ the conductivity is entirely real and coincides with the static Drude-value without any further frequency dependence. This is due to the extremely *dirty limit* under consideration. At $\gamma = 1/\tau \gg \omega$ the Drude model is completely dominated by its static value. For this reason MB theory must not be applied at frequencies in the order of the relaxation rate, which is still present in σ_0.

This limitation is a big disadvantage for the calculation of surface interactions to which the next chapters are dedicated. Here, the optical response functions must hold over a wide range of frequencies. For this reason, the original MB-theory cannot be used and a more general description is desirable.

Zimmermann's formulae

Zimmermann and shortly afterwards Berlinsky *et al.* were the first to consider a general rate of relaxation $\gamma = 1/\tau = v_F/l$ [Zimmermann *et al.* 1991, Berlinsky *et al.* 1993] (and references therein). The basic observation is that outside the extremely anomalous limit, if the integral over $R \neq 0$ is not neglected but performed explicitly, it yields a Lorentzian. Taking just the parts of (1.109) depending on R, the relevant expression is

$$\int_0^{\infty} dR \exp(-R/l)\cos\left(\frac{R}{\hbar v_F}(\varepsilon' - \varepsilon)\right) = \frac{\hbar^2 v_F/\tau}{\hbar^2/\tau^2 + (\varepsilon' - \varepsilon)^2}\,. \qquad (1.122)$$

The complete complex conductivity is therefore given by

$$\frac{\sigma(\omega)}{\sigma_0} = \frac{\hbar}{-i\pi\omega\tau^2}\int_{-\infty}^{\infty} d\varepsilon \int_{-\infty}^{\infty} d\varepsilon' \left[L - \frac{f(\varepsilon) - f(\varepsilon')}{\varepsilon' - \varepsilon}\right] \frac{1}{\hbar^2/\tau^2 + (\varepsilon' - \varepsilon)^2} \qquad (1.123)$$

The contour integration and separation in real and imaginary parts have been performed in the above papers. MB's extremely anomalous limit is recovered in the regime, where $(\varepsilon' - \varepsilon) \ll \gamma \to \infty$, so that

$$\frac{1}{\tau^2}\frac{1}{(\varepsilon \pm \varepsilon')^2 + \hbar^2/\tau^2} \approx \frac{1}{\hbar^2}. \qquad (1.124)$$

Fig. 1.11 and 1.12 show the real and imaginary part of this modified BCS conductivity vs. temperature. Above the transition temperature $T > T_c$ there is no gap, and the material becomes normal-conducting and shows just the Drude model's behavior at the same value of γ, as is shown in fig. 1.11. At lower temperature the response of the superconductor agrees still nicely with the Drude mode at frequencies well above the gap $\omega \gg \Delta(T)$. As in the previous scenario, direct absorption sets in at $\hbar\omega > 2\Delta(0)$.

The temperature dependence of the dissipation rate has been discussed earlier in section 1.1.6. After what has been said there, it seems reasonable to use a constant value of γ because at the relevant temperatures $T \approx T_c$ the vibrational excitations of the lattice are frozen out and the dissipation is dominated by impurities.

Fig. 1.13 shows the conductivity vs. temperature at a constant frequency as compared to the two fluid model. Evidently, above the critical temperature both models take on the temperature independent Drude behavior. A characteristic feature is the so-called coherence peak in the real part, just below the transition temperature. Since the quantum mechanical current density is not identical to the classical particle density, there can be interferences which lead exactly to the peaks under consideration.

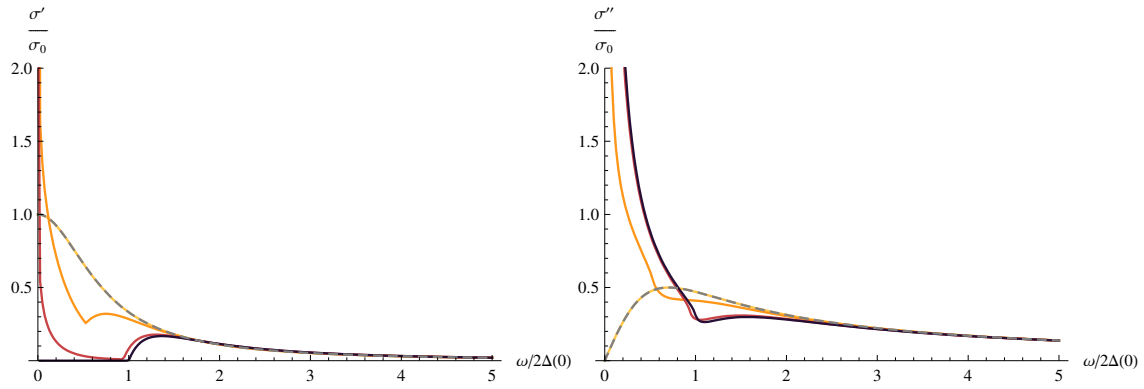

Figure 1.11: *Real and imaginary part (left, right) of the Zimmermann conductivity where* $\gamma = 5 \cdot 10^{-4}\omega_p$ *at* $T/T_c \in \{0.1, 0.5, 0.9, 1.1\}$ *(black - yellow) and the Drude model (dashed). The static Drude conductivity is* $\sigma_0 = \frac{\omega_p^2 \epsilon_0}{\gamma}$.

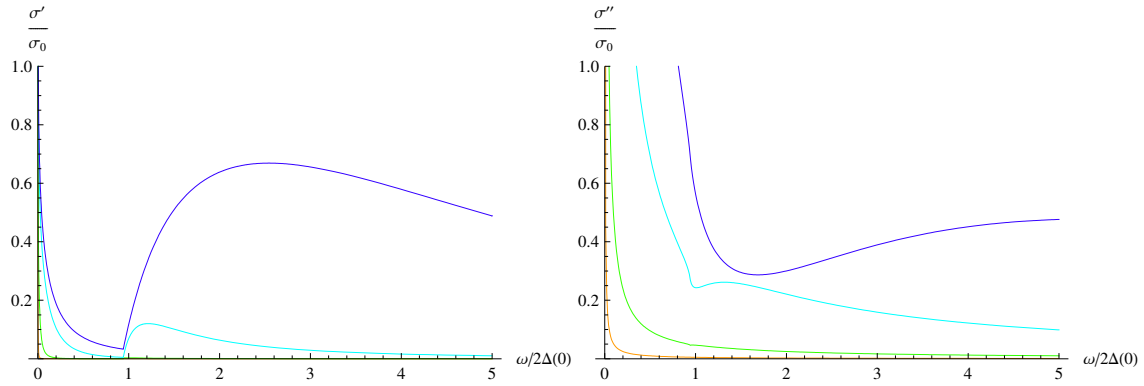

Figure 1.12: *Real and imaginary part of the Zimmerman conductivity at* $T = 0.5T_c, \hbar\gamma/\Delta(0) \in \{0.01, 0.1, 1.0, 10\}$ *(yellow - blue).*

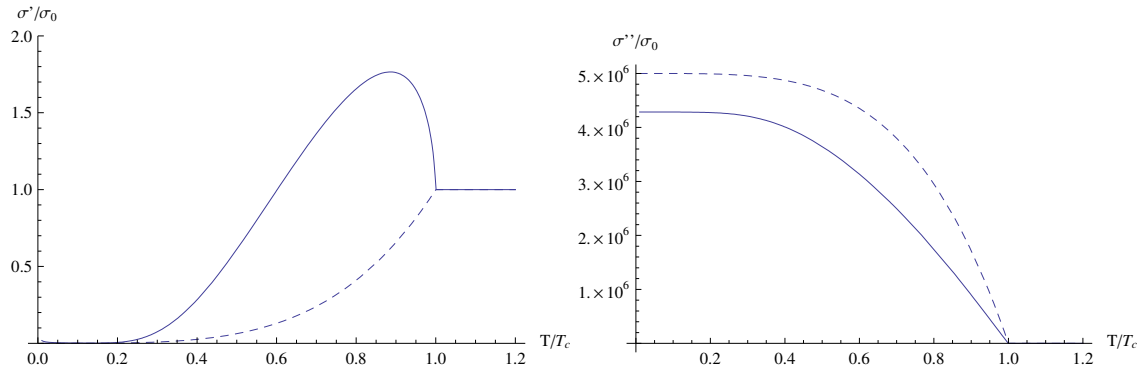

Figure 1.13: *BCS conductivity vs temperature (solid) at* $\omega = 10^{-10}\omega_p, \gamma = 5 \cdot 10^{-4}$ *and the two fluid model (dashed).*

1.6.3 Continuation to imaginary frequencies

To our knowledge of the existing literature, analytical calculations in the framework of Mattis-Bardeen theory have always used real frequencies. Yet, for the application in the Casimir effect, it is desirable to have access to the optical response functions at imaginary frequencies. It is in principle possible, to do an analytical continuation of Mattis-Bardeen theory using the Kramers-Kronig relations. Unfortunately the result is quite ineffective numerically and is therefore useless for practical applications. Nevertheless can they be used to check the consistency of the results obtained analytically.

In the following sections, an original analytical calculation is presented and that leads to expressions for the conductivity at imaginary frequencies both inside and outside the extremely anomalous limit. The results are then compared to the ones obtained with the help of Kramers-Kronig relations.

Continuation in the extremely anomalous limit

An elegant expression for the conductivity at imaginary frequencies can be obtained, if the substitution $\omega = -i\xi$ is done in the unshifted expression[8] (1.110) in the MB-limit $\alpha = 0$ and replacing the quantities $g\pm, \epsilon_\pm, I$ by their complex counterparts $\tilde{g}, \tilde{\epsilon}_\pm, \tilde{I}$ denoted by a tilde

$$g_\mp \to \tilde{g}_\pm := \frac{E^2 \pm i\hbar\xi E + \Delta^2}{\varepsilon\tilde{\varepsilon}_\pm}, \qquad \varepsilon_\mp \to \tilde{\varepsilon}_\pm = \sqrt{(E + i\hbar\xi)^2 - \Delta^2}\,, (\text{ Im } > 0)$$

The conductivity along the positive imaginary axis is then given by

$$\frac{\sigma}{\sigma_0} = \frac{\tilde{I}}{\pi\hbar\xi}\,. \tag{1.125}$$

Here, one must pay attention to the convergence of the integral. Without the cut-off function, there is a contribution in I that does not depend on the gap function Δ. If plugged into σ, this term is generally needed to reproduce the Drude-model at $T > T_c$. The proof is quite involved is not given here in detail [Haakh *et al.* 2009].

In the extremely anomalous limit, the contribution from the Drude term must be replaced by the asymptotic value, which is its static value σ_0. The conductivity can then be written down in terms of these quantities and reads

$$\begin{aligned}\frac{\sigma(i\xi)}{\sigma_0} &= 1 + \frac{i}{2\hbar\xi}\int_\Delta^\infty dE[1 - 2f(E)]\,(2\tilde{g}_- - 2\tilde{g}_+) \\ &= 1 - \frac{2}{\hbar\xi}\int_\Delta^\infty dE[1 - 2f(E)]\ \text{Im}\ (\tilde{g}_+)\ ,\end{aligned} \tag{1.126}$$

where $\tilde{g}_- = \tilde{g}_+^*$ was used.

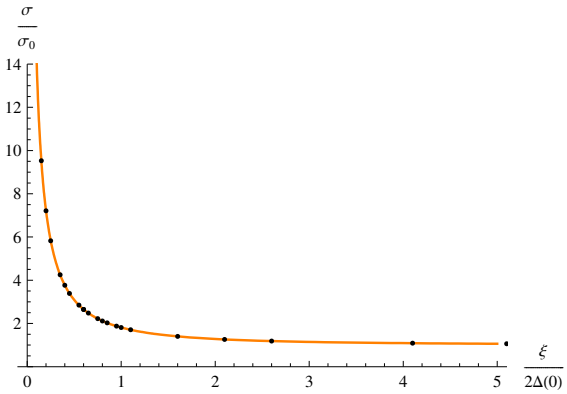

Figure 1.14: *Evaluation of the analytic continuation (line) and the KK results (dots).*

This expression is sufficiently well-behaved to be calculated numerically and shows a good agreement with the values that have been obtained by Kramers-Kronig analysis from the conductivity at real frequencies (fig. 1.14).

[8] No direct continuation can be performed from any form of Mattis' and Bardeens' expressions, where the frequency appears in the integral boundaries of the integral equations because the integration contour would be badly defined after a direct complexification. Note also, that the convention for the sign of ω in the Fourier transformation differs from the one applied previously.

Continuation of Zimmermann's formulae

The analytical continuation outside the extremely anomalous limit is a bit more involved. Starting from (1.123), the complexification is done by replacing $\omega \to -i\xi$. At imaginary frequencies, the function $L(i\xi, \varepsilon, \varepsilon')$ can be written as

$$L(\omega, \varepsilon, \varepsilon') = -\frac{1}{2E}[1 - 2f(E)] \text{ Re } \left[\frac{E^2 + E\hbar i\xi + \Delta^2 + \varepsilon\varepsilon'}{\varepsilon'^2 - \tilde{\varepsilon}_+^2}\right] \tag{1.127}$$

In a second step, the ε' integral is performed by closing the integration contour the upper half-plane. As before, there is a pole $\epsilon' = \tilde{\epsilon}_+$ and the dissipation kernel adds another one at $\epsilon' = \epsilon + i\hbar/\tau$. The residue theorem can be applied and gives the result [Haakh *et al.* 2009]

$$\begin{aligned} \sigma(i\xi) &= \sigma_{Dr}(i\xi) + \frac{\sigma_0}{\xi\tau} 2 \text{ Im } \int_\Delta^\infty dE\,[1 - 2f(E)] \times \\ &\times \left[(\tilde{g}_+ + 1)\frac{\hbar/\tau}{(\tilde{\varepsilon}_+ - \varepsilon)^2 + \hbar^2/\tau^2} - i\frac{E^2 + i\hbar\xi E + \Delta^2 + \varepsilon(\varepsilon + i\hbar/\tau)}{\varepsilon(\varepsilon^2 - \tilde{\varepsilon}_+^2)}\right] . \end{aligned} \tag{1.128}$$

The extremely anomalous limit should be recovered as $\tau \to 0 \Leftrightarrow \gamma \to \infty$. In this regime, the Drude conductivity is then dominated by its static value $\sigma_{Dr}(\omega) \to \sigma_0$ and the term in brackets can be expanded in powers of τ

$$\frac{\tilde{g}_+\tau}{\hbar} + \mathcal{O}(\tau^2) , \tag{1.129}$$

which gives the expected result (1.126).

A consistency check of these results can be done as before by using the Kramers-Kronig relations. The analytical continuation can be done from both real and imaginary part of the conductivity on the real frequency axis but some care must been taken when using the real part because of the localized ($\delta(\omega)$-) contribution.

Bimonte *et al.* [Bimonte *et al.* 2005b] have proposed to evaluate the $\delta(\omega)-$ part by means of a sum rule. This means, that it is the difference between the Drude- and Zimmermann-dielectric function which is considered as the causal transform and then continued analytically by means of (1.68). The result can then be added to the continuation of the pure Drude model. Defining $\sigma_s'(\omega)$ as the real part of the superconducting conductivity without the localized part, the conductivity can be evaluated numerically without much trouble from

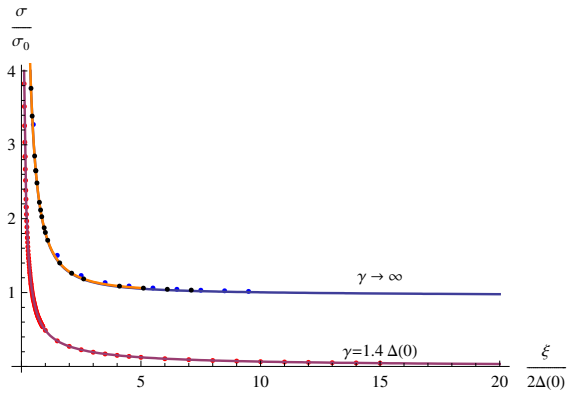

Figure 1.15: *Evaluation of the analytic continuations. Dots are obtained from KK-relations, lines show direct analytical continuations. Extremely anomalous limit (orange), $\gamma = \omega_p \approx 1400\Delta(0)/\hbar$ (blue) and $\gamma = 5 \cdot 10^{-4}\omega_p \approx 1.4\Delta(0)/\hbar$ (red).*

$$\sigma(i\xi) = \sigma_{Dr}(i\xi) - \frac{2}{\pi}\int_0^\infty d\omega \frac{\omega^2(\sigma_s'(\omega) - \sigma_{Dr}'(\omega))}{\xi^2 + \omega^2} , \tag{1.130}$$

Alternatively, a continuation can be done according to (1.67) from the imaginary part, where no distributional contribution occurs, and which works just as well.

The results obtained by KK-continuation and the ones from the above analytical formula coincide very well, as can be seen in fig. 1.15. The anomalous limit is recovered for high values of γ. Note that the analytical continuations give the correct Drude limit at high frequencies and coincide results in the extremely anomalous limit if $\gamma \gg \Delta(0)$.

1.7 Reflectivity

The reflectivity is the basic quantity used in later sections to calculate Casimir and Casimir-Polder interactions between objects. All physical effects in the matter enter the calculation through the optical reflectivity. Therefore it is very instructive to compare directly the reflectivities calculated in the different models.

The numerical evaluation of the TE and TM reflectivities at real frequencies from (1.16ff) for the different models are shown in figures 1.16 - 1.19. The next sections cover physical effects, such as high- or low-frequency transparency or the gap in BCS-superconductors, that show signatures in the reflectivity and which will have significant consequences in the Casimir effects, too.

1.7.1 The plasma edge

All materials become asymptotically transparent at very high frequencies in the order of the plasma-frequency $\omega \gg \omega_p$. Here, the charge carriers cannot follow an external field any more and the response becomes dominated by inertia,so that all models take the asymptotic behavior of the plasma model (cf. section 1.1.5, eq.(1.64)). In the calculation of the Casimir effect, which is due to the introduction of boundary conditions into a system, this property will become very important because it introduces a natural cutoff above which the boundary conditions become irrelevant.

Total reflexion occurs in the plasma model, where $k/c < \omega < \omega_p$ in both polarizations. In this regime, the transmitted fields are evanescent.

The surface plasmon resonance is a resonant collective excitation that occurs the zero of the dielectric function. It is responsible for the prominent peak in the TM reflectivity, where $|r^{TM}| > 1$. The fields are evanescent and do not carry energy, hence a increase of amplitude does not necessarily violate energy conservation. A thorough discussion of the plasmon-modes can be found in [Intravaia and Lambrecht 2005].

1.7.2 Screening by surface charges

In all electrical conductors surface charges can build up and screen very effectively low frequency TM modes, whose electrical fields are perpendicular to the surface. Since dissipation (next section) does not play a big role for the charges in a steady state situation, the TM reflectivity – unlike the TE one – is nearly identical in all models. The screening will work only at low frequencies, where the surface charges can keep up with the field and breaks down somewhere beyond the plasma edge, which gives the asymptotically transparent regime mentioned before.

Of course the screening must be present in Fresnel's equations (1.18), and in fact the low frequency limit in any of the models considered is

$$\lim_{\omega \to 0} r^{TM}(\omega) \quad = \quad 1 \,. \tag{1.131}$$

1.7.3 Dissipation

In the Drude model (section 1.1.5), dissipation is described within the *relaxation time approach*, where the timescale is defined by the Drude parameter $\gamma = 1/\tau$. Dissipation cannot change charge distributions but has an impact only on the velocity distribution of the charge carriers, i.e. the current. Since the TM modes are screened by surface charges (not currents, see previous section), dissipation is irrelevant once the charges are distributed at the surface, unless the field varies very rapidly.

In contrast, TE-modes of low frequency correspond to external magnetic fields that can generally penetrate into normal conductors, but are very sensitive to surface currents and hence to dissipation. Modes $\omega \ll \gamma$ that vary

Reflectivity of the plasma, Drude, two fluid and BCS model

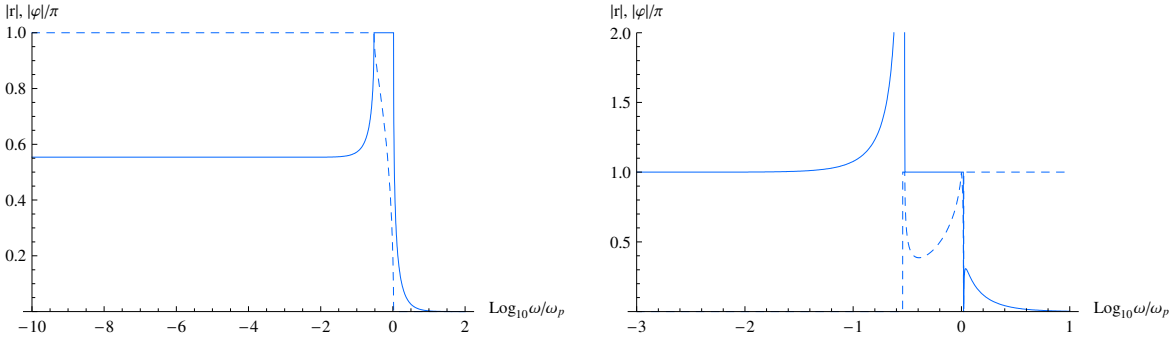

Figure 1.16: *$r = |r| \exp i\phi$ in the plasma model, tangential wave vector $k = 0.3\omega_p/c$. TE-polarization (left) and TM-polarization (right). Solid: Absolute value $|r|$. Dashed: Argument $|\phi|$.*

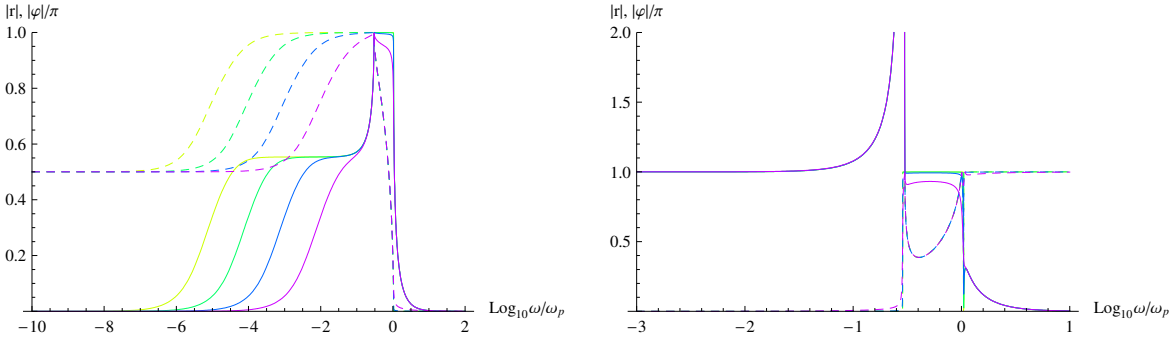

Figure 1.17: *Drude model, where $\gamma/\omega_p \in \{5 \cdot 10^{-5}, 5 \cdot 10^{-4}, 5 \cdot 10^{-3}, 5 \cdot 10^{-2}\}$ (yellow - purple).*

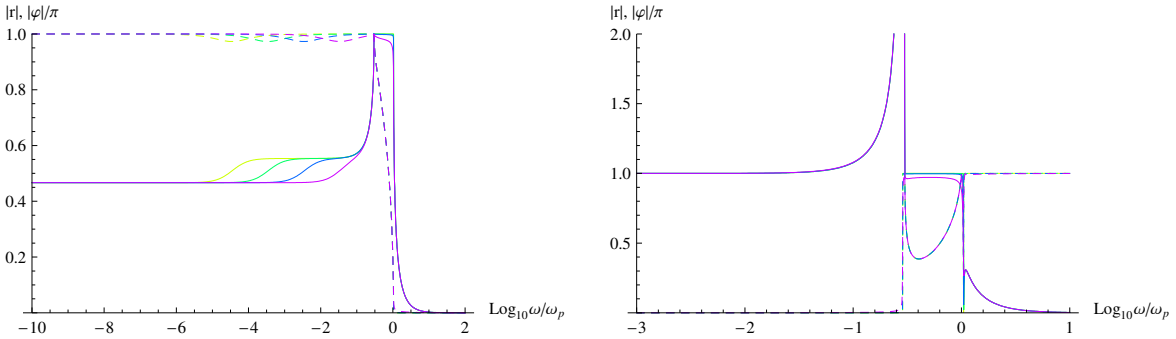

Figure 1.18: *Two fluid model with a Gorter-Casimir order parameter at $T = 0.8T_c$, same value γ.*

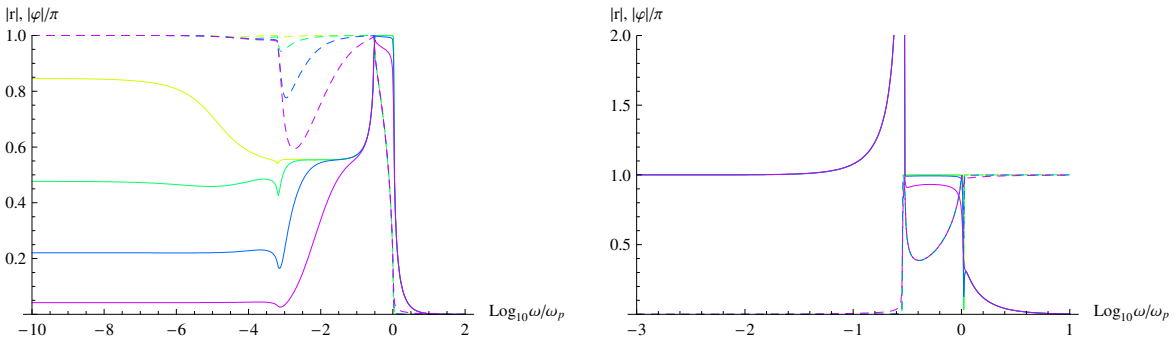

Figure 1.19: *BCS model at $T = 0.6T_c$, same value γ. BCS gap $\Delta(0) \approx 3.5 \cdot 10^{-4}\hbar\omega_p$.*

slower than this time fail completely to excite currents and the material becomes permeable, leading to a characteristic dissipation edge at $\omega \approx \gamma$ in the TE-reflectivity of all dissipative models.

$$\lim_{\omega\to 0} r^{TE}(\omega,\mathbf{k}) = \begin{cases} 0 & \gamma \neq 0 \\ \frac{k-\sqrt{\frac{\omega_p^2}{c^2}+k^2}}{k+\sqrt{\frac{\omega_p^2}{c^2}+k^2}} \approx 1 & \text{at small } k \quad \gamma \equiv 0 \text{ (plasma)} \end{cases} \tag{1.132}$$

The transparent regime at low frequencies can be understood as a consequence of the *Bohr-van-Leeuwen theorem*, that does not allow a diamagnetic response in a system described by classical physics in the absence of static magnetic moments [Soldati 2003]. Hence any material described by classical physics should become transparent to low frequency magnetic fields [Bimonte 2009]. This effect will become extremely important in the discussion of the thermal Casimir effect in section 2.2.2.

In general, high dissipation rates lead to a softening of all structures, especially the sharp plasma edge and the totally reflecting regime. Thus, the transparent regime for low frequency TE fields can also be seen as the smeared out distributional effect that will be shown to appear in the causal plasma model $\gamma = 0^+$ in section 1.8.1.

1.7.4 Superconductors

The optical properties of superconductors and normal conductors are expected to differ enormously, because the Meißner-Ochsenfeld effect in superconductors shields quasistatic magnetic fields from the bulk. Since the superconducting surface currents are not dissipated, they can play a very similar role for TE-modes as the charges do for TM-modes. Thus the expulsion of slowly varying magnetic fields from the bulk in the Meißner state translates directly to a finite value of the static TE-reflectivity $r^{TE}(0) > 0$ as holds indeed for the BCS theory (fig. 1.19), the two fluid model (1.18), and of course also for its low temperature limit given by the plasma model (London superconductor, fig. 1.16).

The TM reflectivity was shown to depend only on the surface charges but not on dissipation. A superconductor is still a metal, though in a very special state, and the surface charges can build up as in any other metal, so that the TM-reflectivities for superconductors and other models are very much alike.

The two parameters relevant in superconductors are the dissipation rate and the temperature. In the two fluid model the dissipation rate determines merely the frequency scale, where the transition between from a plasma- like to a Drude-like behavior sets in. The effects are much stronger in the case of the BCS model. Here, the TE-reflectivity at low frequencies depends strongly on the dissipation rate and the numerical results show, that in the *clean limit* $\hbar\gamma \ll \Delta \Rightarrow r^{TE}(0) \to 1$. The comparison of figures 1.19, 1.16 and 1.18 hints at a dependence of the effective plasma frequency on the relaxation rate. Values $r^{TE}_{BCS}(0) > r^{TE}_{Pl}(0)$ can be obtained formally by using higher values of the plasma frequency and are a consequence of of the coherence effects not covered in the classical model.

Interestingly the BCS model coincides pretty closely with the two fluid model if $\hbar\gamma \gtrapprox 2\Delta(T)$. Here, even the temperature dependence is quite consistent (fig. 1.20, 1.21). At the same time this is a quite realistic regime, since it accounts for $\gamma \approx 10^{-5}\omega_p$, which is about the value in a normal metal like gold at room temperature. The good agreement of the reflectivities at comparable values of the dissipation rate will lead to the astonishing coincidence of the predictions for the Casimir interaction obtained using the BCS and two fluid model section 2.4. The underlying effects and the impact of the coherence effects are an interesting topic for future research.

There is one more small feature TE-reflectivity of the BCS model. Here, a notch occurs at the inset of direct absorption at $\hbar\omega \approx 2\Delta(T)$. Above this frequency, the reflectivity converges quickly to the behavior in other models, which was expected from the previous results for the conductivity.

1.8 The δ-peak in superconductivity

1.8.1 The δ-peak from sum rules

Earlier in this work, it has been proposed to add a δ-peak to the plasma model by taking the limit $\gamma \to 0$ in the Drude model. The result was called the distributional plasma model (1.26) and turned out be a causal transform

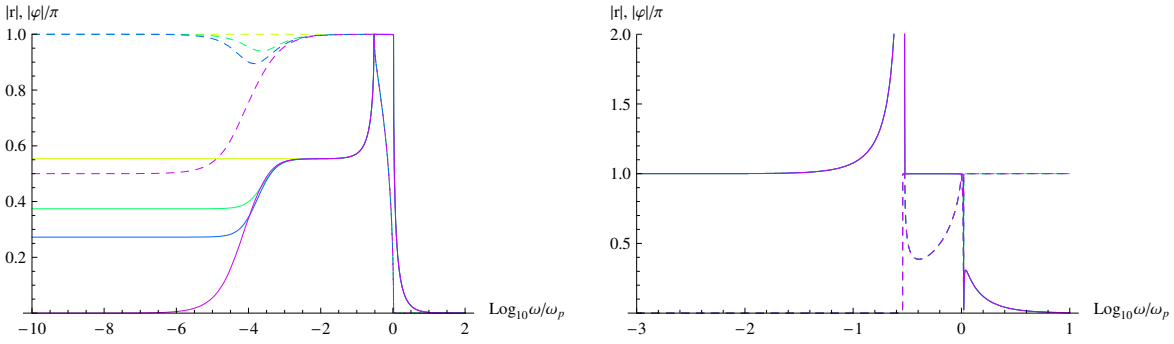

Figure 1.20: *Two fluid model, where* $\gamma = 5 \cdot 10^{-4}\omega_p$ *at* $T/T_c \in \{0.1, 0.9, 0.95, 1.2\}$ *(yellow-purple).*

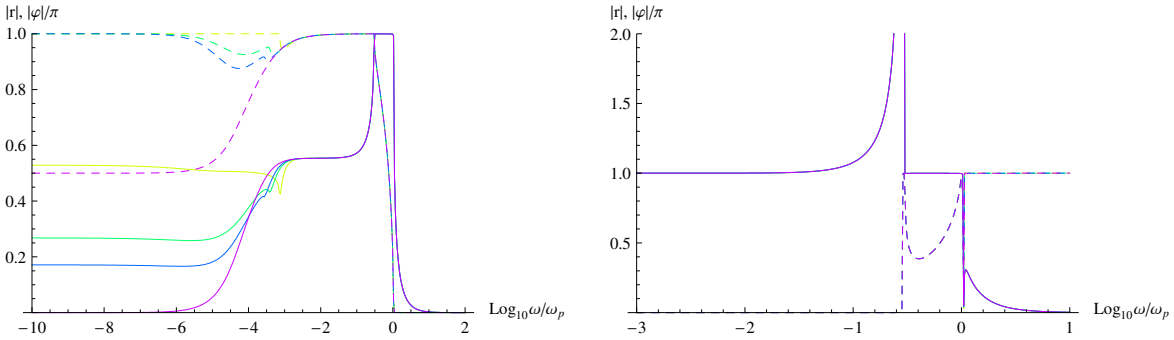

Figure 1.21: *BCS model, same values of* γ *and* T.

(sec. 1.2.4) while the "common" plasma model in the form (1.23) is not causal and does not fulfill the Kramers-Kronig relations [Ferrell and Glover 1958, Glover and Tinkham 1957, Dressel and Grüner 2002].

Another way of introducing the localized contribution uses the oscillator strength sum rule (1.66). The rule is valid for general conductivities and there is no reason, why the total spectral weight should not be conserved through the superconducting transition. At $T = 0$, the two fluid superconductor coincides with the plasma model and the conductivity is purely imaginary $\sigma = \sigma''$. Using the oscillator strength sum rule

$$\int_0^\infty \sigma_s'(\omega')d\omega' \quad = \quad \int_0^\infty \sigma_n'(\omega')d\omega' = \frac{\pi\epsilon_0\omega_p^2}{2}$$

Since, $\sigma'(\omega) \equiv 0$ at any finite frequency $\omega \in (0, \infty)$, any effect must take place at the lower boundary of the the integration domain. The spectral weight can be preserved, if a $\delta(\omega)$-contribution is introduced [Ferrell and Glover 1958, Glover and Tinkham 1957, Dressel and Grüner 2002]

$$\sigma_s' \quad = \quad \pi\epsilon_0\omega_p^2\delta(\omega). \tag{1.133}$$

The factor 2 is introduced to take into account the integration domain in (1.133).

At $T = 0$ *all* the spectral weight (or oscillator strength) is in the collective mode at $\omega = 0$ [Glover and Tinkham 1957, Berlinsky *et al.* 1993]. Generalizing this to temperatures $0 < T < T_c$, some spectral weight is given by the dissipation due to the normal current, and the relative spectral weight of the collective mode is just given by the order parameter $\eta(T)$.

1.8.2 BCS and two fluid model

The collective mode is closely connected to the existence of supercurrents, and it is natural to ask, whether a localized contribution occurs also in descriptions other than the two fluid models. The answer is yes, it does. The

plasma model is recovered in the limit of low temperature and small frequencies from the BCS theory [Bardeen *et al.* 1957, Berlinsky *et al.* 1993], and it was shown there, that a δ-distribution occurs. The optical effects found in the two-fluid model connected to this peak should therefore occur also in the other descriptions.

In the context of analogies between the models it may be interesting to mention, that notwithstanding the complex structure of BCS theory and the coherence effects, the BCS model can still be read in some way as a two fluid model, in the sense that a normal and a supercurrent coexist. A first attempt to interpret the gap-function as an order parameter of a two-fluid model was given Bardeen in [Bardeen 1958]. More recently, Berlinsky *et al* [Berlinsky *et al.* 1993] proposed a decomposition of the BCS conductivity with the goal of identifying the equivalents to the normal and superconducting contribution in the two fluid model. Basically, the direct absorption component accounts for the first one and the superfluid is given by the rest. The authors used the oscillator strength sum rule to obtain the spectral weight of the δ-contribution, which they considered as an extra contribution.

1.8.3 Reflectivity revisited

The introduction of a δ-peak to the plasma model changes not only the causal properties of the response but also the reflectivity. Earlier, the distributional plasma model was introduced as a limit of the Drude model, where $\gamma = 0^+$ is infinitesimal.

It was shown in section 1.7.2 that the low frequency TM reflectivity is determined by the surface charges, does not depend on the specific model and holds hence at all values of γ, including the distributional limit $\gamma = 0^+$.

Things are quite different in the case of TE-modes. The dissipation is highly relevant and it was shown in section 1.7.3 that in the Drude model $r^{TE}(\omega) \to 0$ for $\omega \ll \gamma$, while it remains finite for the "normal" plasma model. Now, in the distributional limit, the regime $\omega \in [0;\gamma]$ is compressed the single frequency $\omega \equiv 0$, and it becomes important, in which order the limits are performed:

$$\lim_{\gamma\to 0}\lim_{\omega\to 0} r^{TE}(\omega,\mathbf{k}) = 0 \tag{1.134}$$

$$\lim_{\omega\to 0}\lim_{\gamma\to 0} r^{TE}(\omega,\mathbf{k}) = \frac{k-\sqrt{\frac{\omega_p^2}{c^2}+k^2}}{k+\sqrt{\frac{\omega_p^2}{c^2}+k^2}} \approx 1 \qquad \text{at small } k\,. \tag{1.135}$$

This result and its physical interpretation are quite puzzling for two reasons:

- *The Meißner-Ochsenfeld effect*: Since the plasma model describes a superconductor at $T = 0$, there is an apparent contradiction with the requirement that static magnetic fields be expelled from the bulk, which is a well-established experimental fact for low-frequency fields.
- *Thermal Casimir effect*: In section 2.2.3 the effect of a vanishing $r^{TE}(0)$-reflectivity for the thermal Casimir effect will be discussed in detail. Limits like the above ones will be shown to have a significant effect on the Casimir forces at large distances and for the entropy at low temperatures. No such effects occur for the "normal" plasma model, but the problems encountered in other models could be reproduced, if the δ-peak is included in the description of the plasma.

The usual way of dealing with these difficulties is to just ignore the $\delta(\omega)$-contribution for *optical descriptions* but leave it in the model when looking at causality. Still, there is no final answer to the question yet. Meanwhile one can think of different arguments that point into this direction:

- *Dissipation at $\omega = 0$:* Tinkham and Glover [Glover and Tinkham 1957] argued that according to the fluctuation-dissipation theorem, a mode without any time-dependence cannot contribute to dissipation, which is furthermore proportional to the mode energy.
- *Definition of reflectivity for $\omega = 0$:* The concept of a reflectivity $r^{TE}(0) > 0$ for a static field is not a very well-defined quantity. One can think of the *extra field* created by the object in contrast to *externally applied fields*. This would connect the static TE reflectivity to the magnetization response. In any way, $r^{TE}(0)$ is certainly not directly accessible to any measurement in frequency space, since any finite experimental time scale limits the uncertainty of frequency measurements so that it is experimentally impossible to be sure a supposedly static field has really $\omega \equiv 0$. If the response at $\omega = 0$ has a measure in some integral, it should be *chosen* such that the resulting observable quantities are consistent with experiments or fundamental principles of physics.

- *Adiabatic and isothermal processes:* If not an adiabatic but an isothermal process is considered, the susceptibilities are slightly different. It is not improbable, that for the static fields under consideration the adiabatic approximation breaks down. More attention should therefore be paid to the influence of the specific thermodynamic process under consideration in order to understand the topic fully.

1.9 Conclusions

This chapter has given an introduction to the electrodynamical and optical properties of solids needed in the rest of this work, and some tools from the theory of distributions and complex analysis have been presented and applied to important models commonly used to describe metals and superconductors. Normal metals were described in terms of the Drude model, in which the dissipation can depend on impurity scattering or electron-phonon scattering.

The plasma model, which in the context of Casimir physics has often been used to describe metals, was shown to be the low-temperature limit of the two most prominent descriptions of superconductors: the two-fluid model and BCS theory. If was found that the usual form of the plasma model is not a causal response function. The introduction of a δ-peak at zero frequency is a remedy to this problem, but leads to a transparency of the superconductor for *exactly* static magnetic fields $\omega \equiv 0$ which is in contradiction with the Meißner-Ochsenfeld effect. A possible solution to this conundrum recovers the commonly used recipe to just neglect the localized contribution in the optical description.

The most important original result in this chapter was found in the framework of BCS theory. Here, it was shown how the expressions by Mattis-Bardeen and Berlinsky-Zimmermann for the optical conductivity valid at real frequencies can be analytically continued to purely imaginary frequencies. The results were found to coincide with results independently by G. Bimonte and were checked against numerical data obtained from Kramers-Kronig relations. This result is very valuable for the calculation of the Casimir effect.

A direct comparison of the reflectivities calculated in the different models has been done and shown that ability of all metals to build up surface charges leads to an almost dissipation-independent behavior of the TM-reflectivity, while the TE-reflectivity is determined mostly by surface currents and is therefore very sensitive to dissipative effects. The comparison between the two fluid model and BCS theory showed an overall good agreement, especially where the dissipation rate is comparable to the superconducting gap energy $\hbar\gamma \approx \Delta(0)$.

2 Casimir interaction

2.1 Casimir interaction

2.1.1 Vacuum interactions

The first chapter of this thesis has dealt the optical and electrodynamical properties of superconductors and metals. The descriptions and methods introduced there will be applied in this and the following chapter to calculate the vacuum interaction between metallic plates or a plate and an atom. What are those vacuum interactions?

It was J. D. van-der-Waals [Van der Waals 1873] who had the idea, that electrically neutral atoms or molecules in a gas interact attractively, which leads to the deviation from the ideal gas law. His explanation depicted the interaction of fluctuation-induced dipoles with their mirror-charges. A first quantitative calculation was done by F. London [London 1930].

In 1948, Casimir and Polder calculated a QED description of the interaction between two atoms and the effects of retardation [Casimir and Polder 1948, Casimir 1948]. What they found more or less by the way, was that not only atoms attract, but that attractive forces occur between perfectly reflecting plates, too. In this special scenario, no properties of the matter were introduced in the description, and so the interpretation was, that the zero-point-energy of the electromagnetic vacuum is sensitive to the boundary conditions and responsible for the effect.

These and similar interactions between metallic plates are covered in this chapter. The next chapter will then come back to the interaction of atoms with a surface.

In honor of the four researchers mentioned above, today all kinds of vacuum-interactions are known indiscriminately under the names *van-der-Waals forces, London dispersion forces* or *Casimir-Polder forces*. For this reason, it necessary to introduce the nomenclature used in this work before going deeper into the subject,

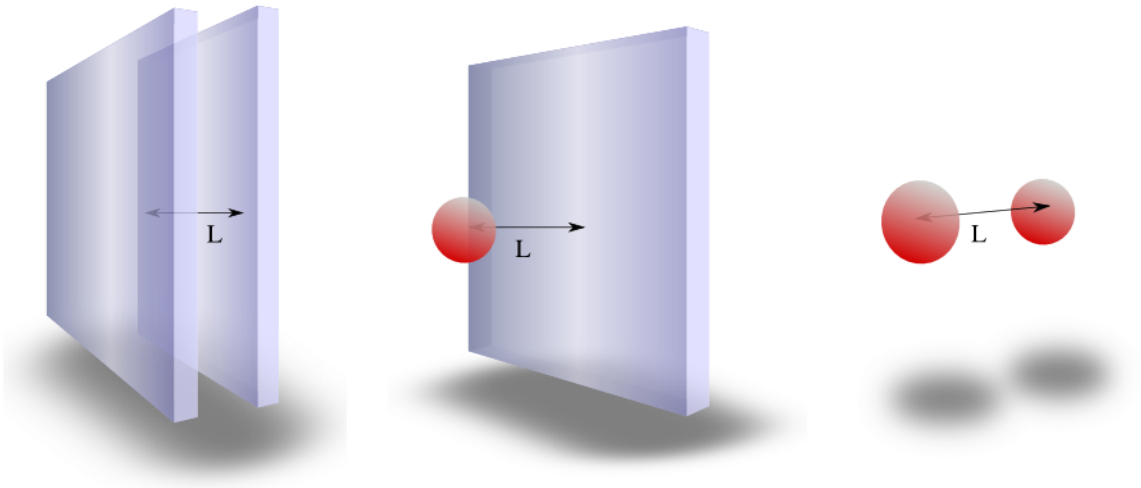

Figure 2.1: *a)* Casimir interaction *between macroscopic objects , b)* Casimir-Polder interaction *between an atom or molecule and a macroscopic object and c)* Casimir-Polder interaction *between two atoms or molecules.*

It is common to distinguish the effects according to the objects involved as shown in figure 2.2 and call

- *Casimir interaction* the interaction between two macroscopic bodies.
- *Casimir-Polder effect* the interaction involving one or two microscopic objects, i.e. atoms or molecules.

Anyway, this is not completely settled in the literature. Each configuration involves characteristic power laws of the force in function of the separation, and quite often the above terms are used rather to describe forces in special regimes, where these power laws apply. As an example, the term *van-der-Waals interaction* is often used for the non-retarded atom-surface interaction to distinguish it from the retarded one also known as *Casimir-Polder interaction*. To avoid confusion, the nomenclature in this text refers always to configurations and not to power law regimes.

2.1.2 Vacuum expectation values in bosonic fields

In classical physics, the vacuum was considered to be just free, empty space with no physical properties of its own. But at the beginning of the 20th century, it became clear that in a quantum world this vision does not work any more. Space became much more complex a thing and the quantum vacuum turned out to be not at all empty nor static but rather endowed with energy and fluctuations that lead to physical effects, especially in the presence of boundaries[1].

The origin of these energies lie in the quantization of bosonic fields, such as the photon field, Bose-Einstein-condensates, the phonon-field, etc. All these fields are described by Hamiltonians that can be decomposed into an ensemble of harmonic oscillators

$$H = \sum_k \frac{\hbar\omega_k}{2}\left[a_k^\dagger a_k + a_k a_k^\dagger\right] = \sum_k \frac{\hbar\omega_k}{2}\left[2a_k^\dagger a_k + 1\right] . \tag{2.1}$$

The creation and annihilation operators $a_k^\dagger, a_k$ of a one-particle state with quantum numbers k and energy eigenvalue $E_k = \hbar\omega_k$ adhere to bosonic commutation relations

$$[a_k, a_k^\dagger]_- = 1, \qquad [a_k, a_{k'}]_- = [a_k^\dagger, a_{k'}^\dagger]_- = 0 . \tag{2.2}$$

The Hamiltonian has a vacuum expectation value $\langle 0|H|0\rangle \neq 0$ and a vacuum or zero point energy $E_k^0 = \frac{\hbar\omega_k}{2}$ per mode. Summed up, the vacuum energy may well be divergent. The usual way of coping with this difficulty is the introduction of a *normally ordered* Hamiltonian

$$H \rightarrow :H: := H - \langle 0|H|0\rangle = \sum_k \hbar\omega_k a_k^\dagger a_k . \tag{2.3}$$

Physically, this subtraction fixes the level from which energy is measured, but the offset may well be infinite! This procedure works in many cases presented in a lecture in quantum statistics, but a lot more of attention is required, whenever the mode spectrum and subsequently the vacuum energy is modified by the boundary conditions or control parameters of the system α. Then the system will feel a generalized force $F_\alpha = \langle -\frac{\partial H}{\partial \alpha}\rangle$, even if there are no excitations present in the system. These general *Casimir forces* arise from the dependence of the quantum-vacuum state of a bosonic system on the boundary conditions.

2.1.3 Casimir interaction of ideal mirrors

In his original paper Casimir [Casimir 1948] considered a cavity made of parallel and ideally reflecting plates[2] (fig. 2.2a). This defines a Dirichlet problem for the electromagnetic field inside the cavity, which is solved by harmonic

[1] In some sense it looks as if the physical properties connected to the quantum vacuum make it a new kind of *ether*. This is not as scandalous at it seems at first sight, because the vacuum not a medium in the sense of the theory of relativity. Einstein [Einstein 1920] put it this way:

More careful reflection teaches us, however, that the special theory of relativity does not compel us to deny ether. We may assume the existence of an ether; only we must give up ascribing a definite state of motion to it, i.e. we must by abstraction take from it the last mechanical characteristic which Lorentz had still left it.

In this context it must be mentioned, that the vacuum energy may have a great impact not only in the quantum world, considered in this thesis but also in cosmology and relativity. It might for instance give rise to a cosmological constant or vacuum drag (e.g. [Davies 2005] and references therein).

[2] *Ideally reflecting* means plates of unit reflectivity $r^{TM} = -r^{TE} = 1$ for both polarizations. The term *ideal conductor* should be avoided in this context. It is misleading since a vanishing resistivity does not automatically imply unit reflectivity for TE-modes (cf. sections 1.4.2 and 1.7.3).

waves. Each mode of the electromagnetic field inside the cavity has a zero-point energy $E_n^0 = \frac{\hbar\omega_n}{2}$. The frequency follows the dispersion relation

$$\omega(n,\mathbf{k}) \quad = \quad c\sqrt{\mathbf{k}^2 + \frac{n^2\pi^2}{L^2}}\,, \tag{2.4}$$

where $\mathbf{k}$ is the two-dimensional wave vector component parallel to the plate and the third component is quantized in units of the inverse plate-distance L. In a cavity of finite size, only discrete resonant waves $n \in \mathbb{N}$ are allowed, but sending $L \to \infty$ leads to the *continuum limit* where $n \in \mathbb{R}$. The total zero-state energy diverges at both finite and infinite L, but Casimir's amazing result was that their difference does not. This difference is known as the Casimir energy

$$E_C = g_P \sum_{n=0}^{\infty}{}' \int \frac{Ad^2\mathbf{k}}{(2\pi)^2}\frac{\hbar\omega(n,\mathbf{k})}{2} f(\omega) - g_P \int_0^\infty dn \int \frac{Ad^2\mathbf{k}}{(2\pi)^2}\frac{\hbar\omega(n,\mathbf{k})}{2} f(\omega)\,. \tag{2.5}$$

The function $f(\omega)$ is a regulator such that $f(0) = 1, f(\omega \to \infty) \to 0$, which introduces a frequency cut-off into the system but does not appear in the final result, and $g_P = 2$ takes into account the two polarizations. Casimir [Casimir and Polder 1948] justified it by comparison to the realistic media, which become asymptotically transparent at high frequencies (see 1.7.1). The zero-point energy of modes of very high frequency that do not see the boundary, will not be changed by the presence of a boundary.

The sum prime symbol has been introduced because there is only one polarization of the mode $n = 0$ and frequent use of this notation is made in the rest of this work. It is defined as follows

$$\sum_{n=0}^{\infty}{}' := \sum_{n=0}^{\infty}\left(1 - \frac{1}{2}\delta_{n,0}\right) \tag{2.6}$$

The angular integration can be performed and by a change of variables $k = \frac{\pi c}{L}y$ the remaining integrals can be made adimensional

$$E_C = \frac{A\hbar c\pi^2}{4L^3}\left[\sum_{n=0}^{\infty}{}' - \int_0^\infty dn\right]\int_0^\infty dyy\sqrt{y^2+n^2} f\left(\sqrt{y^2+n^2}\pi c/L\right)\,. \tag{2.7}$$

The difference between the integral and the sum can be evaluated using the *Euler-MacLaurin formula* (e.g. [Gourdon and Sebah 2002])

$$\sum_{n=0}^{\infty}{}' F(n) - \int_0^\infty dnF(n) \quad = \quad -\sum_{m=1}^{\infty}\frac{B_{2m}}{(2m)!}F^{(2m-1)}(0) = -\frac{F'(0)}{12} + \frac{F'''(0)}{3\cdot 240} + ... \tag{2.8}$$

where B_m are Bernoulli's numbers (e.g. *loc. cit.*) and the derivatives must be taken with respect to n. In the case of the Casimir energy one more substitution $x = \sqrt{y^2+n^2} \Rightarrow xdx = ydy$ gives

$$F(n) \quad = \quad \int_n^\infty dxx^2 f\left(xc\pi/L\right)\,, \tag{2.9}$$

$$\Rightarrow F'(0) = 0, \qquad F'''(0) \quad = \quad -4, \qquad F^{(n>3)}(0) = 0. \tag{2.10}$$

from which follows Casimir's famous formulae for the interaction energy and the Casimir force

$$E_C \quad = \quad -\frac{\hbar c\pi^2}{3\cdot 240}\frac{A}{L^3}\,, \tag{2.11}$$

$$F = -\frac{\partial E_C}{\partial L} \quad = \quad -\frac{\hbar c\pi^2}{240}\frac{A}{L^4}\,. \tag{2.12}$$

The appearance of Planck's constant $\hbar$ indicates a generic quantum effect. Apart from this constant, the Casimir effect between perfect mirrors depends only on the speed of light and the geometry of the system.

The physical interpretation of the force [Milonni *et al.* 1969] seems straight forward: The continuous mode spectrum outside the cavity exerts a radiation pressure on the wall that does not depend on the plate separation, while

the inside mode spectrum and the radiation pressure do (2.2). Hence, the Casimir force is due to a difference of radiation pressures from both sides of the wall and the Casimir energy is just the work done on the system while approaching the plates from infinite distance to L.

Since the mode density inside the cavity is always discrete and hence more "dilute" than the one outside, it is intuitive to assume, that the pressure from the outside always dominates and the Casimir force is always attractive. This notion is incorrect as was shown in [Boyer 1974, Hushwater 1997]. They considered the force in a cavity made of one perfect reflector and an imperfect one, so that the boundary conditions are of a mixed Dirichlet-von Neumann type, and found a repulsive interaction.

This shows, that the formalism exposed above holds only for "flat" plates and perfect mirrors. Of course it is necessary to include the boundary conditions imposed by real materials and more general geometries.

2.1.4 General boundary conditions

The Lifshitz formula

Another way of calculating the Casimir energy was given by Lifshitz in 1956 [Lifshitz 1956], who had obtained his result using a somewhat different approach. Rather than comparing the modes inside a resonator at finite and infinite distances, Lifshitz considered the fluctuations in the dielectric cavity walls to calculate the electromagnetic stress-tensor on both sides of the plate directly. The physical picture from which he started considers the fluctuations in the matter as the fundamental quantity, that produces the zero-point field. This can be seen as complementary to Casimir's approach, but as Milonni [Milonni and Shih 1992] stated it: *Interpretation of the Casimir force in terms of the vacuum field is largely a matter of taste.* While Lifshitz' approach includes dissipation from the very beginning, the same was not easily obtained within Casimir's description.

In an imperfect cavity made of a dispersive but non-dissipative medium the resonances will be somewhat shifted with respect to the ideal mirror case due to the partial penetration into the mirrors, but they will still be discrete poles. In this case it is possible to find an expression for the Casimir energy or force between which coincides exactly with Lifshitz's. This is shortly outlined in this paragraph.

Rather than calculating the energies independently and performing a subtraction as before, it is useful to introduce a regularized density of states which counts the difference due to the boundaries and integrate over frequency and wave vectors in the end:

$$[\varrho(\omega,\mathbf{k},L)]_{\infty}^{L} := \varrho(\omega,\mathbf{k},L) - \lim_{L\to\infty}\varrho(\omega,\mathbf{k},L) \quad (2.13)$$

In Casimir's calculation this was implemented by taking the difference between the sum and integral (2.5), which could also have been written in terms of a density of states

$$\varrho(\omega,\mathbf{k},L) = {\sum_{m=0}^{\infty}}' \delta(\omega-\omega(\mathbf{k},n,L)) \quad (2.14)$$

$${\sum_{n=0}^{\infty}}' \frac{\hbar\omega(n,\mathbf{k})}{2} = \int_0^{\infty} d\omega \frac{\hbar\omega}{2}\varrho(\omega,\mathbf{k},L)\ . \quad (2.15)$$

Since this holds only for ideal mirrors, it is natural to look for a generalization to imperfect boundary conditions, including in a first step dispersion, but no dissipation.

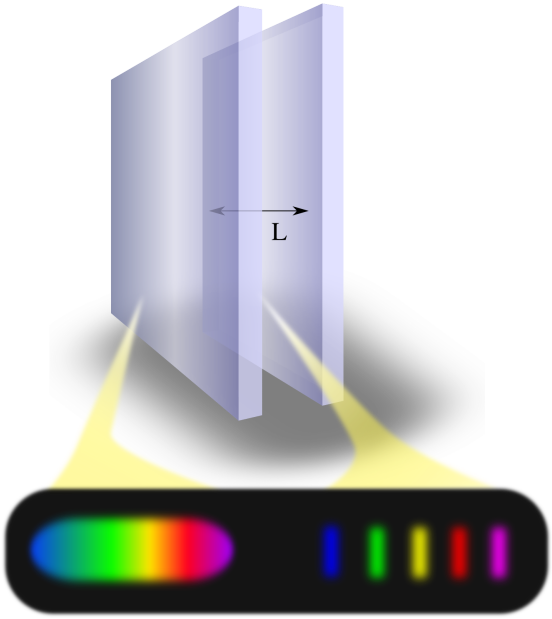

Figure 2.2: *Scheme of a Casimir setup. The spectra inside the cavity made of two parallel mirrors differ strongly from the one outside, where only one boundary condition is imposed.*

Cavities made up by two parallel mirrors are commonly
known as *Fabry-Pérot etalons* and the calculation of the mode structure inside is a textbook problem. From the Fresnel reflectivities (1.16) it is easy to obtain the field amplitude after one cycle of reflection (*open-loop-function*) and after an infinite number of cycles (*closed-loop-function*). For the polarizations $p \in \{TE, TM\}$ they are given by

$$\rho^p_{\mathbf{k}}(\omega) = r^p_{1,\mathbf{k}}(\omega) r^p_{2,\mathbf{k}}(\omega) \exp(-2\kappa L) \leq 1 \,, \tag{2.16}$$

$$f^p_{\mathbf{k}}(\omega) = \sum_{n=1}^{\infty} (\rho^p_{\mathbf{k}})^n = \frac{\rho^p_{\mathbf{k}}}{1-\rho^p_{\mathbf{k}}} \,. \tag{2.17}$$

Here, $\kappa = \sqrt{k^2 - \frac{\omega^2}{c^2}}$ is the wavenumber inside the cavity, chosen such that $\mathrm{Re}\ \kappa \geq 0$. The factors r in ρ account for the changes in phase and amplitude due the reflections from the walls and the exponential describes the propagation inside the cavity.

If $\varrho^p_{\mathbf{k}}(\omega) = 1$, the field is mapped to itself after one round trip in the cavity, which is just the characteristic of a cavity mode. The function $f^p_{\mathbf{k}}(\omega)$ will be show up again later.Schram [Schram 1973] (cf. also [Intravaia and Henkel 2008]) used this property of $\rho^p_{\mathbf{k}}(\omega) = 1$ to give an expression for the regularized density of states between general dispersive mirrors, by applying the *argument principle* of complex analysis, which counts the number of poles and zeros of a complex function within an integration contour.

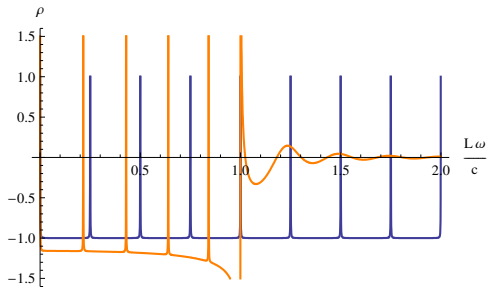

Figure 2.3: *TM contribution to the regularized density of states at normal incidence $k = 0$ for a perfect reflector (blue) and the plasma model (orange). The plates distance is set to $L = 2\lambda_p$.*

The regularized density of states is given by

$$[\varrho_p(\omega, \mathbf{k})]^L_\infty = -\frac{1}{\pi} \,\mathrm{Im}\, \frac{d}{d\omega} \ln\left(D_p(\omega, \mathbf{k})\right) \,, \tag{2.18}$$

$$D_p(\omega, \mathbf{k}) = 1 - \rho^p_{\mathbf{k}}(\omega) = 1 - r^i_{1,\mathbf{k}} r^i_{2,\mathbf{k}} \exp(-2\kappa L) \,. \tag{2.19}$$

As an example, Fig. 2.3 shows the regularized density of states in TM polarization for a perfect reflector and for plates described by the plasma model. It is evident from the above formulae, that in a perfectly reflecting cavity $\rho^p_{\mathbf{k}}(\omega) = 1 \Leftrightarrow D_p(\omega, \mathbf{k}) = 0$ wherever a mode is resonant. Any non-resonant mode in such a cavity cancels out by destructive interference and does not contribute to the density of states.

The first one features just the equidistant spectrum of Casimir's calculation and the density of states of the plasma model shows the effects of dispersion and the asymptotic transparency beyond the plasma edge. The Casimir energy can now be written in terms of the density of states or the mode function D respectively. In a second step a partial integration is performed, in which the evaluation of at the boundaries $[\omega \ln D_p(\omega, \mathbf{k})]^\infty_0$ vanishes, because of the transparency at high frequencies and because (hopefully) $\ln D_p(\omega) < \infty$.

$$E = \sum_p \int_0^\infty d\omega \int \frac{A d^2\mathbf{k}}{(2\pi)^2} \frac{\hbar\omega}{2} \left[\varrho_p(\omega, \mathbf{k}, L)\right]^L_\infty \tag{2.20}$$

$$= -\,\mathrm{Im} \sum_p \int_0^\infty d\omega \int \frac{A d^2\mathbf{k}}{(2\pi)^2} \frac{\hbar\omega}{2\pi} \frac{d}{d\omega} \ln\left(D_p(\omega, \mathbf{k})\right) \tag{2.21}$$

$$= \mathrm{Im} \sum_p \int_0^\infty d\omega \int \frac{A d^2\mathbf{k}}{(2\pi)^2} \frac{\hbar}{2\pi} \ln\left(D_p(\omega, \mathbf{k})\right) \,. \tag{2.22}$$

The Casimir force is again obtained from the derivative with respect to the cavity length L, and since

$$\frac{d}{dL} \ln(D_p) = \frac{-2\kappa\rho^p_{\mathbf{k}}(\omega)}{1-\rho^p_{\mathbf{k}}(\omega)} = -2\kappa f^p_{\mathbf{k}}(\omega) \,, \tag{2.23}$$

$$\Rightarrow F = -\frac{dE}{dL} = \frac{\hbar}{\pi} \,\mathrm{Im} \sum_p \int_0^\infty d\omega \int \frac{A d^2\mathbf{k}}{(2\pi)^2} \kappa f^p_{\mathbf{k}}(\omega) \,. \tag{2.24}$$

The last equation (2.24) is just the celebrated *Lifshitz formula* which expresses the Casimir interaction in terms of Fresnel's reflectivities at the interface between the vacuum and a dielectric. It should be stressed again that equation (2.24) as obtained by Lifshitz holds for both dispersive and dissipative media and is the basis of most contemporary calculations in the field of Casimir physics.

The above derivation included only dispersion. If dissipation is to be included in the description, the eigenfrequencies become complex and it is no longer possible to just define a zero-point energy per mode $E^0 = \frac{\hbar\omega}{2}$ and take the difference (2.7) as before. A way of defining the zero-point energy and write it as a sum over modes in such systems was worked out in the nineties [Jaekel and Reynaud 1991, Lambrecht and Reynaud 2000, Genet *et al.* 2003, Genet *et al.* 2004, Intravaia and Lambrecht 2005, Intravaia 2005]).

Representation by real and imaginary frequencies

So far, real frequencies have been used, and the fields can be distinguished into two kinds with clearly differing properties:

- *Propagating* $\kappa \in i\mathbb{R}$: fields can propagate in the cavity,
- *Evanescent* $\kappa \in \mathbb{R}$: fields decay exponentially.

Analytical continuation of optical functions to the imaginary frequency axis has already been introduced in section 1.2.5, but no use has been made of the formalism until now. It is possible to express the Casimir energy or force as an integral over purely imaginary frequencies $\omega = i\xi$, using the analyticity of κf in the upper complex half-plane. In this representation, both κ and $\ln(D)$ become real quantities, so there is no need to write the Re explicitly. The difference between propagative and evanescent fields however, is no longer evident. The Casimir free energy and force as integrals over imaginary frequencies read:

$$E = \frac{\hbar}{2\pi}\sum_p \int_0^\infty d\xi \int \frac{Ad^2\mathbf{k}}{(2\pi)^2} \ln\left(D_p(i\xi,\mathbf{k})\right) \tag{2.25}$$

$$F = \frac{\hbar}{\pi}\sum_p \int_0^\infty d\xi \int \frac{Ad^2\mathbf{k}}{(2\pi)^2} \kappa f^i_{\mathbf{k}}(i\xi)\,. \tag{2.26}$$

Example: Perfect reflection revisited

The formalism presented in the last sections can be used to calculate the Casimir force between perfectly reflecting plates in a very elegant way. As the reflectivities are $r_p = \pm 1$, the sum over polarization becomes a degeneracy factor $\sum_p = g_P = 2$. Direct evaluation gives

$$\kappa f^p_{\mathbf{k}}(i\xi) = \frac{\sqrt{k^2 + \frac{\xi^2}{c^2}}}{\exp\left(2L\sqrt{\mathbf{k}^2 + \frac{\xi^2}{c^2}}\right) - 1}\,. \tag{2.27}$$

The integral over wave vectors can be transformed to spherical coordinates in three dimensions including the frequency integral, setting $K = \sqrt{k^2 + \frac{\xi^2}{c^2}}$, so that

$$c\int_{-\infty}^{\infty} d^2\mathbf{k} \int_0^\infty d\left(\frac{\xi}{c}\right) = \frac{1}{2}c\int_{-\infty}^{\infty} d^3\mathbf{K}\,.$$

$$\Rightarrow F = A\hbar c g_P \int_{-\infty}^{\infty} \frac{d^3\mathbf{K}}{(2\pi)^3} \frac{K}{\exp(2KL) - 1} \tag{2.28}$$

$$= \frac{A\hbar c g_P}{2^5\pi^2 L^4}\Gamma(4)\zeta(4) = \frac{A\hbar c\pi^2}{240L^4} \tag{2.29}$$

This is of course just Casimir's result for the force (2.12).

2.1.5 Experiments measuring the Casimir force

Measuring the Casimir force has been a challenge for experimentalists since Casimir's prediction of the effect in 1948. At this point only the most important setups are sketched. More extensive reviews are given in [Bordag *et al.* 2001, Milton 2004, Klimchitskaya *et al.* 2009].

First measurements were done by Sparnaay in 1957 using a spring balance [Sparnaay 1957]. He measured the forces between parallel plates made of different metals at distances in the order of $1\ \mu\mathrm{m}$ and failed to give decisive answers due to a big range of uncertainty of about 100%. Follow-up experiments during the fifties and seventies by Derjaguin and van Blokland and Overbeek reached experimental uncertainties of about 50% using curved objects close to a surface rather than two plane surfaces [Derjaguin *et al.* 1956, Blokland and Overbeek 1978]. This eliminates one of the largest sources of error, i.e. the non-parallelism of the plates, and is still used today.

Recently, thanks to advancing nanotechnology and quantum-optics, interest in the vacuum-induced effects has risen again and experimentally it has become possible to measure Casimir forces to the precision of some percent. A milestone experiment was done by Lamoreaux in 1997, who used a spherical lens close to a surface and a torsion pendulum and reached an estimated uncertainty of about $5\% - 10\%$. At this level of accuracy, it becomes important to include conductivity and thermal corrections into the theoretical description [Lamoreaux 1997].

Further experiments were done by Mohideen *et al.* using a sphere attached to the cantilever of an atomic force microscope (AFM) and measuring its displacement to high precision by the reflection angle of a laser beam. This setup reached very high precision up to 1% at distances smaller than $1\mu m$ [Mohideen and Roy 1998, Harris *et al.* 2000, Chen *et al.* 2005].

Yet another setup developed by Capasso *et al.* exploited the change of the eigenfrequency of a nano-mechanical oscillator if a metal-coated sphere mounted to the tip of the AFM is approached [Chan *et al.* 2001, Iannuzzi *et al.* 2004, Lisanti *et al.* 2005]. This type of experiment measures the curvature of the surface potential in function of the distance. A conceptually similar experiment has recently performed in the context of atom-surface interaction (cf. 3.1.2).

Only one recent experiment by Bressi *et al.* tried to measure the force between even surfaces and reached a precision of 15% [Bressi *et al.* 2002]. As in the older experiments, the alignment of the plates turned out to be the crucial point and main source of inaccuracy.

Still it is highly desirable to measure the Casimir force in the two plates geometry, because it is the only setup, where a rather complete theory exist. Other geometries are compared to predictions obtained from the plane plate geometry by means of the *proximity force theorem*. It must be mentioned, that even for plane plates, the theory is not universal, because the inclusion of roughness, conductivity, etc. requires generally the use of material data.

2.1.6 The thermal Casimir effect

Finite temperature $T \neq 0$

At non-zero temperature, the electromagnetic field inside the cavity is not only due to the vacuum fluctuations, but there is also a thermal field. The first ones to include temperature into the calculation of the Casimir effect were Mehra and Lifshitz [Mehra 1967, Lifshitz 1956]. Here, the relevant thermodynamical potential for the system at a constant temperature is the Helmholtz free energy[3]

$$\mathcal{F}(T,V) = E - TS\,. \tag{2.30}$$

Once this potential is known, the toolbox of thermodynamics can be used to derive many other quantities such as entropy, the Casimir force, etc. In this text, a calligraphic $\mathcal{F}$ is used for the Casimir free energy to distinguish it from the force F.

The complete free energy per mode including both the thermal and the zero-point contribution can be obtained from the well-known formulae of quantum statistics, but exploiting the complete Hamiltonian (2.1) instead of the

[3] The term *free energy* is often used indiscriminately for two different quantities. The first is the *Helmholtz free energy* $\mathcal{F}(T,V) = E - TS$ with the differential $d\mathcal{F} = -SdT - pdV$, which is the thermodynamical potential minimized at constant temperature and volume. It should not be confused with *Gibb's free enthalpy* $G(T,p) = F + pV,\ dG = -SdT + Vdp$, which becomes relevant if the pressure is held constant rather than the volume.

normally ordered one (2.3). Using the common abbreviation $\beta = 1/k_B T$, the partition function of a mode with quantum numbers k is obtained from

$$\mathcal{Z}_k = \mathrm{Tr}\left[e^{-\beta\hbar\omega_k(a_k^\dagger a_k + 1/2)}\right] = \sum_m e^{-\beta\hbar\omega_k m} e^{-\beta\hbar\omega_k/2} = \frac{\exp\left(-\beta\hbar\omega_k/2\right)}{1-\exp\left(-\beta\hbar\omega_k\right)} \tag{2.31}$$

The corresponding Casimir free energy and force per mode are given by [Mehra 1967]

$$\begin{aligned}
\mathcal{F}_k &= -k_B T \ln(\mathcal{Z}_k) \\
&= k_B T \ln\left(1-\exp\left(-\beta\hbar\omega_k\right)\right) + \frac{\hbar\omega_k}{2} && (2.32)\\
&= k_B T \ln\left(2\sinh\left(\frac{\hbar\omega_k}{2k_B T}\right)\right) && (2.33)\\
F_k &= -\frac{\partial \mathcal{F}_k}{\partial L} = -\coth\left(\frac{\hbar\omega_k}{2k_B T}\right)\frac{\partial E_k^0}{\partial L}\,, && (2.34)
\end{aligned}$$

so that the Casimir free energy and the Casimir force at finite temperature can be obtained from the expressions (2.20, 2.24) at $T = 0$ by a simple replacement $E_k^0 \to \mathcal{F}_k$ or by introducing a thermal kernel $\coth\left(\frac{\hbar\omega}{2k_B T}\right)$ respectively.

Expansion in Matsubara frequencies

A very useful representation of the thermodynamic functions can be obtained, if the ω-integral is continued analytically to the complex plane and rotated to imaginary frequencies, as has been done before. Here, the thermal kernel $\coth\left(\frac{\hbar\omega}{2k_B T}\right)$, which is a slowly varying function at real frequencies, is purely imaginary apart from a discrete number of poles. Fig. 2.4 shows the behavior along both axes.

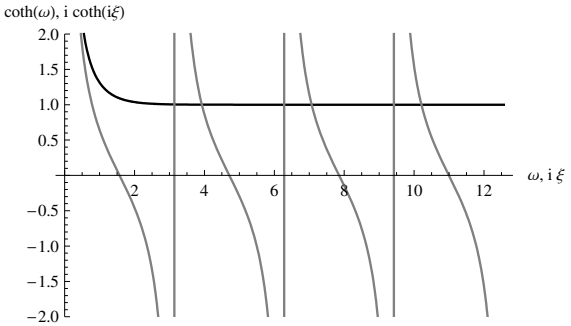

Figure 2.4: *Hyperbolic cotangent* $\coth(\omega)$ *and* $i\coth(i\xi)$ *evaluated at real (black) and imaginary (gray) arguments.*

This property of the hyperbolic cotangent makes it possible to use the series expansion, e.g. [Mostepanenko and Trunov 1997]

$$\mathrm{Re}\,\coth\left(\frac{i\xi\hbar}{2k_B T}\right) = \frac{2\pi k_B T}{\hbar}\sum_{n=-\infty}^{\infty}\delta(\xi-\xi_n)\,. \tag{2.35}$$

The quantities $\xi_n = 2\pi n k_B T/\hbar$ are known as the *Matsubara frequencies*.

The Casimir force at finite temperature can now be written directly using equations (2.34) and (2.26) and writing the real part explicitly

$$F(L,T) = \frac{\hbar}{2\pi}\,\mathrm{Re}\int_0^\infty d\xi \sum_{p,\mathbf{k}} \kappa f_{\mathbf{k}}^i(i\xi)\coth\left(\frac{\hbar i\xi}{2k_B T}\right) = k_B T {\sum_{n=0}^{\infty}}' \sum_{p,\mathbf{k}} \kappa f_{\mathbf{k}}^i(i\xi_n)\,. \tag{2.36}$$

In the case of the free energy (2.21), the internal energy per mode must be replaced by the corresponding free energy (2.33). A partial integration yields again a hyperbolic cotangent. The result is rotated to imaginary frequencies, where the series expansion of coth gives a very compact expression for the thermal Casimir free energy.

$$\begin{aligned}
\mathcal{F} &= -\operatorname{Im}\sum_{p,\mathbf{k}}\int_0^\infty d\omega k_B T \ln\left[2\sinh\left(\frac{\hbar\omega}{2k_BT}\right)\right]\frac{1}{\pi}\left[\frac{d}{d\omega}\ln D_p(\omega)\right] \\
&= \frac{\hbar}{2\pi}\operatorname{Im}\sum_{p,\mathbf{k}}\int_0^\infty d\omega \coth\left(\frac{\hbar\omega}{2k_BT}\right)\ln D_p(\omega) \qquad (2.37)\\
&= \frac{\hbar}{2\pi}\operatorname{Re}\sum_{p,\mathbf{k}}\int_0^\infty d\xi \coth\left(\frac{\hbar i\xi}{2k_BT}\right)\ln D_p(i\xi) \qquad (2.38)\\
&= k_BT\sum_{p,\mathbf{k}}{\sum_{n=0}^{\infty}}'\ln D_p(i\xi_n)\,. \qquad (2.39)
\end{aligned}$$

The thermal fluctuations introduce a new physical energy scale into the system which translates directly to a change of the characteristic power laws of the thermodynamical quantities. It is natural to expect thermal effects to occur at lengths comparable to the thermal wave length

$$\lambda_T = \frac{2\pi\hbar c}{k_BT} \approx \frac{0.014\,\mathrm{K}\cdot\mathrm{m}}{T} \qquad (2.40)$$

As a general feature of the Casimir interaction, the free energy is enhanced by a Bose factor $k_BT/E_k \approx \frac{k_BTL}{\hbar c}$ in the high T regime. The next section will use perfect reflectors to illustrate this effect further and demonstrate how asymptotic expressions can be obtained. In this case there are no intrinsic spectral effects from the optical properties of the material surface and it becomes clear, that the change of power law is a purely thermo-geometric effect.

Example: Perfect reflection

Once again, the perfectly reflecting resonator is a simple model to try out the formalism. A similar treatment was given in [Mostepanenko and Trunov 1997]. Since $|r^{TE}| = r^{TM} = 1$, both polarizations behave identically and the sum over both contributions yields simply a degeneracy factor $g_P = 2$. The free energy expressed through the Matsubara expansion reads now

$$\mathcal{F} = \frac{k_BTAg_P}{2\pi}\int dk k{\sum_n}'\ln(1-e^{-2\kappa(n)L}), \quad (2.41)$$

where again $\kappa = \sqrt{k^2+\xi_n^2/c^2}$. Hence, the Casimir force can be obtained by differentiating with respect to L. In a second step the integration variable is substituted $k \to 2L\kappa$ which yields a dimensionless integral.

$$\begin{aligned}
F = -\frac{\partial\mathcal{F}}{\partial L} &= -\frac{k_BTAg_P}{2\pi}{\sum_n}'\int_0^\infty dk k\frac{2\kappa}{e^{2\kappa L}-1} \\
&= -\frac{Ak_BTg_P}{8\pi L^3}\underbrace{{\sum_n}'\int_{2L\xi_n/c}^\infty du\frac{u^2}{e^u-1}}_{I}\,.
\end{aligned} \qquad (2.42)$$

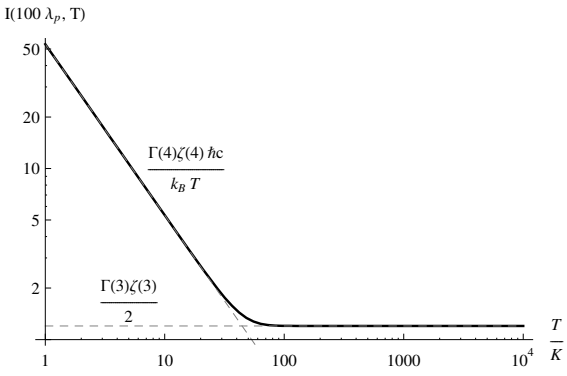

Figure 2.5: *Numerical evaluation of the function $I(L,T)$ vs. temperature (equivalently distance, since $I(T,L) = I(TL)$), calculated at $L = 100\lambda_p$. Dashed lines show the asymptotes at low and high T.*

The dimensionless function I has a structure similar to (2.9) and must generally be calculated numerically. Its behavior in function of temperature is shown in fig. 2.5. Since $I(T,L)$ is a function of the product TL only, the plot of I vs. distance at fixed temperature would be identical.

In the two limiting regimes of very high and low T it is possible to obtain asymptotic expressions for I and the functions derived from it, such as the Casimir force, free energy or entropy [Mehra 1967] (see also [Mostepanenko and Trunov 1997, Milton 2004]).

- *High temperatures or large distances $L \gg \lambda_T$*: In the calculation of I, the temperature enters only via the Matsubara frequencies $\xi_n = 2\pi n k_B T/\hbar$. If the temperature is sufficiently high, the zeroth frequency $\xi_0 = 0$ is separated from the other ones by a big interval and gives the only non-vanishing contribution, because it is the only mode that is thermally excited. Thus, the high temperature limit is given by the zeroth term of the Matsubara expansion, i.e. in the free energy $\sum_n{}' \to \frac{1}{2}\sum_{n=0}^{0}$ which can be evaluated immediately

$$I \approx \frac{1}{2}\int_0^\infty du \frac{u^2}{e^u - 1} = \zeta(3) \approx 1.202\ .$$

The free energy law can be recovered from the force by integration, and from there the limits of other thermodynamical quantities such as the Casimir entropy can be obtained.

$$\mathcal{F}(T,L) \approx -\frac{Ak_BT}{8\pi L^2}\zeta(3) \tag{2.43}$$

$$\Rightarrow S = -\frac{\partial \mathcal{F}}{\partial T} \approx \frac{k_B A \zeta(3)}{8\pi L^2}\ . \tag{2.44}$$

- *Low temperatures or small distances $L \ll \lambda_T$*: At low values of T, the Matsubara frequencies are quasi-continuous. In this regime, the sum can be replaced by an integral and a correction to first order in T can be calculated by means of the Euler-MacLaurin formula (2.8). Doing so, and substituting $y = n/u$, the integration boundaries can be made independent of n.

$$I \approx \underbrace{\int_0^\infty dn \overbrace{\int_{2L\xi_1/c}^\infty dy \frac{y^2 n^3}{e^{ny}-1}}^{F(n)}}_{I_1} - \underbrace{\frac{1}{12}\frac{d}{dn}F(n)\Big|_{n=0}}_{I_2} + \underbrace{\frac{1}{720}\frac{d^3}{dn^3}F(n)\Big|_{n=0}}_{I_3} + \ldots$$

Now, with the substitution $n \to N = yn$, the first term can easily be calculated. The following term vanishes identically and the third one gives in after some algebra.

$$\begin{aligned} I_1 &= \int_{2L\xi_1/c}^\infty dy \frac{1}{y^2}\int_0^\infty dN \frac{N^3}{e^N - 1} = \frac{\hbar c}{4\pi L k_B T}\Gamma(4)\zeta(4) \\ I_2 &\equiv 0 \\ I_3 &= \frac{1}{240}\int_{2L\xi_1/c}^\infty dy y^2 = \frac{1}{720}\left(\frac{4\pi L k_B T}{\hbar c}\right)^3 .. \end{aligned}$$

The final result for the force recovers Casimir's result for $T = 0$ plus an correction and again, the free energy and entropy asymptotics can be obtained.

$$F(T,L) \approx -\frac{\hbar c A \pi^2}{240 L^4} - \frac{\pi^2}{45}\frac{A(k_BT)^4}{(\hbar c)^3} + \ldots \tag{2.45}$$

$$\Rightarrow \mathcal{F}(T) \approx -\frac{\hbar c A \pi^2}{720 L^3} - \frac{\pi^2}{45}\frac{A(k_BT)^4 L}{(\hbar c)^3} + \ldots \tag{2.46}$$

$$S \sim ALT^3\ . \tag{2.47}$$

The thermal contribution to the free energy shows the T^4 law of the Stefan-Boltzmann law, so that the additional Casimir-pressure can be interpreted as the pressure of black-body radiation. The entropy connected to this thermal field is an extensive quantity, proportional to the cavity volume $V = AL$. At low temperatures the entropy vanishes, and the system fulfills Nernst's theorem - better known as the third law of thermodynamics. While this is a nice property of the perfectly reflecting cavity, it will show in the following sections, that $S(T \to 0) = 0$ does not necessarily hold, once the boundary conditions are imposed by reflectivities derived from a dielectric function.

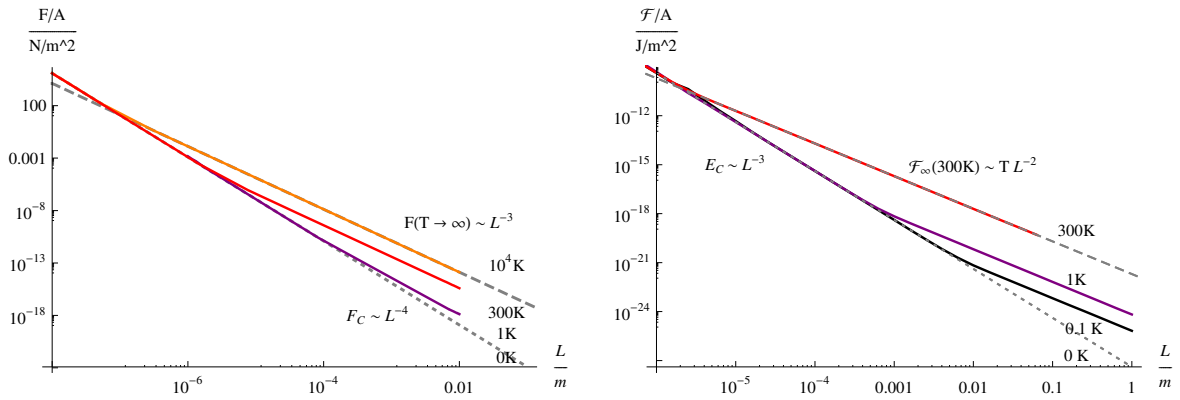

Figure 2.6: *Casimir force (left) and free energy (right) between perfect mirrors for different temperatures and its low and high temperature limits (dotted/dashed lines).*

The results of numerical calculations of the thermal Casimir force and free energy vs. distance is given in fig. 2.6. Both feature the characteristic changes of the temperature power law postulated earlier and now derived asymptotically. The comparison of the numerical results and the asymptotic power laws shows very good agreement.

The distance at which the transition between the power laws takes place is given about by the intersection of the low and high T asymptotics, i.e. where

$$\frac{\hbar c A \pi^2}{720 L^3} \approx \frac{k_B T A \zeta(3)}{8\pi L^2} \Leftrightarrow L \approx \lambda_T \frac{\pi^2}{180\zeta(3)} \approx 0.045\lambda_T := \Lambda_T \, . \tag{2.48}$$

This recovers the thermal wavelength λ_T as the characteristic length scale in this problem, which does not come as a surprise, since it is the only physical scale in the system. Anyhow, it is astonishing to find it multiplied by so small a numerical factor, such that the transition takes place at distances a factor ≈ 20 smaller than λ_T. The calculations in other systems including more realistic boundary conditions will show closely related effects.

2.1.7 Numerics

Evaluation of Matsubara sums

Already in the last section, numerical calculations were performed to obtain values of the Casimir free energy or force respectively and a big part of the results in this thesis are based on numerical calculations. The two main problems that one meets doing numerical calculations are, that firstly computers are always too slow and secondly the results most of the time too imprecise.

The numerical calculation of Casimir energies requires the calculation of integrals over the perpendicular wave vector and the frequencies. There are basically two different approaches to perform the frequency integral. Either one can do an integration along the real frequency axis (2.33) or move to the imaginary frequency axis according to (2.38). Due to the expansion of the hyperbolic cotangent at imaginary frequencies (2.35), the latter collapses to a sum over discrete Matsubara frequencies as in (2.39).

This has another advantage: Each point in the $\omega, \mathbf{k}$ plane used in the numerical integrations requires the calculation of the optical reflectivities. This step is not a big issue for models where an analytical form is known for the dielectric function, like in the Drude oder plasma model, but e.g in BCS theory the calculation of $\epsilon(\omega)$ involves a numeric integration itself. Here, it is preferable to evaluate reflectivities only for a rather small number of Matsubara frequencies and not quasi-densely as necessary in a frequency-integral.

The starting point of the calculation of the thermal Casimir free energy is usually a spectral free energy density g. A discussion of these functions and a more precise definition is given in section 2.2.2. They decay rapidly at sufficiently high frequencies because of the exponential damping with $\exp(-2\kappa L)$. This property can be used to

truncate the infinite sum and approximate the remaining infinite partial sum by an integral

$$\begin{aligned} \mathcal{F}(T) &=: \sum_{n=0}^{\infty}{}' g(n) \\ &\approx \sum_{n=0}^{N}{}' g(n) + \int_N^\infty g(n)dn + \dots . \end{aligned} \tag{2.49}$$

If the upper summation limit N is chosen correctly, the free energy density $g(n > N)$ at frequencies $\xi > \xi_{max}$ varies very slowly and the difference between the integral and the sum is small. The error can be estimated with help of the Euler-MacLaurin-formula.

In practice it is necessary to obtain an estimate for the summation limit N in an algorithmic, fast and reliable way. A scheme proposed in [Boström and Sernelius 2004] used a fixed number of Matsubara-terms $N = 10$. Such a recipe puts a lower limit to temperatures where the algorithm works, because as the Matsubara summands are proportional to the temperature, for any fixed number N there is a maximum value of T, for which $\xi_N > \xi_{max}$, and at lower temperatures the integral is used in a regime, where the free energy density has not yet the required slow variance.

A basic criterion for N is, that the integral must be only a small correction to the total result, so that fixing the relation between the partial sum and the remainder integral gives a value for N that does not depend on the specific form of g. Along the way $u_{F,max}$ can be used as an estimate for the numerical error.

$$\frac{\int_N^\infty g(n)dn}{\sum_{n=0}^{N}{}' g(n)} < u_{F,max} . \tag{2.50}$$

Such a recipe can be used as the final condition in a loop. In this case it is essential that the first partial sum give a non-vanishing contribution, which can be secured by fixing $N > N_{min} \gg 0$.

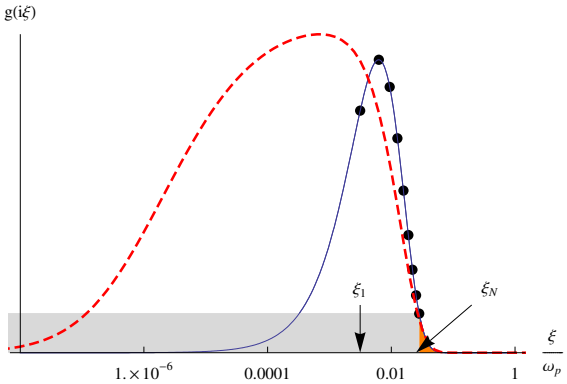

Figure 2.7: *Matsubara-terms on a toy energy density (solid) at imaginary frequencies. Dashed: TE-modes in the Drude model. For numerical evaluation the remaining terms of the sum is approximated by an integral, where its relative weight is small enough. For some functions the integral (orange area) may be estimated by $N \cdot g(N)$ (gray area).*

Another possibility opens if the asymptotic behavior of the energy density is known. Often there is an approximately exponential decay at high n. Then g varies slower than a heuristic toy-model G.

$$g(n) \sim \exp(-\alpha n) < n \exp(-\alpha n) =: G(n) .$$

This is a rather pessimistic estimate, but the extra factor n guarantees an overall similar qualitative behavior as in the Drude model and the curves match well at high frequencies (see fig. 2.7 for a comparison of the toy model with the Drude energy density). The toy-model allows to perform the integral which yields

$$\int_N^\infty G(n) = \frac{1+\alpha N}{\alpha^2} \exp(-\alpha N) \approx \frac{N}{\alpha} \exp(-\alpha N)$$

at high N. This gives a coarse estimate for N, which is very quick to calculate and is therefore an advantage in numerical calculations. The criterion (2.50) in this approximation becomes:

$$\frac{N g(N)}{\sum_{n=0}^{N}{}' g(n)} < u_{F,max} . \tag{2.51}$$

For appropriate models, the values of N stemming from the two estimates (2.50) and (2.51) are very similar and the approximation can save much time. But in other cases, especially for non-monotonous behavior of the energy density at $n > N_{min}$ it must be used with care because it may give too low values of N.

In this work (2.50) is usually used, because it turned out to be more reliable at very low temperatures and for general models. The parameters used were $u_{F,max} \in \{10^{-3}, 10^{-6}\}$, $N_{min} \in \{10^1, 10^3\}$ and the result include sums over $N \in \{10^2, 10^5\}$ terms. In some cases like BCS theory, due to the time-consuming calculation of the optical response, the remainder integral was neglected completely, which may be done if $u_{F,max}$ is chosen high enough and the contribution from the integral is vanishing anyway, but will yield a systematic numeric error and yield generally too small values of the energy.

As a last point one should mention that in the algorithmic evaluation of the Matsubara sum, the zeroth term must usually be evaluated separately, since it requires performing the limit $\xi \to 0$ in the Fresnel's reflectivities, which can be done much more efficiently using analytical or asymptotic techniques rather than numerical ones.

Numerical differentiation

The Casimir free energy is not the only relevant quantity of the system. Experimentalists will mostly be interested in forces and in the context of thermodynamics also the entropy is very interesting. Both quantities are related to the free energy by a derivative

$$S = -\frac{\partial \mathcal{F}}{\partial T} \qquad \text{and} \qquad F = -\frac{\partial \mathcal{F}}{\partial L} \, .$$

It is possible to perform the differentiation first analytically and evaluate the Matsubara sums afterwards, but to save time it can be often convenient to use already generated data for the free energy first and extract the entropy or force using a numerical differentiation. In this, one uses difference quotients as an approximation for differential quotients. This is of course an additional source of numerical errors but can be minimized by the right choice of the sample points. From the Taylor expansion of a function $f(x)$ one obtains

$$\begin{aligned} f'(x) &= \frac{f(x+a)-f(x)}{a} - \frac{a}{2} f''(x) + \mathcal{O}(a^2) && (2.52) \\ &= -\frac{f(x)-f(x-b)}{b} + \frac{b}{2} f''(x) + \mathcal{O}(b^2) && (2.53) \\ \Rightarrow f'(x) &= \frac{1}{2}\left[\frac{f(x+a)-f(x)}{a} + \frac{f(x)-f(x-b)}{b}\right] + \mathcal{O}(a-b) + \mathcal{O}(a^2, b^2) \, . && (2.54) \end{aligned}$$

Hence, the error of a non-central difference quotient ($a \neq b$) goes in first order as the non-centrality $a - b$ which is directly connected to the interval length, but this order can be suppressed if the difference quotient is chosen centrally $a = b$. In this case

$$f'(x) = \frac{f(x+a)-f(x-a)}{2a} + 2\mathcal{O}(a^2) \, , \qquad (2.55)$$

the error is in second order of the interval length. A similar or higher precision could also be obtained including higher orders or the Taylor expansion, but this requires usually the calculation of more sample points of the free function f at special values of x.

Therefore, the optimal way (at least to this order) to calculate entropies, forces, etc. numerically from the existing free energy data, is just in between two of the sample points.

2.2 Casimir interaction in the Drude and plasma model

2.2.1 Thermal surface plasmons

Energy correction at general distances

The mode spectrum of a free electron gas filling the whole space by a neutral background ($\epsilon_r = 1$) features collective longitudinal charge oscillations known as *Bulk plasmons* or *plasma polaritons*, that occur at the zeros of the dispersion relation [Ibach and Lüth 1981]

$$k^2 - \epsilon(\omega)\frac{\omega^2}{c^2} = 0 \, .$$

These excitations can propagate inside the bulk material and are not further considered here. They correspond to the collective plasma oscillations in the bulk introduced earlier in section 1.1.5. The characteristic frequency is the plasma frequency ω_p.

Bounded system with interfaces can carry a second kind of plasmonic modes, known as *surface plasmons*. They belong to the solutions of

$$1 - r_p(\mathbf{k}, \omega)^2 \exp(-2\kappa L) = 0$$

in the evanescent sector of the mode spectrum. Therefore they are confined to the interface and are connected to electric fields that decay both inside and outside the medium.

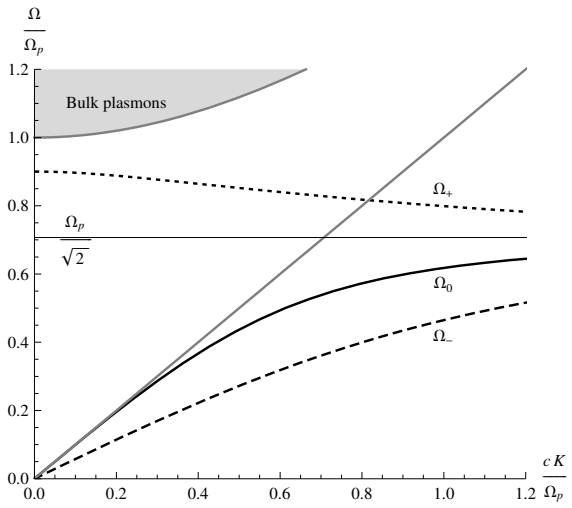

Figure 2.8: *TM plasmonic dispersion relations. Surface modes $\Omega\pm, \Omega_0$ and continuum of bulk-modes (gray area). One branch of the surface dispersion relation crosses the light cone (gray).*

It is worthwhile noticing that the collective excitations in superconductors are very similar to the ones in a normal metal [Rickayzen 1959, Bardasis and Schrieffer 1961]. In the 1980s surface plasmons raised new interest, as they may be connected to the yet unknown coupling mechanism in some high T_c superconductors [Ruvalds 1987], which are typically layered structures. Today, the advances in nanotechnology offer precise tools to tailor (meta-)materials with specific optical properties, that are often determined by plasmonic excitations. This branch of material science is therefore also known as *(nano-) plasmonics*.

The relevance and impact of surface plasmons on the Casimir effect at zero temperature has been discussed thoroughly in [Intravaia and Lambrecht 2005, Intravaia 2005, Intravaia *et al.* 2007]. The presentation in this paragraph follows closely the third of the references and uses the same notation, but includes the effects of finite temperature.

Figure 2.8 shows the plasmonic dispersion relations obtained in TM-polarization. An isolated surface has only one surface plasmon mode Ω_0, which splits in two branches $\Omega_\pm$ in the case of two plates at finite distance because of the electromagnetic coupling. The plasmon dispersion curve Ω_0 of an isolated surface is recovered in the limit of large plate separation. The upper branch crosses the light cone. In contrast, all TE-modes (not shown here) lie inside the light cone. The dispersion relation for the surface-modes at given distance L can be expressed in a parametric form [Intravaia 2005]

$$z = (\kappa L)^2, \qquad \Omega = \frac{\omega L}{c}, \qquad K = kL \tag{2.56}$$

$$\Omega_{0,\pm} = \sqrt{g_{0,\pm}(z)}, \quad K_{0,\pm} = \sqrt{z + g_{0,\pm}(z)}, \quad dK^2_{0,+,-} = dz + g'_{0,\pm}(z)dz \tag{2.57}$$

$$g_{0,\pm}(z) = \frac{\Omega_p^2 \sqrt{z}}{\sqrt{z} + \sqrt{z^2 + \Omega_p^2}[\tanh(\frac{z}{2})]^{0,\pm 1}} \, . \tag{2.58}$$

The variable $z = 0$ where the dispersion relations cross the light cone. To obtain the complete dispersion curves shown in fig. 2.8, z must run over the interval $\Gamma_- = \Gamma_0 = [0, \infty]$ in the branches Ω_0, Ω_-, but in the Ω_+-branch $z \in \Gamma_+ = [-z_+, \infty]$, where $\sqrt{z_+} = \Omega_p \cos(\sqrt{z_+}/2)$, so that an additional contribution to the integral must be taken into account.

Knowing the dispersion relation, there is no need to calculate a density of states, and the integration over modes can be done at once. The difference w.r.t isolated plates is obtained by the subtraction $\Omega_\pm - \Omega_0$ for each branch:

$$E(L) = \frac{cA\hbar}{4\pi L^3} \int_0^\infty K dK \left[\Omega_+(K) + \Omega_-(K) - 2\Omega_0(K)\right] \tag{2.59}$$

$$= \frac{cA\hbar}{8\pi L^3} \sum_{a=0,\pm} c_a \int_{\Gamma_a} dz \sqrt{g_a(z)} \left(1 + g'_a(z)\right) \, . \tag{2.60}$$

The K-integral is replaced by the parametrization over z, and $c_+ = c_- = 1, c_0 = -2$ realizes the subtraction.

The general case including $T > 0$ is obtained by substituting the internal energy per mode with the respective free energy as in (2.32)

$$E(g_a(z)) \to \mathcal{F}(g_a(z)) = \begin{cases} \frac{\hbar c}{L}\sqrt{g_a(z)}, & T = 0 \\ k_B T \ln[1 - \exp(\frac{\hbar c\sqrt{g_a(z)}}{k_B T L})] + \frac{\hbar c}{L}\sqrt{g_a(z)}, & T > 0 \end{cases}$$

Now, the second term in the integrals (2.60) can be evaluated by a substitution of the variable $dz \to dg(z)$

$$\begin{aligned} \mathcal{F}(L,T) &= \frac{A}{8\pi L^2}\left[\left(\sum_{a=0,\pm} c_a \int_{\Gamma_a} dz \mathcal{F}(g_a(z))\right) + \left(\sum_{a=0,\pm} c_a \int_{g_a(\Gamma_a)} dg \mathcal{F}(g)\right)\right] \\ &= \frac{A}{8\pi L^2}\left[\left(\sum_{a=0,\pm} c_a \int_{\Gamma_a} dz \mathcal{F}(g_a(z))\right) - [A(g_+(-z_+)) - A(0)]\right] . \end{aligned} \tag{2.61}$$

The integral can be performed and is expressed through the antiderivative $A(g) = \int dg' \mathcal{F}(g')$. Contributions arise only from the lower limit of the Ω_+-branch (minus the free space value), because the other two branches coincide here $g_0(0) = g_-(0) = 0$. The other integration boundary has no contribution at all, because all three branches converge to $\Omega_p/\sqrt{2}$ as $z \to \infty$. The evaluation of $A(g)$ gives

$$A(0) = \frac{2(k_B T)^3}{(c\hbar/L)^2}\zeta(3) \tag{2.62}$$

$$\begin{aligned} A(g) = {} & \frac{2c\hbar}{3L} g^{3/2} + \left\{ \frac{c\hbar}{3L} g^{3/2} + k_B T g \log\left[\frac{1 - e^{-\frac{c\hbar\sqrt{g}}{k_B T L}}}{1 - e^{\frac{c\hbar\sqrt{g}}{k_B T L}}}\right]\right. \\ & \left. - \frac{2(k_B T)^2}{c\hbar/L}\sqrt{g}\,\mathrm{Li}_2\left[e^{\frac{c\hbar\sqrt{g}}{k_B T L}}\right] + \frac{2(k_B T)^3}{(c\hbar/L)^2}\,\mathrm{Li}_3\left[e^{\frac{c\hbar\sqrt{g}}{k_B T L}}\right]\right\} . \end{aligned} \tag{2.63}$$

The term in curly brackets involves polylogarithms $\mathrm{Li}_s(z) = \sum_{k=1}^{\infty} \frac{z^k}{k^s}$ and collapses to $A(0)$ as $T \to 0$. In this case the term vanishes in the subtraction of the free space value and the contribution from the second integral in (2.61) is just the single term $\frac{2c\hbar}{3L} g^{3/2}$, which recovers the surface plasmon interaction energy at $T = 0$ [Intravaia and Lambrecht 2005, Intravaia 2005, Intravaia *et al.* 2007]

$$E(L) = -\frac{A\hbar c\pi^2}{720 L^3} \underbrace{(-1)\frac{90}{\pi^3}\left[-\frac{2}{3}z_+^{3/2} + \sum_{a=0,\pm} c_a \int_{\Gamma_a} dz \sqrt{g_a(z)}\right]}_{\eta(L)} . \tag{2.64}$$

Fig. 2.9 shows the free energy and the correction factor $\eta(L,T) = \mathcal{F}_{pl}(L,T)/E_C(L)$, which is the plasmon energy measured in units of the Casimir energy of a perfectly reflecting cavity of equal size at $T = 0$ as introduced in [Intravaia *et al.* 2007].

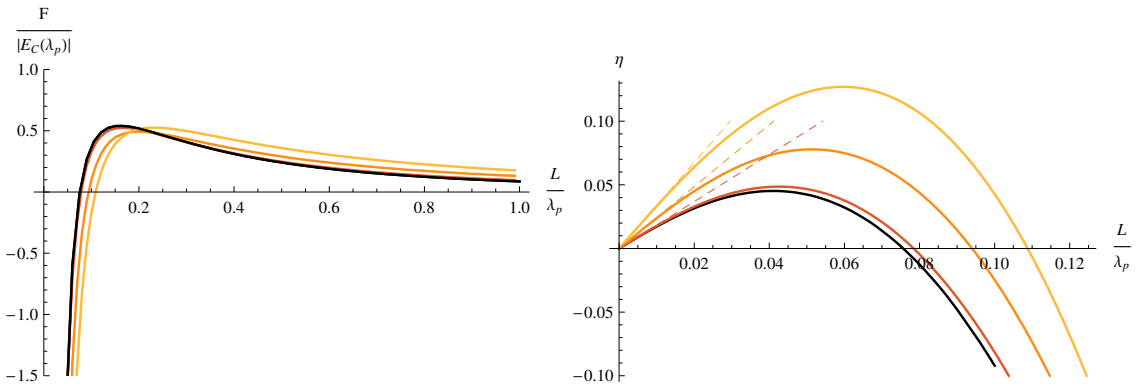

Figure 2.9: *TM plasmonic energy vs. the plate distance L at $T/T_p \in \{0, 0.1, 0.2, 0.3\}$ normalized to the Casimir energy at the plasma-wavelength (left) and at the same distance (right). Dashed: Small-distance asymptotics.*

The surface plasmon Casimir energy has two characteristic features already present at $T = 0$:

- *Repulsive regime*: The plasmonic Casimir energy changes its sign i.e. there is a transition from an attractive to a repulsive force. This was a very surprising result, since the Casimir effect between perfect reflectors and metals was known to be purely attractive. The transition from an attractive to an repulsive force occurs at approximately $L \approx 0.08\lambda_p$ at $T = 0$, but sets in at larger distances as the temperature increases. Here, the characteristic length scale is the *plasma wavelength*

$$\lambda_p = \frac{2\pi c}{\omega_p} \,. \tag{2.65}$$

- *Small distance correction:* The correction-factor $\eta(L,T)$ is linear in L at small distances (see the next section for a detailed calculation). This means, that the Casimir interaction in this regime does not follow Casimir's power law, but is enhanced by one power of L so that

$$\mathcal{F}(T,L) \sim L^{-2} \qquad \text{at small } L \ll \lambda_p \,. \tag{2.66}$$

  This effect is common to all conducting media with *finite bandwidth* [Lambrecht *et al.* 1998] and will appear again in other models, showing that at small plate separations the electrostatic interaction of the surface plasmons dominates the Casimir interaction [Van Kampen *et al.* 1968].

The small distance limit

The correction-factor $\eta(L,T)$ can be calculated asymptotically in the limit of small plate separations. An expansion of the dispersion relations to first order in $\Omega_p = \frac{2\pi L}{\lambda_p}$ yields

$$\Omega_0 = \frac{\Omega_p}{\sqrt{2}}, \qquad \Omega_\pm = \Omega_0\sqrt{1 \pm \exp(-\sqrt{z})} \tag{2.67}$$

In the calculation of the energy correction factor to first order, the propagative contribution can be neglected, because it gives contributions to the third order in L (as at zero temperature). The result consists then of two parts, one of which survives at $T = 0$ while the other depends explicitly on temperature and accounts for the steepening of the curves at small distance with temperature (see fig. 2.9). Introducing the plasma temperature $T_p = \hbar\omega_p/k_B$ for a more compact notation, the energy correction is given by

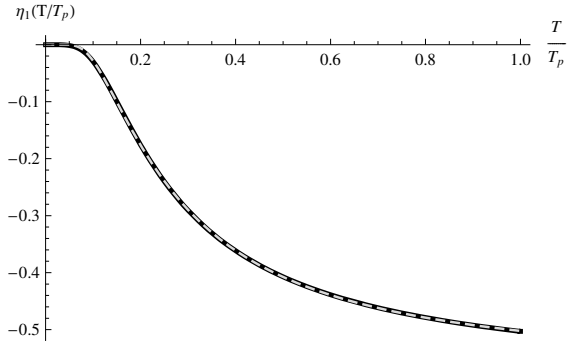

Figure 2.10: $\eta_1(T/T_p)$*, thermal contribution to the free energy correction factor at small distances* $L \ll \lambda_p$ *(solid black line) and the fit (gray dashed line).*

$$\eta(L,T) = -\frac{90}{\pi^3}\left(\frac{2\pi L}{\lambda_p}\eta_0 + \frac{2\pi L}{\lambda_p}\frac{T}{T_p}\eta_1(T/T_p)\right) \tag{2.68}$$

where

$$\eta_0 = \int_0^\infty dz\left\{\frac{\sqrt{1-e^{-\sqrt{z}}}}{\sqrt{2}} + \frac{\sqrt{1+e^{-\sqrt{z}}}}{\sqrt{2}} - \sqrt{2}\right\} \approx -0.0981 \tag{2.69}$$

$$\eta_1(\tau) = \int_0^\infty dz\left\{2\ln\left[1-\exp\left(-\frac{\sqrt{1-e^{-\sqrt{z}}}}{\sqrt{2}\tau}\right)\right] + 2\ln\left[1-\exp\left(-\frac{\sqrt{1+e^{-\sqrt{z}}}}{\sqrt{2}\tau}\right)\right] - 4\ln\left[1-\exp\left(-\frac{1}{\sqrt{2}\tau}\right)\right]\right\} . \tag{2.70}$$

Figure 2.10 shows the thermal contribution $\eta_1(\tau)$ in function of temperature. The curve saturates against a constant value at high temperatures. The integral can be evaluated analytically, which involves the asymptotic evaluation of polylogarithms similar to the ones encountered before, and gives the nice result

$$\lim_{\tau\to\infty}\eta_1(\tau) \quad = \quad -\frac{\zeta(3)}{2} \approx -0.601\ , \tag{2.71}$$

so that the slope of the energy correction at small distances grows linearly with temperature in this regime.

At low temperatures, $\eta_1(\tau)$ decays exponentially, so that no expansion in powers of $\tau = T/T_p$ can be done. A numerical fit to an ansatz with similar qualitative behavior gives the approximation

$$\eta_1(\tau) \approx -0.575 \exp\left(-0.135\ \tau^{-1.345}\right)\ , \tag{2.72}$$

which shows quite good agreement with the exact function over a wide range of temperatures, though the high T limit is not reproduced exactly (see the plot). Note that the prefactor of $\eta_1(T/T_p)$ can be written as $\frac{2\pi L}{\lambda_p}\frac{T}{T_p} = \frac{k_B T L}{\hbar c}$. It links the geometric and the thermal energy scale and does not depend on the value of the plasma frequency.

2.2.2 Plasma and Drude model

Distance power laws

The surface plasmon modes covered explicitly in the last section, give important contributions to the mode spectrum of metals, but they are not the only ones. In fact, the repulsive regime created by them is overcompensated by other contributions. Numerical results for the Casimir energy vs. distance calculated in the plasma and Drude model are shown in figures 2.11. As in the case of the perfect reflector, there are different regimes, each of which features

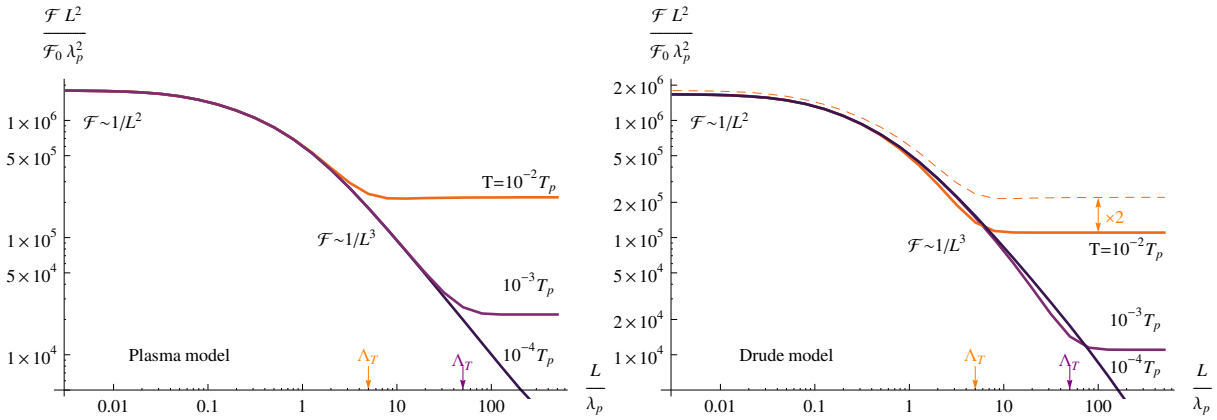

Figure 2.11: *Casimir free energy vs. distance in the plasma (left) and Drude model (right). The free energy is scaled to the value $\mathcal{F}_0$, obtained in the plasma model at $T = 0, L = 100\lambda_p$ and scaled to L^2/λ^2. Thermal effects set in at $\Lambda_T \approx 0.045\lambda_T$. The dashed line in the right plot shows the corresponding curve in the plasma model, which differs from the drude curve by a factor ≈ 2 at large L.*

a characteristic power law connected to characteristic length scales of the system. The thermal wavelength plays the same role as before, but unlike the case of perfect reflectors, the material of the cavity walls can carry plasmonic excitations. This introduces a new energy scale into the system, given by the plasma wavelength $\lambda_p = 2\pi c/\omega_p$ and new effects occur when the plate distance becomes comparable. The distance regimes determined by these scales are

- *Non-retarded regime* $L \ll \lambda_p$: At distances below the plasma wavelength, the non-retarded electrostatic interaction between surface plasmons is dominant and Casimir free energy follows a distance power law $\mathcal{F} \sim L^{-2}$ as in (2.66). Qualitatively, there are no big differences between the plasma and Drude model in this regime , so that any dissipative effects (cf. next section) result merely in a scaling of the free energy but do not influence the power law.
- *Retarded regime* $\lambda_p \ll L \ll \lambda_T$: Where the electrostatic surface interaction becomes less important and retardation sets in, the power law is just the one known from Casimir effect for perfect reflectors $\mathcal{F} \sim L^{-3}$. The arrows in the plot indicate the length scale $\Lambda_T \approx 0.045\lambda_T$ originally found for perfect reflectors in

(2.48), where the crossover to the thermal regime takes place. Interestingly, the finite temperature curves in the Drude model fall below the one at $T = 0$ in this regime. This indicates a (small) repulsive correction due to dissipative effects.

- *Thermal regime* $\lambda_T \ll L$: Exactly as for the perfect reflector, the thermal wavelength is the scale that determines the thermal regime. The zeroth Matsubara summand dominates the behavior and the free energy follows $\mathcal{F} \sim L^{-2}$. Dissipation has a strong influence on this value, and the plasma and Drude model differ by a factor 2 (solid and dashed line in plot 2.11) as will be discussed in the next sections. At very low temperatures the thermal wavelength becomes very long, so that the thermal regime is suppressed and the retarded regime extends to infinity instead.

Effects of dissipation

If the complete mode spectrum of the plasma or Drude model is included into the calculation of the Casimir effect, dissipation becomes relevant and results in big differences between the two models in at both zero- and nonzero-temperature. The Casimir free energy is usually calculated from (2.39) and it is useful to introduce a spectral Casimir free energy density $g(i\xi)$, such that

$$\mathcal{F} = k_B T {\sum_{n=0}^{\infty}}' g(i\xi) \Leftrightarrow g(i\xi) = \sum_{p,\mathbf{k}} \ln D_p(\mathbf{k}, i\xi) \; . \tag{2.73}$$

Fig. 2.12 shows the spectral Casimir free energy density for the plasma and Drude model. The solid lines show the total free energies and the dashed lines separate the contributions from TE and TM-modes. Note that the TE energy density of the Drude model goes to zero below the dissipation rate $\xi \ll \gamma$, while nothing alike occurs for the plasma.

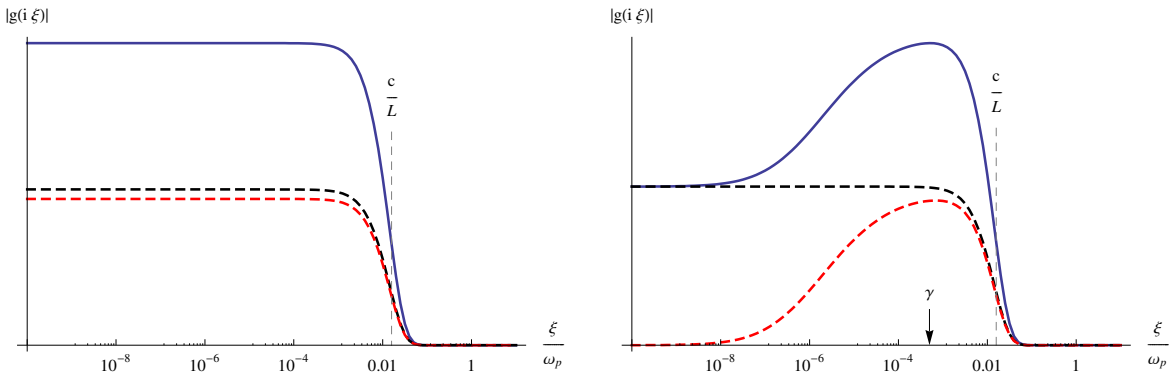

Figure 2.12: *Spectral free energy density* $g(\omega) = \frac{\partial \mathcal{F}}{\partial \omega}$ *in the plasma model (left) and Drude model (right), where* $\gamma = 5{\cdot}10^{-4}\omega_p$, $L = 10\lambda_p$. *Total energy density TE+TM (solid), contributions from TM (dashed black) and TE polarization (dashed red).*

In the plasma model, the contributions from both polarizations have a very similar qualitative behavior and their absolute values are very close, too, due to the the high value of the plasma frequency ω_p in a good conductor. In the *bad conductor* limit with small values of ω_p, the contribution from TE polarization results much smaller, so that difference to the corresponding Drude model would become less pronounced. This was pointed out recently by Klimchitskaya *et al.* [Klimchitskaya 2009] in the discussion of the data analysis for a semiconductor.

As expected from the discussion of the optical properties in section 1.7, surface charges can build up in a very similar way in both a plasma and a Drude metal, and so TM reflectivities and subsequently the free energies contributions do not differ greatly.

Things are of course different for TE-modes. It was shown in section 1.7.3, that the dissipation in the Drude model creates leads to a transparency for low frequency TE-modes, i.e. (quasi-) static magnetic fields with $\omega \ll \gamma$. This set of TE-modes decouples from the resonator and does not contribute to the Casimir effect. This difference between the Drude and the plasma model becomes relevant for the thermal correction. In the calculation of the Casimir free energy, the spectral free energy is evaluated at the Matsubara frequencies. This leads to the smaller thermal

correction in the Drude model, that have been seen in figures 2.11 and will be discussed in more detail in the next section.

Thermal effects and the thermal problem

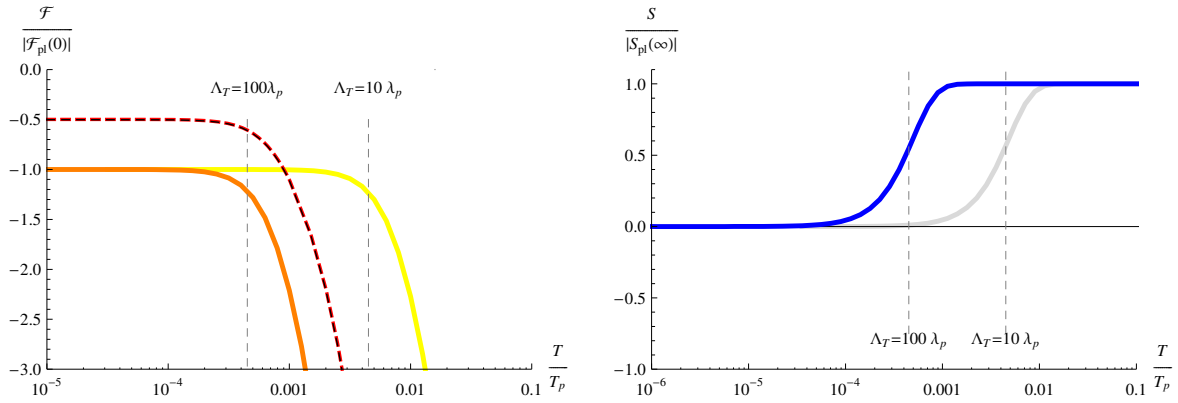

Figure 2.13: *Casimir free energy and entropy in the plasma model between plates at distances $L = 100\lambda_p$ (orange, blue) and $L = 10\lambda_p$ (yellow, gray). TE- (dashed red) and TM-contributions (dashed black) are indistinguishable on this scale (shown for $L = 100\lambda_p$ only). Energies are scaled to the value $\mathcal{F}_{pl}(T = 0)$ of the plasma model, and the entropies to the value $S_{pl}(T \to \infty)$, cf. (2.44). Thermal effects become dominant where $L = \Lambda_T \approx 0.045\lambda_T$.*

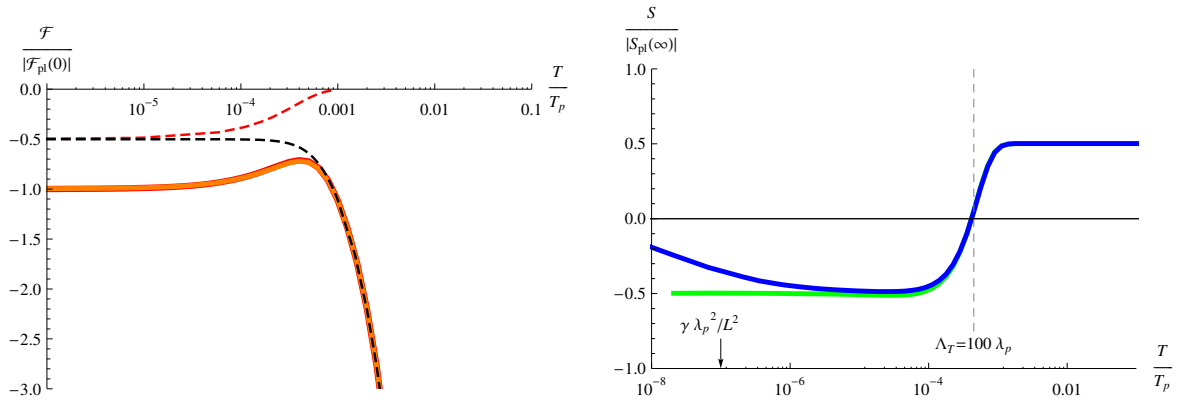

Figure 2.14: *Drude model (orange, blue), where $\gamma = 10^{-3}\omega_p, L = 100\lambda_p, T = 2 \cdot 10^{-2}T_p$, and for the perfect crystal (red, green) $\gamma(T) = \omega_p \left(1 - e^{-(T/T_0)^2}\right), T_0 = 0.02T_p$. Scales as before.*

Figures 2.13 and 2.14 show the numerical calculation of the thermal Casimir free energy between metals described by the plasma model, Drude model and also for the perfect crystal. At high and low temperatures, an asymptotic evaluation can be done as before.

- *High temperatures*: In this limit, the zeroth Matsubara term dominates and as in section 2.1.6, it is possible to obtain asymptotic expressions. The integrals can be evaluated with help the asymptotic values of the TE and TM reflectivities from equations (1.131, 1.132). In all models $r^{TM}(0) = 1$ so the contribution gives just half the value of the perfect reflector (2.43). The low frequency transparency of the Drude model gives $r^{TE}(0) = 0$ so the TE modes give no contribution whatsoever to the Casimir free energy in this limit. No difference occurs in this limit between the perfect crystal and the Drude model, because $\lim_{T\to\infty} \gamma(T) = \gamma \neq 0$. In the plasma model on the other hand, the contribution is non-vanishing and goes again to the perfect

reflector limit at large distances.

$$\mathcal{F}(T\to\infty) \approx \frac{k_BT}{4\pi}\sum_p\int dkk\ln D_p(0,\mathbf{k}) \tag{2.74}$$

$$= \underbrace{\frac{k_BT}{4\pi}\int dkk\ln[1-e^{-2kL}]}_{\frac{1}{2}\mathcal{F}_C\approx-\frac{k_BTA}{16\pi L^2}\zeta(3)} + \underbrace{\frac{k_BT}{4\pi}\int dkk\ln[1-r^{TE}(0)^2e^{-2kL}]}_{=\begin{cases}0 & \text{Drude}\\ \frac{1}{2}\mathcal{F}_C, & \text{Plasma, } L\gg\lambda_p\end{cases}} \tag{2.75}$$

So, in the limit of large distances and high temperatures, the plasma model recovers the perfect mirror case and the Drude model gives just half the value.

$$\mathcal{F}_{Pl}=\mathcal{F}_C=2\mathcal{F}_{Dr} \qquad \text{as } T\to\infty\ .$$

Of course this translates directly to entropies and forces and it is exactly this factor 2 that has aroused a very hot debate in the last decade: Within the Drude model, it is not possible to retrieve the perfect reflector limit.

- *Low temperatures:* In this case it is not possible to do a simple asymptotic evaluation of the free energy analogous to the perfect reflector, because the integral over wave vectors now involves the reflectivities in a nontrivial way. Asymptotic expansions have been performed e.g. in [Ellingsen *et al.* 2008]. It is possible though to calculate the Casimir entropy directly in a very elegant way, presented in the next section 2.2.3. Before that, a first step is to look at the numerical free energy data, which turn out to differ greatly between the models.

  The only really well-behaved entropy seems to come from the plasma model, which has $S(0)=0$ and goes to a finite positive value $S_{Pl}(\infty)$ at high temperatures. The transition between the low and high T regime occurs, where the thermal scale meets the geometric one, as has been shown for the perfect reflector. This can be seen in fig. 2.13 where the free energy and entropy are given for two different plate distances.

  A striking feature in the Drude model (fig. 2.14) is the regime of negative entropy. Here, the entropy decays from $S(0)=0$ (this cannot be shown in a logarithmic plot) to a negative value on a temperature scale related to the dissipation rate $\gamma L^2/\lambda_p^2$ (*Thouless-energy*). At the onset of the high T regime, the entropy approaches rapidly to the asymptotic value $S_{Dr}(\infty)=\frac{1}{2}S_{pl}(\infty)$.

  Even more challenging is the interpretation of the perfect crystal, given in the same plot, because it features a finite negative entropy $S(0)<0$ at zero temperature. Thus it apparently violates Nernst's theorem, i.e. the third law of thermodynamics (cf. next section), which states that for a non-degenerate system $S(T)\to 0$ as $T\to 0$.

The nonzero entropies, together with the factor 2 in the large distance behavior at finite T have provoked harsh controversies on what has become known as the *thermal problem*. See [Bordag *et al.* 2000, Brevik *et al.* 2006, Klimchitskaya *et al.* 2009] for more extensive reviews.

It was put forward, that a negative ground state entropy should not occur in a supposedly well-defined system like the perfect crystal. On the other hand any tiny dissipation rate - present in any realistic system - is sufficient to at least formally fulfill Nernst's theorem as $T\ll\gamma$ [Boström and Sernelius 2000,Boström and Sernelius 2004,Bezerra *et al.* 2004,Brevik *et al.* 2006,Sernelius 2006a,Hoye *et al.* 2007,Svetovoy 2007,Klimchitskaya and Mostepanenko 2008]. There are also claims, that recent high precision experiments measuring the Casimir force between metallic plates favors the plasma model, even though the Drude model seems to be a far more realistic description for a normal metal. So far, there is not even a consensus on the analysis and interpretation of the data [Boström and Sernelius 2000, Decca *et al.* 2005, Brevik *et al.* 2005, Bezerra *et al.* 2006, Mostepanenko *et al.* 2006, Brevik and Aarseth 2006] and the discussion keeps stirring minds.

2.2.3 Casimir entropy

Calculation of the Casimir entropy

The problem of negative entropy makes it necessary to discuss the origin of Nernst's theorem and the very concept of a Casimir entropy.

In thermodynamics, entropy is obtained from free energy as the negative temperature derivative while a force is the negative derivative with respect to a spatial degree of freedom. In the case of the Casimir force, this is the separation of the cavity boundaries. Force and entropy are thus connected by the Maxwell relation

$$-\frac{\partial^2 \mathcal{F}}{\partial L \partial T} = \left(\frac{\partial F}{\partial T}\right)_L = \left(\frac{\partial S}{\partial L}\right)_T . \tag{2.76}$$

It has recently been stressed by L. P. Pitaevskii [Pitaevskii 2008b, Pitaevskii 2008a], that in a Casimir context, the quantity obtained from the Lifshitz formula is the force, not the free energy. For Nernst's theorem to hold, it is vital, that the L is held constant in the calculation of $\partial F/\partial T$ and taking the limit $T \to 0$. All quantities are regularized by subtraction of the free space value, so there is a constant of integration

$$\Delta S = S(T,L) - S(T,\infty) = -\int_L^\infty \left.\frac{\partial F}{\partial T}\right|_L dL' . \tag{2.77}$$

If the two summands display a different distance behavior and the limit $S(T,\infty)$ remains finite (some support has been given that this is possible), then there is no reason why the Casimir entropy ΔS could not take negative values at finite temperatures. Another open question is, whether a global thermal equilibrium can be assumed in the case of two bodies separated by infinite distance.

It was shown in the last section, that negative entropy occurs in the model of a perfect crystal with a temperature dependent dissipation rate as e.g. in the Bloch-Grüneisen law (1.28) and it turned out to give a finite negative value $S(T \to 0) < 0$. On the other hand, a constant rate of dissipation $\gamma = \text{const.}$ was shown to fulfill Nernst's theorem. The following paragraph presents the formalism from a paper by Intravaia and Henkel [Intravaia and Henkel 2008], who put the results by Sernelius and Boström [Boström and Sernelius 2000] and the model specific calculation by Bezerra *et al* [Bezerra *et al.* 2004] in a general context.

The free energy is represented by a free energy per mode (similar to (2.73), but without performing the k-integral) $k_B T g_{p,\mathbf{k}}(\omega,T) = k_B T g_{p,\mathbf{k}}(i\xi,T) = k_B T \ln\left[1-(r^p(\mathbf{k},i\xi,T))^2 \exp(-2\kappa L)\right]$ evaluated at the Matsubara frequencies $\omega_n = i\xi_n = \frac{2\pi i n k_B T}{\hbar}$

$$\mathcal{F} = k_B T \sum_{p,\mathbf{k}} \sum_{n=0}^{\infty} g_{p,\mathbf{k}}(i\xi_n,T) \tag{2.78}$$

$$\Rightarrow S = -k_B \sum_{p,\mathbf{k}} \sum_{n=0}^{\infty} \left[g_{p,\mathbf{k}}(i\xi_n,T) + i\xi_n \frac{\partial}{\partial\omega} g_{p,\mathbf{k}}(i\xi_n,T) + T\frac{\partial}{\partial T} g_{p,\mathbf{k}}(i\xi_n,T)\right] . \tag{2.79}$$

If the optical properties of the plates depend on temperature, generally the limits

$$\lim_{T\to 0} (\alpha T)^2 \epsilon(\alpha T,T) \neq \lim_{T\to 0}\lim_{\omega\to 0} \omega^2 \epsilon(\omega,T) , \tag{2.80}$$

occurring in the reflectivities, need not coincide. These effects were discussed earlier in sections 1.7.3 and 1.8.3 and it was shown, that TM polarization is not affected by the problem. The order in which the limits are taken has manifest effects only on the zeroth Matsubara term. Introducing a function

$$\hat{g}_{p,\mathbf{k}}(i\xi_n,T) := \begin{cases} \lim\limits_{T\to 0} g(\alpha T,T) & n=0 \\ g_{p,\mathbf{k}}(i\xi_n,T) & n\neq 0 \end{cases} \tag{2.81}$$

which coincides with g at all $\xi_n \neq 0$, the zeroth summand can be isolated and the entropy can be expressed as

$$S = -k_B \sum_{p,\mathbf{k}} \left(\frac{g_{p,\mathbf{k}}(0,T) - \hat{g}_{p,\mathbf{k}}(0)}{2} + {\sum_{n=0}^{\infty}}' \left[\hat{g}_{p,\mathbf{k}}(i\xi_n,T) + i\xi_n \frac{\partial \hat{g}_{p,\mathbf{k}}}{\partial\omega} + T\frac{\partial \hat{g}_{p,\mathbf{k}}}{\partial T}\right]\right) \tag{2.82}$$

$$\Rightarrow S(T\to 0) \approx -\sum_{p,\mathbf{k}} \left(k_B \frac{g_{p,\mathbf{k}}(0,0) - \hat{g}_{p,\mathbf{k}}(0)}{2} + \frac{\hbar}{2\pi}\int_0^\infty d\xi \frac{\partial \hat{g}_{p,\mathbf{k}}}{\partial T}\right) . \tag{2.83}$$

In the limit $T \to 0$, the Matsubara sum can be replaced again by the integral and only two terms survive, the others being proportional to T. The last term vanishes for the plasma and the standard Drude model, because these do not depend explicitly on T, but needs to be considered in the case of the perfect crystal or later in the two fluid superconductor, where such a dependence exists.

Only the first summand depends on the limits $\omega, T \to 0$ and the order in which they are taken. For a plasma and the simplest Drude model $\gamma = \text{const.}$, it is easy to see that the limits (2.80) commute and thus the total entropy at $T = 0$ vanishes.

To check condition (2.80) for a general dissipative model of the Drude form, including a temperature dependent dissipation rate $\gamma(T)$, one has to compare the limits

$$\lim_{T\to 0} \frac{\gamma(T)}{T} \stackrel{?}{=} \lim_{T\to 0} \lim_{\omega\to 0} \frac{\gamma(T)}{\omega} , \tag{2.84}$$

At low temperatures, an ansatz $\gamma(T) \sim T^\beta$ can be used to recover the two interesting cases of the perfect crystal model, where $\beta > 2$, and the impurity dominated Drude model, where $\beta = 0$ (section 1.1.6). The limits depend on the exponent β and since the limit on the right hand side does not exist, the limits cannot commute for $\beta \geq 1$.

In the "normal" Drude model, both limits in (2.84) are divergent but identical (it is also easy to show and that (2.80) is fulfilled), so there is no effect from the first term in (2.83), and also the other term vanish as $T \to 0$ because $\hat{g}$ has no explicit temperature dependence of its own, as was said before. Therefore, Nernst's theorem is fulfilled by the Drude model with constant γ.

If as in the perfect crystal model the dissipation is dominated by electron-phonon scattering or electron-electron scattering, $\beta \geq 2$, so the limits do not coincide. Nicely, in these cases, the last term in the entropy (2.83) vanishes (cf. [Intravaia and Henkel 2008])

$$\frac{\partial \hat{g}}{\partial T} = \frac{\partial \hat{g}}{\partial \gamma} \underbrace{\frac{\partial \gamma(0)}{\partial T}}_{\to 0} \to 0 \qquad \text{as } T \to 0 .$$

Only the contribution from the TE polarizations can show this kind of defect and so the zero-point entropy of the perfect crystal is finally given by the finite negative value

$$S(0) = k_B \sum_{\mathbf{k}} \frac{1}{2} \hat{g}_{TE,\mathbf{k}}(0) < 0 \tag{2.85}$$

$$\approx \frac{\mathcal{F}_C(L)}{2T} \qquad \text{if } L \gg \lambda_T . \tag{2.86}$$

The large distance limit is found by comparing the equation to (2.74), having in mind that the $\hat{g}_{TE,\mathbf{k}}$ behaves like the plasma model at low frequencies. This recovers half of the free energy calculated for the perfect reflector. All results from this section comply well with the numerical data shown in fig. 2.14.

Nernst's theorem

The finite zero-point entropy at $T = 0\,\mathrm{K}$ resulting from some models is apparently in contradiction with Nernst's fundamental theorem [Nernst 1906b, Nernst 1906a], which in its most common form reads

$$T \to 0 \Rightarrow S(T) \to 0 .$$

So far, the theorem, which is at the very heart of the discussion of the thermal problem, has only been quickly introduced in section 2.2.2. This section will discuss its origin and validity.

In his original paper Nernst formulated his principle for the entropies S, S' of a substance in two different states with heat capacities C, C' and claimed that the difference of entropy vanishes

$$\Delta S = S - S' = \int dT \frac{C - C'}{T} \tag{2.87}$$

$$\lim_{T\to 0} \Delta S = 0 , \tag{2.88}$$

leaving the absolute value for $S(T = 0)$ arbitrary. Planck [Planck 1927] subsequently imposed the stronger condition

$$\lim_{T\to 0} C = 0 , \tag{2.89}$$

and thus fixed the constant of integration $S(0) = 0$. The vanishing heat capacity at low temperatures leads to the statement of phenomenological thermodynamics, that "it is impossible to reach $T = 0$ by cooling".

The connection between thermodynamics and statistical physics brought about a more intuitive interpretation of entropy by means of Boltzmann's celebrated formula

$$S = k_B \ln(\Omega) \; . \tag{2.90}$$

while Ω denotes the number of phase space cells connected to a macrostate of given energy in the microcanonical ensemble of classical statistical mechanics. In quantum statistics Ω is the number of quantum-mechanical states of a given energy. In a quantum system with a non-degenerate ground state, the system must necessarily be in just this state at $T = 0$, such that the multiplicity is $\Omega = 1$ and the entropy vanishes $S = 0$. A textbook example for a quantum system with a non-degenerate ground state is the harmonic oscillator. Also, the vibrational degrees of freedom of a solid (phonons) can be modeled as a collection of harmonic oscillators (Einstein-Debye model), and have this property.

On the other hand a system with a degenerate ground state may have a non-zero entropy at zero temperature. Beyond of what can be found in every textbook on thermodynamics and statistical physics, references [Dugdale 1996, Schwabl 2002] cover the topic very thoroughly.

Violation of Nernst's theorem

When Max Planck presented his version of Nernst's theorem, he also pointed out a special case where it does not apply: The model of the *ideal non-interacting gas* [Planck 1927, Fermi 1956], whose entropy is given by

$$S = C_V \log T + R \log V + a \; , \tag{2.91}$$

where a is an integration constant. Obviously $S(T \to 0)$ diverges, unless a is chosen infinite[4]. The reason is easy to find: The description assumes a constant heat capacity C_V, which stands in contrast to (2.89) and is certainly not true for any real gas at low temperatures, where quantum statistics become important.

In the framework of statistical physics it is easier to find systems that feature a physical zero-temperature entropy, connected to a degenerate ground state [Schwabl 2002]. A very simple system of this type is another type of ideal gas, made of *particles with uncoupled spins* s and in the absence of external fields. The partition function decomposes into the single particles' ones, where $\mathcal{Z}_0(T)$ includes all degrees of freedom except the one due to the spin

$$\mathcal{Z}(T) = (2s+1)^N \mathcal{Z}_0(T) \tag{2.92}$$

$$\Rightarrow S(T=0) = k_B N \ln(2s+1) \; . \tag{2.93}$$

Thus, even at $T = 0$ the entropy is extensive and the entropy per particle does not vanish in the thermodynamical limit. Usually it is argued, that in such systems some symmetry breaking must occur at low temperatures, e.g. when the spin coupling starts to dominate over mechanical degrees of freedom. The system is not "ideal" any more and a single ground state is created, so that Nernst's theorem holds eventually.

A related and very common system in everyday life is *ice*, where a ground state degeneracy occurs due to realization of a specific distribution of hydrogen bonds between oxygen and hydrogen atoms, where other possibilities would be energetically equivalent [Schwabl 2002].

But there are also systems that feature a *metastable state* in which the system can get stuck if the temperature drops very quickly, because thermal fluctuations will only very seldom lift the system above the activation threshold. Thus the relaxation to the fundamental state is suppressed by the kinetics of the thermodynamical process and the system will remain in the metastable state for all experimentally accessible times. Obviously such systems do not meet the requirements of *ergodicity*[5]

[4] The volume must be held constant. Nernst's theorem does not apply, if temperature and volume vary at the same time [Pitaevskii 2008b]

[5] In an ergodic system, the phase space trajectory ϕ fills the iso-energetic subspace Γ densely and homogeneously, i.e. it gets arbitrarily close to any state that is energetically allowed at some point. In this case the time average along the trajectory and the phase-space average coincide.

$$\langle A \rangle_t = \lim_{T\to\infty} \frac{1}{T} \int_0^T dt A(\phi(t)) \equiv \langle A \rangle_\Gamma = \frac{1}{\Gamma} \int_\Gamma d\phi A(\phi)$$

So, in some sense, in the metastable systems described above, the trajectory is just not long enough to fill the phase space.

and hence are not thermal equilibrium states in the sense of statistical mechanics. In this case it may be very reasonable to introduce a finite zero-temperature entropy, which can be calculated in the microcanonical ensemble[6] .

Such behavior is known from *glasses* made of SiO or from polymers. These materials feature a glass-transition (liquid to crystalline or amorphous). A special example given e.g. in [Schwabl 2002] are *binary alloys* like brass CuZn in the β-phase, which show a phase transition that depends crucially on the kinetics. A slow cooling will lead to a well-ordered structure of low residual entropy, while fast cooling makes it impossible for an equilibrium structure to be reached. The resulting lattice is not well ordered and can be attributed a considerable entropy that persists even at low T. Even though these systems are not in total thermal equilibrium, some degrees of freedom decouple and can be considered in thermal equilibrium. For instance the phonon gas will relax quickly to a distribution well-described by equilibrium thermodynamics (Einstein-Debye statistics). As a result of the decoupling of different subsystems, one can introduce more than one effective temperature present at once.

2.2.4 Diamagnetism and diffusive modes

Now, how is the negative Casimir entropy to be interpreted? Is it a relict of a inconsistent renormalization or is it a physical entropy related to a degenerate ground state?

1. $T > 0$: Here a negative value of the Casimir entropy $S < 0$ does not create problems. It was shown before, that this can happen just because the Casimir entropy is a entropy difference w.r.t. isolated plates.

2. $T = 0$: The value $S(T \to 0) < 0$ in the perfect crystal is more puzzling. An elegant solution to the conundrum could be a glassy state.

Intravaia and Henkel [Intravaia and Henkel 2009] have recently shown, that the negative entropy in the Drude model stems from a set of diffusive *Foucault* or *eddy current modes*. The finite entropy attributed to these modes, motivates the postulation of a *Foucault glass* state present in the perfect crystal at low temperatures. If the eddy contribution were suppressed in a normal metal, the negative entropy supposedly violating Nernst's theorem would not appear.

It is not very intuitive though, why this should happen, after what has been said on the influence of dissipation on causality and optics. A recent argument by Bimonte [Bimonte 2009] stresses this yet again: Since any material described by classical physics cannot be diamagnetic according to Bohr-van Leeuwen's theorem (e.g. [Soldati 2003]), it should always become transparent to low frequency magnetic fields. This coincides with the value of $r^{TE}(0) = 0$ in the Drude model and imposes a strong condition on the possible mechanisms that could suppress the diffusive modes in a normal metal. It would have to be a quantum effect that survives in the classical limit where commonly the models works quite well. Interestingly, such an effect could also explain the large distance behavior.

It is interesting, to think of what happens in a superconductor. Here, the $U(1)$ gauge symmetry is broken (see chapter 1.5) and a diamagnetic response is no problem, because superconductivity is a manifest quantum effect. At $T = 0$ the superconductor can be safely assumed to be completely in the London-state, i.e. it is well-described by the plasma model. The eddy currents must collapse to the collective mode which in a superconductor is the only mode on the imaginary axis. This can be seen as a rearrangement of the eddies, which now produce the diamagnetic surface current responsible the Meißner-Ochsenfeld effect. Hence there is some different level of order present in a superconductor and a change of entropy seems reasonable. At this point it is not yet possible to give a final statement on neither of the topics of this paragraph and further investigation is necessary.

[6] Conceptually, one should spend some thoughts on the differences between the *microcanonical* and the *canonical ensemble* description. Entropy and temperature can be defined in either description and coincide.

Ergodicity is usually introduced as a property of an isolated system, described by the microcanonical ensemble and characterized by its fixed energy. The system considered here is coupled to a thermal bath and thus described in the canonical ensemble, where not the energy is fixed but its average value [Soldati 2003].

Let Γ_A be the phase space of the system and Γ_B the one of the bath. If a microcanonical picture is to be applied, the bath must be included into the description and the total phase space is given by $\Gamma(E) = \prod_{E_B} \Gamma_A(E-E_B) \otimes \Gamma_B(E_B)$. Nevertheless, if the trajectories $\phi \subset \Gamma_A$ fail to fill the subspace Γ_A, the system A is non-ergodic leaving out the bath, and so neither is the complete system Γ including it.

2.3 Two-fluid superconductors

2.3.1 The superconducting transition

From the experimental point of view, the thermal problem is basically the question, to which model data should be fitted. In this context, different experimental setups involving superconductors have recently been brought into the discussion by Bimonte [Bimonte *et al.* 2005b, Bimonte *et al.* 2005a, Bimonte *et al.* 2006, Bimonte 2008]. The basic idea is that the plasma model should describe well a superconductor below $T = T_c$ and above it is just a normal metal (Drude model). Thus, there should be a significant change in the interaction energy *if* the normal metal is described by the Drude model, and the change should be much smaller or even vanishing, if the normal metal, too, is better described by the plasma model (for whatever physical reason). Thus, superconductors might be a means for investigating the mechanisms responsible for the thermal anomalies encountered in the thermal Casimir effect.

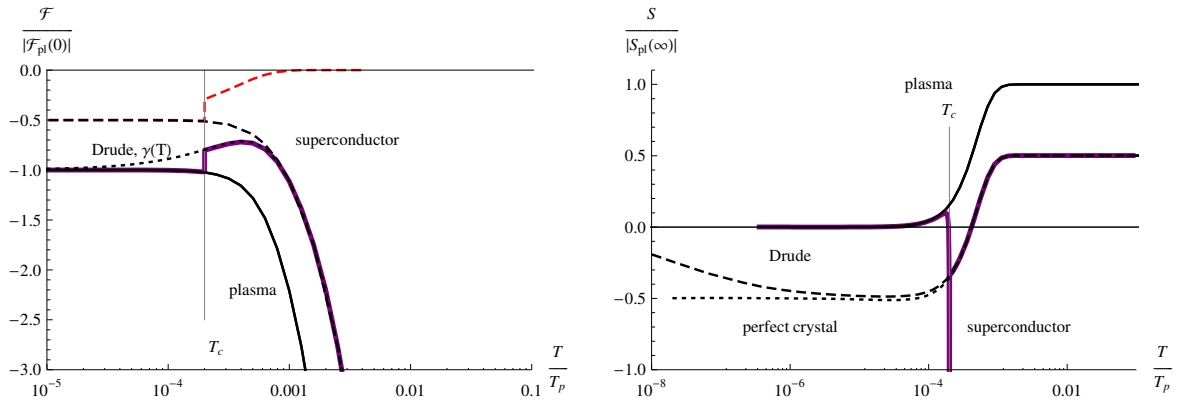

Figure 2.15: *Casimir free energy (left) and entropy (right) in a two fluid model (purple) and the other models for comparison. The critical temperature is $T_c = 2 \cdot 10^{-4} T_p$, $L = 100\lambda_p$, $\gamma = 10^{-3}\omega_p$. As before, dashed red and black lines show the TE and TM contributions to the free energy.*

In his first papers on the Casimir interaction involving superconductors, Bimonte considered a abrupt transition between the plasma and the Drude-model at T_c (later work has also included BCS-superconductors using the evaluation at imaginary frequencies developed previously).

A next step towards a more realistic description of the phenomena can be obtained using the two fluid model. The results of numerical calculations of the Casimir free energy for such a model are shown in fig. 2.15. Rather than use an abrupt transition between plasma and Drude behavior, it features a continuous interpolation of the optical properties that occurs below T_c. The change of the material properties translates to a continuous transition of the free energy from the plasma curve at $T = 0$ to the Drude curve, with which it must of course coincide for $T \geq T_c$. A plot of the free energy in this interval is given in fig. 2.16. A non-intuitive effect occurs in the entropy. Very slightly below T_c it decays to large negative value and then jumps back onto the Drude curve at the critical temperature. This is a consequence of the form of the order parameter, whose intrinsic temperature dependence dominates the thermodynamics at temperatures close to the critical transition. In the following these effects will be investigated in more detail.

2.3.2 Casimir entropy

Entropy at $T = 0$

A two fluid model interpolates between the plasma and the Drude model. It must asymptotically approach the plasma model at low temperatures $\epsilon \approx \epsilon_{Pl}$ and a Drude-like behavior above the superconducting phase transition $\epsilon(T > T_c) = \epsilon_{Dr}$.

A class of two fluid models is given by

$$\epsilon(\omega,T)=\eta(T)\epsilon_{Pl}(\omega)+[1-\eta(T)]\epsilon_{Dr}(\omega)\;, \tag{2.94}$$

where the order parameter $\eta(T)$ needs not necessarily be of the Gorter-Casimir type[7] (1.84) but must fulfill several conditions in order to guarantee the interpolation properties:

1. $\eta(T)\in[0,1]\Leftrightarrow$. Since $\eta(T)=n_s/n$ is fraction of charge carriers contributing to the supercurrent, this is just the conservation of charge[8].
2. $\eta(0)=1\Leftrightarrow$ Full superconductivity at $T=0$.
3. $\eta(T)$ has no discontinuities $\Leftrightarrow$ Continuous phase transition.
4. $\frac{d}{dT}\eta(0)=0\Leftrightarrow$ Ensures, that the plasma model holds in an environment of $T=0$. This can also be seen as a requirement obtained from experimental results in the regime, where the measured gap function coincides well with the order parameter.

With help of the formalism from [Intravaia and Henkel 2008] exposed in section 2.2.3 the entropy at $T=0$ can be calculated from the free energy densities as before. For the superconductor there is an additional explicit temperature dependence of the order parameter and the relevant derivative in eq. (2.83) becomes

$$\frac{\partial\hat{g}}{\partial T}=\underbrace{\frac{\partial\hat{g}}{\partial\gamma}}_{(*)\;\to 0\text{ at }T=0}\frac{\partial\gamma(T)}{\partial T}+\frac{\partial\hat{g}}{\partial\eta}\underbrace{\frac{\partial\eta(0)}{\partial T}}_{(**)\;\equiv 0}\;. \tag{2.95}$$

Since the two fluid model approaches the plasma value at $T=0$, a possible thermal dependence through $\gamma(T)$ becomes irrelevant, since it is quenched by the order parameter (condition 1): Even if the dissipative current contribution is described through a perfect crystal model (*clean superconductor*), the previously troublesome part (*) is simply switched off at low T.

The additional term due to the order parameter (**) might also cause an entropy defect at $T=0$, but only if $\frac{\partial\eta(0)}{\partial\tau}\neq 0$. These models are excluded by condition 4, because though they would approach the plasma model value of $\epsilon(\omega)$ at $T=0$, the plasma model would not describe the asymptotic behavior which is well established experimentally. Therefore there is no contribution to entropy at $T=0$ from any explicit temperature dependence of the model.

The last remaining term in (2.83) is the one connected to the order of the limits. This term, too, vanishes, again due to the plasma model asymptotics. As before, one must compare the limits

$$\lim_{T\to 0}(\alpha T)^2\epsilon(\alpha T,T)\overset{?}{=}\lim_{T\to 0}\lim_{\omega\to 0}\omega^2\epsilon(\omega,T)\;. \tag{2.96}$$

A direct calculation gives

$$\begin{aligned}
\lim_{T\to 0}\lim_{\omega\to 0}\omega^2\epsilon(\omega,T) &= -\omega_p^2\lim_{T\to 0}\eta(T)=-\omega_p^2\\
\lim_{T\to 0}(\alpha T)^2\epsilon(\alpha T,T) &= -\omega_p^2-\lim_{T\to 0}[1-\eta(T)]\cdot\left[\frac{1}{1+\frac{i\gamma(T)}{\alpha T}}\right]\\
&= -\omega_p^2+0\cdot\underbrace{\lim_{T\to 0}\frac{1}{1+\frac{i\gamma(T)}{\alpha T}}}_{:=A}\;.
\end{aligned} \tag{2.97}$$

Conditions 3 - 4 make sure for $T=0$ to be an accumulation point of the domain of $\eta(T)$, so the limits can be separated[9] and even though $\gamma(T)/\alpha T\to 0$ or ∞, the limit $A\to 1$ or 0 is always finite.

[7] The Gorter-Casimir like models are of course a special case. Here $\eta_a(T)=1-(T/T_c)^a$, where typically $a=4$. Note that all models with $a>1$ meet the conditions 1 - 4. The special value $a=1$ violates number 4 and gives a pseudo-two fluid model, without the plasma asymptotic which - if evaluated asymptotically or numerically - features a non-vanishing zero-point entropy, in agreement with the results of this section.

[8] It was mentioned earlier that in BCS theory, due to the quantum nature of the charge carriers, interference effects occur and lead e.g. to the coherence peak (cf. sections 1.4.1, 1.7.4 and 1.6.2). To obtain a similar peak in a classical model, one would require $\eta>1$.

[9] *Let $f,g:\;D\subseteq\mathbf{R}\mapsto\mathbf{R}$ and p an accumulation point of D, i.e. $p\in\bar{D}$. If the limits $\lim_{x\to p}f(x)=a,\lim_{x\to p}g(x)=b$ exist, then $\lim_{x\to p}f(x)\cdot g(x)=a\cdot b$.*

It has now been shown, that due to asymptotic plasma-like behavior at low temperatures, Nernst's theorem holds for the whole class of two fluid models and order parameters as specified above, including those where γ depends on temperature.

A minimum of entropy

The Casimir entropy in the two fluid model features a local minimum at temperatures slightly below T_c, i.e. before the entropy discontinuity.

The free energies $\mathcal{F}(T)$ must be continuous through the superconducting transition and it has been shown that $\mathcal{F}_{Dr}(T) \geq \mathcal{F}_{Pl}(T)$ and $S_{Dr}(T) \leq S_{Pl}(T)$ at all T. So there must be a transition between the asymptotic regimes, and it follows from the mean value theorem applied to $\mathcal{F}$ and S that either

- $\mathcal{F}(T)$ must be monotonous and grow with T
- or have at least one inflection point where the derivative changes from $+$ to $-$.

The second case is the mathematical definition of a minimum of the entropy and in the first, the minimum coincides with the entropy discontinuity.

This shows that the local minimum of the Casimir entropy is a general feature of superconductors and not a relic of the description used: It is just the consequence of the fact that the free energy must in some way arrive at the Drude curve starting from the plasma value. Until now, the effect has only been presented in the two fluid model, but it can be expected to arise similarly from BCS theory, too. In fact this will be one of the results shown in the next section.

In a two fluid model, the minimum can be deduced directly from the order parameter. If the order parameter is differentiable at the phase transition ($\eta(T_c) = 0$, $\frac{d}{dT}\eta(T_c) = 0$), there is no discontinuity of free energy or entropy and a minimum of entropy must occur at $T < T_c$ in contrast to the scenario, where $\partial\eta/\partial T$ is discontinuous as in the Gorter-Casimir model and the entropy minimum occurs at $T = T_c$.

Entropy jump at T_c

The numerical results for a two fluid model with a Gorter-Casimir oder parameter given in fig. 2.15, feature a cusp of the free energy at T_c, connected to a jump of entropy or equivalently a latent heat.

It is possible to identify the source of the jump: Writing the entropy in terms of the free energy

$$\begin{aligned} S &= \int d\omega \sum_{p,\mathbf{k}} \frac{d}{dT} \left[k_B T \ln D_p(\omega, \mathbf{k})\right] \\ &= \int d\omega \sum_{p,\mathbf{k}} k_B \ln D_p(\omega, \mathbf{k}) + \int d\omega \sum_{p,\mathbf{k}} k_B T \frac{\partial \ln D_p(\omega, \mathbf{k})}{\partial \epsilon} \frac{\partial \epsilon}{\partial \eta} \frac{\partial \eta(T)}{\partial T} \qquad (2.98) \\ \Delta S &= -\lim_{\tau \to 0} [S]_{T_c - \tau}^{T_c + \tau} \qquad (2.99) \end{aligned}$$

The first integral for ΔS vanishes, since drastic changes near T_c stem from the dielectric function $\epsilon(\omega, T)$ and not from the explicit prefactor T. The second one is identically zero above T_c, where $\eta(T) \equiv 0$, so only the limit of the superconductor at T_c is relevant, where $\partial\epsilon/\partial\eta = \epsilon_{Pl} - \epsilon_{Dr}$

$$\Delta S = -k_B T_c \underbrace{\frac{\partial \eta(T_c - 0^+)}{\partial T}}_{=:\delta_T \eta} \int d\omega \sum_{p,\mathbf{k}} \frac{\partial \ln D_p(\omega, \mathbf{k})}{\partial \epsilon}\bigg|_{\epsilon = \epsilon_{Dr}} \left[\epsilon_{Pl}(\omega) - \epsilon_{Dr}(\omega)\right] \qquad (2.100)$$

As before, the low frequencies give the important contribution to the entropic effects, since $\epsilon_{Pl}(\omega) - \epsilon_{Dr}(\omega)$ vanishes at high frequencies, introducing a kind of cut-off in the order of γ into the integral. In the Gorter-Casimir model, the term $\delta_T \eta = -\frac{4}{T_c}$ but in a model, where the order parameter is differentiable at $T = T_c$, $\delta_T \eta = 0$ and $\Delta S = 0$. On the other hand, if the BCS gap function $\Delta(T)/\Delta(0)$ is used as the order parameter in a two fluid model, $\delta_T \eta \to -\infty$ and so does the entropy discontinuity.

2.4 BCS superconductors

As a next step, it is highly interesting to compare the previous results of the two fluid model to the BCS theory. The Casimir free energy has been calculated using Zimmermann's version of Mattis-Bardeen theory. In practice it turned out to be impossible to do the numerics in decent time using either the real frequency version or the continuation through Kramers-Kronig relations, which involves another integral for each frequency. This was the reason, why the direct analytical continuation to imaginary frequencies as presented in section 1.6.3, was calculated to start with.

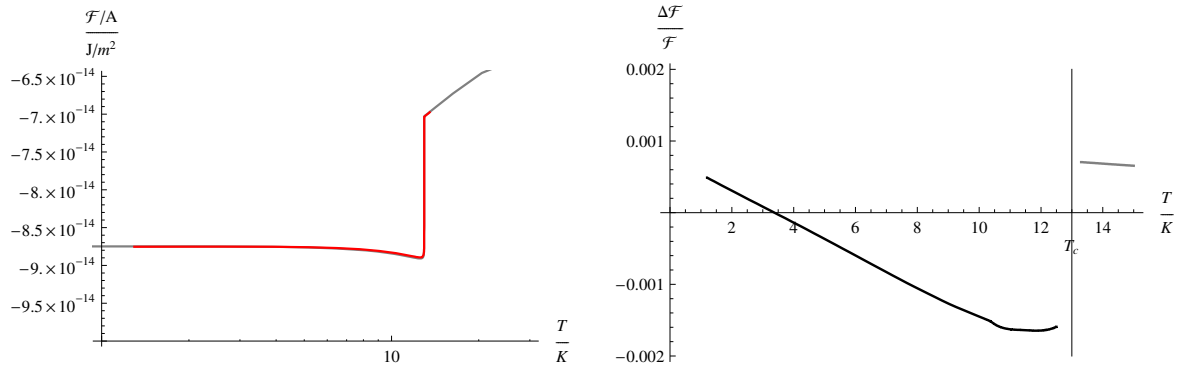

Figure 2.16: *Left: Casimir free energy in the BCS model (red) and two fluid model (gray), critical temperature* $T_c \approx 13K$, $\omega_p = 8.95 \cdot 10^{15} s^{-1}, \gamma = 5 \cdot 10^{-3}\omega_p$ *and at a plate separation of* $L = 2\mu m$. *Right: Relative difference between the results obtained in the BCS and two fluid description.*

The numerical results of the BCS model are shown in fig. 2.16 together with the data obtained in the two fluid model (cf. previous section) and show a complete coincidence at the parameters chosen up to a relative precision of $\leq 2 \cdot 10^{-3}$ for all temperatures below T_c. Near the critical temperature the differences are largest. Beyond the critical temperature, the models coincide exactly and the resulting deviation (gray line in the right plot) is comparable to the numerical error from the Matsubara summation, i.e. the value fits well with the one used for the cut off criterion (2.50).

This high agreement is somewhat fortuitous due to the choice of parameters. In section 1.7.4 it was shown, that in the regime $\hbar\gamma \approx \Delta(0)$, the optical response of the two fluid and BCS descriptions coincide very well. This may put a limit to the application of the two-fluid model instead of the numerical more challenging BCS model, but it was shown earlier, that this regime of γ is not unreasonable for common metals.

In any case, after what has been said in the previous section about the dependence of the entropy-jump in a two-fluid model of the slope of $\eta(T)$ at T_c, it is relieving to see, that the discontinuity obtained from the BCS-theory is finite and coincides well with the prediction from the Gorter-Casimir model.

In future work, the dependence on the value of γ will be considered also outside the regime of good coincidence. It would be especially desirable to find a precise interval in which the application of the two fluid model is justified.

2.5 Conclusions

In this chapter the interaction of two metallic or superconducting plates was investigated. Two alternative descriptions due to Casimir and Lifshitz were presented, and it was shown, how the Lifshitz formula covers more general classes of systems including dissipative ones. In a next step nonzero temperatures have been included in the calculation. It was shown, how the infinite Matsubara sums can be evaluated to good precision numerically using a self-adjusting cut-off criterion.

The perfectly reflecting cavity was presented as a first instructive example and showed characteristic features which survive also for more realistic cavities. The most important result was a crossover to a distance power law $\mathcal{F} \sim TL^{-2}$ in the thermal regime where the thermal wavelength is small compared to the plate distance.

In metals, the surface plasmons were shown to dominate the interaction at small distances, where they give rise to another crossover to power law to for the free energy vs. distance to $\mathcal{F} \sim \omega_p L^{-2}$ at distances small compared to the plasma wavelength. The thermal correction to the plasmonic Casimir energy was calculated numerically and asymptotically for the first time, and the energy correction factor was found to be $\eta(T, L) = \mathcal{F}(\mathcal{L}, \mathcal{T})/E_C(L) \sim L$ at small distances, where its slope depends on temperature.

Then the complete spectrum of modes in a plasma, Drude metal and perfect crystal was considered, previous results were recovered. These included a notorious factor 2 between the free energies of the plasma and the Drude model, and negative entropies occurring in the dissipative models at low temperatures. Some arguments have been given, why negative Casimir entropies – measuring entropy differences – at finite temperatures are not unphysical, and how the violation of Nernst's theorem at $T = 0$ featured by some models could be understood in terms of a *Foucault glass*.

From there it was a natural step to consider superconductors, for which is known that the plasma model is a decent description at very low temperatures. The description of superconductors in terms a two fluid model lead to a characteristic jump of entropy in the superconducting transition at T_c and to a minimum of entropy slightly below and it was proven that Nernst's theorem holds for a general class of two fluid models.

Finally the optical description obtained from BCS theory at imaginary frequencies obtained in the first chapter was used to describe the optical properties of the superconducting surface in the calculation of the Casimir effect. The numerical results for the Casimir free energy obtained in this model agree to great accuracy with the ones calculated for the two fluid model, at least in the reasonably realistic regime $\hbar\gamma \approx \Delta(0)$ encountered already earlier. This shows, that for the purpose of predicting the Casimir effect between superconducting plates, it is sufficient (at least in this regime) to use the two fluid description. This is much easier accessible to analytical calculations and also advantageous for numerical simulations.

3 Casimir-Polder interaction

3.1 Casimir polder interaction

3.1.1 Atoms near surfaces

Until now, the interaction of two macroscopic bodies has been studied in a framework in which the microscopic structure of matter has been used only to determine macroscopic electrodynamic response functions. This chapter will investigate the interaction of single atoms with a surface, where the dynamics of the atom becomes relevant.

Starting from the Casimir configuration involving two plates in global thermal equilibrium, this new scenario can be thought to be obtained in a *dilute limit*, first considered by Lifshitz [Lifshitz 1956]: If one of the plates is made ever less dense, the collective effects such as the Lorentz polarization field or conductivity vanish and what remains are the single non-interacting atoms of the wall, which are characterized by a magnetic and electric polarizability. It is not generally possible to do the calculation the other way round, i.e. to recover the Casimir interaction of two macroscopic bodies outside the dilute limit from summing up the single atoms' interactions. This is because in the dilute limit, nonadditivity and screening effects are excluded from the beginning. See also [Spagnolo 2009] and [Buhmann and Scheel 2008] for non-equilibrium situations.

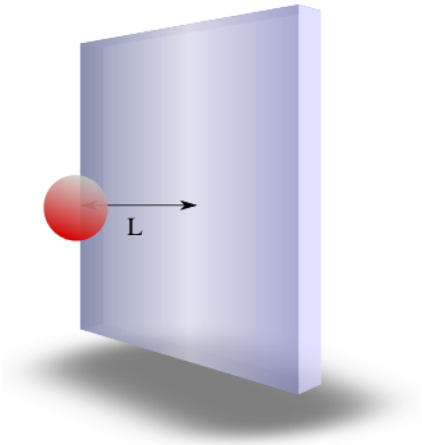

Figure 3.1: *Atom near a metallic surface. The atom is characterized through its electric and magnetic dipole moments.*

Historically, the idea of dispersion forces was proposed by van der Waals [Van der Waals 1873]. He assumed, that close to a polarizable medium (another atom or a metallic surface) a *spontaneously* polarized atom will feel the field created by its own mirror charge. Fritz London [London 1930, London 1937] was the first to give a quantitative description of the interaction. A complete calculation for perfect reflection including the retardation effects was done by Casimir and Polder [Casimir and Polder 1948].

The idea of the charge/mirror-charge interaction is catchy but it does not give the complete picture. The reason is, that there is more than one contribution to an atom's polarization:

- *Spontaneous fluctuations* of the charge densities in the atom.
- *Mirror polarization* due to induction from the mirror(-charge), which is statistically perfectly correlated to the atom's spontaneous fluctuations.
- *Induced polarization* due to other atoms' (or the mirror's) own spontaneous fluctuations. This contribution is statistically independent from the spontaneous fluctuations of the atom.

Therefore in a setup with physical mirrors or two atoms, the other object will not only mirror the first atoms' fluctuation but also show fluctuations of its own that will "blur" the mirror image.

Casimir and Polder considered the interaction of an atom, characterized by its static electric polarizability α with a perfectly reflecting wall at the distance L. Their result for the interaction energy (at zero temperature) in the retarded regime reads

$$U(L) = -\frac{3\hbar c\alpha}{\pi L^4} \,. \tag{3.1}$$

In this section, energies will be labeled U, to distinguish them from electric field components.

3.1.2 Experiments

A handful of recent experiments have probed the atom-wall interaction. Reviews can be found in [Aspect and Dalibard 2002, Spagnolo 2009]. There are different approaches, the most important of which are the following:

- *Scattering of thermal atom beams*: Early experiments used a thermal atom beam of scattering of atoms from a crystalline surface. If the deBroglie wavelength of the atoms is in the order of the lattice distance of the crystal, Bragg-diffraction occurs. On these length scales, the Casimir-Polder forces have a relatively long range, and can be extracted from the diffraction pattern – similar to a surface form factor. A theoretical work on this field was given in [Beeby and Thomas 1974].
- *V-setup*: In this setup described by Sukenik *et al.* [Sukenik *et al.* 1993] atoms travel slowly through a cavity made of plates that form a small angle (V-shape). Thus, the setup allows to change the cavity width by moving the source vertically. Inside the cavity, already the (classical) transverse momentum distribution leads to a certain geometric loss of the atoms that hit the walls. Further loss is due to the attractive Casimir-Polder forces. The actual number of atoms arriving at a detector is then measured and compared to Monte-Carlo simulations. At large plate distances, the purely geometric losses dominate, but below a critical width, the Casimir-Polder losses become significant. This experiment allowed for the use of ground-state atoms and showed good agreement at both retarded and non-retarded distances with an accuracy of about 10%.
- *Light force potential*: Here, the equilibrium between a repulsive light force and the attractive surface interaction is used to establish a potential barrier, that can be well controlled by changing the light field. The barrier height influences is then probed through the reflectivity for incident atoms [Landragin *et al.* 1996].
- *Quantum reflection*: Atoms move under a small angle towards a surface, carrying a small kinetic energy in the perpendicular direction. Classically, a potential gradient leads to an attractive force and adsorption of the atoms. Due to quantum reflection in the potential gradient, most of the atoms will not reach the plate but are deflected from the surface. It can be shown, that very slow atoms will actually be reflected perfectly. Experiments demonstrating quantum deflection have been conducted with H atoms on a liquid helium surface and also for Ne atoms at solid surfaces. Measuring the atom-reflectivity in function of the atoms' velocity, the reflecting potential can be reconstructed. This has been done [Shimizu 2001] for the Casimir-Polder potential in the retarded regime quite far from the surface, where quantum deflection is mostly sensitive.
- *Spectroscopic measurements*: The atom-wall interaction leads to a distance-dependent shift of the atomic energy levels which may be detected by resonant spectroscopic techniques. These techniques offer a very high precision, but involve necessarily energy shifts for excited atoms which behave very differently from atoms in the ground state. The Casimir-Polder forces have successfully been probed in such experiments [Laliotis *et al.* 2007, Sandoghdar *et al.* 1992, Failache *et al.* 1999].
- *Oscillation frequency shift*: Very precise measurements of the Casimir-Polder force including the thermal correction have been done by Obrecht *et al.* [Harber *et al.* 2005, Obrecht *et al.* 2007, Obrecht 2007] by measuring the frequency of center of mass oscillations of the atoms inside chip-based trap. As the trap-minimum is moved closer towards the surface, the Casimir-Polder forces change the curvature of the potential which leads to a relative change of the oscillation frequency in the order of 10^{-4} [Antezza *et al.* 2004]. The same basic concept was applied by Capasso *et al.* [Chan *et al.* 2001, Iannuzzi *et al.* 2004, Lisanti *et al.* 2005] to measure the Casimir effect between macroscopic bodies (section 2.1.5).
- *Deformed trapping potential*: In modern atom chip setups, cold neutral atoms can be trapped close to a surface in a magnetic trap. The trapping potential is usually measured by direct imaging of an atomic cloud inside the trap. Close the surface the Casimir-Polder interaction deforms and finally destroys the trap potential which is frequently seen (see e.g. [Petrov *et al.* 2008] for an example in a trap involving a carbon nanotube). This kind of measurement seems basically possible, e.g. [Yuju *et al.* 2004].

3.1.3 Atom-surface interaction at $T = 0$

The interaction of a neutral atom with an external field can be expressed through its multipole coefficients. The most important contributions stem from the lowest electric and magnetic multipole moments, because the atom size is small compared to the relevant wavelengths. Usually, the dominating one is the electric dipole moment

(E1), followed by the magnetic dipole moment (M1) and the electric quadrupole contribution (E2). In atoms, the multipole moments are connected to specific transitions between energy states. In alkali atoms, for example, E1-transitions connect to electronic ground state to excited states with transition frequencies in the visible range ($\approx 10^{15}$ Hz) and M1 transitions occur between Zeeman- or hyperfine states with much lower transition frequencies (MHz $-$ GHz) [Henkel 2005].

The electric dipole case has been investigated thoroughly e.g. [Antezza *et al.* 2004, Spagnolo *et al.* 2006, Scheel and Buhmann 2008, Bezerra *et al.* 2008] so this chapter will focus mainly on the magnetic dipole contribution and use previous work done by Power [Power *et al.* 2005b, Power *et al.* 2005a] and Spagnolo [Spagnolo and Intravaia 2008, Spagnolo 2009]. A comparison to the electric case will be done on the basis of the numerical data. Generally, the magnetic dipole coupling is much smaller than its electric counterpart. Anyhow this is partially compensated, because it has been shown in [Joulain *et al.* 2003] that the local magnetic density of states (LMDOS) close to a surface is higher than its electric equivalent (LEDOS) by orders of magnitude.

In the case of the Casimir-Polder interaction, the multipole-moments involved are not static due to fluctuations and induction, but physically this does not change the form of the interaction Hamiltonian, e.g. [Spagnolo 2009]. Splitting the contributions to the magnetic dipole moment into spontaneous fluctuations and the induced part $\boldsymbol{\mu} = \boldsymbol{\mu}_{ind} + \boldsymbol{\mu}_{fl}$, the interaction energy with an external magnetic field $\mathbf{B} = \mathbf{B}_{ind} + \mathbf{B}_{fl}$ is

$$U = -\frac{1}{2}\langle \boldsymbol{\mu} \cdot \mathbf{B} \rangle \, . \tag{3.2}$$

The induced dipole is due to the polarizability β and the induced part of the field is the response to the fluctuations of the source dipole (using a Green's tensor H)

$$\mu_i^{ind}(\omega) = \beta_{ij}(\omega) B_j^{fl}(\omega) \tag{3.3}$$

$$B_i^{ind}(\omega) = H_{ij}(\omega) \mu_j^{fl}(\omega) \, . \tag{3.4}$$

Assuming statistical independence of the dipole and field fluctuations, the interaction energy at zero temperature can be evaluated with help of the dissipation-fluctuation theorem and gives an expression obtained by Wylie and Sipe [Wylie and Sipe 1984, Wylie and Sipe 1985]

$$U(\mathbf{r}) = -\frac{\hbar}{2\pi} \, \mathrm{Im} \int_0^\infty d\omega \beta_{ij}(\omega) H^{ji}(\mathbf{r}, \omega) \, . \tag{3.5}$$

So, very similar to the two-plates scenario, the interaction energy of a dipole with a surface, which enters the description via the Green's tensor, is given by an integral over a spectral energy density. At $T = 0$, the atom is in the ground-state and so only transitions from and to the ground state can contribute to the magnetic polarizability, which is given by

$$\beta_{ij}(\omega) = \sum_m \frac{\langle 0|\mu_i|m\rangle\langle m|\mu_j|0\rangle}{\hbar} \frac{2\omega_{0m}}{\omega_{0m}^2 - (\omega - i0)^2}, \qquad \omega_{0m} = \frac{E_0 - E_m}{\hbar} \tag{3.6}$$

In the upcoming calculations, the atom was modeled as a two-level system, so the sum collapses to only one transition with a transition frequency $\omega_{01} =: \Omega_m$. Here the magnetic moment is due to electron spin only (orbital angular momentum $L^2 = 0$), the two states correspond to the spin orientation and the matrix element can be assumed to be in the order of Bohr's magneton μ_B

$$\mu_i = -\frac{\mu_B g_s \sigma_i}{2} \Leftrightarrow |\langle 0|\mu_i|1\rangle|^2 = \frac{\mu_B^2 g_s^2}{4}, \tag{3.7}$$

where $g_s \approx 2.0$ is the Landé g-factor for the electron and σ_i is a Pauli matrix.

To obtain the analog equations for the electric dipole contribution, the magnetic polarizability β and the Green's tensor H have to be replaced by the corresponding electric quantities α, G. The electric and magnetic Green's functions at a surface are obtained from one another by interchanging the reflectivities $r^{TM} \leftrightarrow r^{TE}$, and the polarizabilities require the replacement of the transition frequency $\Omega_m \leftrightarrow \Omega_e$ and the dipole moment $\langle 0|\mu_i|1\rangle \leftrightarrow \langle 0|d_i|1\rangle$, i.e. $\frac{\mu_B^2 g_s^2}{4} \leftrightarrow \frac{e^2 a_0^2}{3}$, where a_0 is the Bohr's radius [Power *et al.* 2005b, Power *et al.* 2005a].

3.1.4 Atom-surface interaction at finite temperature

At non-zero temperature the free energy rather than the internal energy is the relevant thermodynamic potential. As in the Casimir effect, the thermal effects can be included by introducing a thermal kernel [Novotny and Henkel 2008, Wylie and Sipe 1985]

$$\mathcal{F}(\mathbf{r}) = -\frac{\hbar}{4\pi}\,\mathrm{Im}\int_{-\infty}^{\infty} d\omega \beta_{ij}^{T}(\omega) H^{ji}(\mathbf{r},\omega)\coth\left(\frac{\hbar\omega}{2k_BT}\right)\,. \tag{3.8}$$

The polarizability itself depends on temperature, which must be taken into account according to the system under consideration.

- *Thermal equilibrium:* The system is in total thermal equilibrium and at finite temperature the atoms near the surface will no longer be in the electronic ground state (or its Zeeman-/hyperfine states), but thermally excited . The following sections will deal with such situations.

- *Non-equilibrium:* Typically, in magnetic traps including the ones integrated on a microchip, there are not single atoms but a cloud of ultracold atoms or a Bose-Einstein condensate (BEC). Thus the system is not in global thermal equilibrium, and while the chip surface has room temperature, the ensemble of atoms can be attributed an effective temperature which lies typically in the order of μK [Spagnolo 2009] and is often modeled as zero [Buhmann and Scheel 2008]. This is not a bad choice, since ground state cooling is possible, and especially in BECs the ground state is populated macroscopically. A different non-equilibrium situation describes field due to two different temperatures scales, one for the chip surface and one for the "surrounding chamber" [Antezza *et al.* 2005, Antezza *et al.* 2008, Antezza 2008].

The polarizability of an excited atom differs from the one in the ground state, because now the transitions between different excited states must be taken into account, too:

$$\beta_{ij}^{T} = \sum_{n,m}\frac{\exp\left(-\hbar E_n/k_BT\right)}{\mathcal{Z}}\frac{\langle n|\mu_i|m\rangle\langle m|\mu_j|n\rangle}{\hbar}\frac{\omega_{nm}}{2\omega_{nm}^2-(\omega-i0)^2}\,, \tag{3.9}$$

where $\mathcal{Z}$ is the partition function of the system. For the two-level system the thermal polarizability takes the very simple form [Spagnolo 2009]

$$\beta_{ij}^{T}(\omega) \;=\; \tanh\left(\frac{\hbar\Omega_m}{2k_BT}\right)\beta_{ij}(\omega)\,. \tag{3.10}$$

At $T=0$, both the thermal kernel and the factor in the polarizability, $\coth\left(\frac{\hbar\Omega_m}{2k_BT}\right)=\tanh\left(\frac{\hbar\Omega_m}{2k_BT}\right)=1$ which recovers (3.6). On the other hand, at finite temperature an analytic continuation to imaginary frequencies $\omega=i\xi$ can be performed to obtain an expansion in Matsubara frequencies as before.

The magnetic Green's tensor evaluated at imaginary frequencies $\omega=i\xi$ and setting $\kappa=\sqrt{k^2+\xi^2/c^2}$ reads [Wylie and Sipe 1984, Wylie and Sipe 1985]

$$H_{ij} \;=\; \frac{\mu_0}{8\pi^2}\int_0^{2\pi}d\phi\int_0^{\infty}\frac{kdk}{\kappa}\left(-\frac{\xi^2}{c^2}\right)\left[r^{TE}(\hat{p}_0^{+}\hat{p}_0^{-})_{ij}+r^{TM}(\hat{s}\hat{s})_{ij}\right]\exp(-2\kappa L)\,. \tag{3.11}$$

Here, the unit vector $\hat{z}$ is perpendicular to the surface. The angular integration of the tensor-components yields then

$$\frac{1}{2\pi}\int d\phi(\hat{s}\hat{s})_{ij} \;=\; \frac{1}{2}\left[\hat{x}\hat{x}+\hat{y}\hat{y}\right] \tag{3.12}$$

$$\frac{1}{2\pi}\int d\phi(\hat{p}_0^{+}\hat{p}_0^{-})_{ij} \;=\; -\frac{c^2}{\xi^2}\left[k^2\hat{z}\hat{z}+\frac{\kappa^2}{2}(\hat{x}\hat{x}+\hat{y}\hat{y})\right]\,. \tag{3.13}$$

Now, both the Green's tensor and the polarizability tensor are known and the traces will be calculated in two special configurations for later use in numerical evaluations:

- *Anisotropic dipole*: The transition-dipole is parallel to the surface. Then, the shift does not depend on the $\hat{z}\hat{z}$-element of the Green's function, and the polarizability tensor has components $\beta_{xx} = \beta_{yy} = \beta^T, \beta_{zz} = 0$.

$$\beta_{ij}H^{ji} = \frac{\mu_0}{4\pi}\int_0^\infty \frac{kdk}{\kappa}\left[\left(-\frac{\xi^2}{c^2}\right)r^{TM} + \kappa^2 r^{TE}\right]\beta^T \exp(-2\kappa L) \tag{3.14}$$

  This applies in atom chips, where static trapping fields parallel to the surface exist. Here, $\Omega_m \sim B$ the trapping field.

- *Isotropic dipole*: The average is taken over all directions, which gives $\beta_{ij} = \beta^T \frac{1}{3}\delta_{ij}$.

$$\beta_{ij}H^{ji} = \frac{1}{3}\frac{\mu_0}{4\pi}\int_0^\infty \frac{kdk}{\kappa}\left[\left(-\frac{\xi^2}{c^2}\right)[r^{TM} + r^{TE}] + 2\kappa^2 r^{TE}\right]\beta^T \exp(-2\kappa L)\,. \tag{3.15}$$

  This is relevant in optical traps and Ω_m can be assumed in the order of the hyperfine splitting.

In these expressions, the temperature dependent diagonal polarizability elements

$$\beta^T(\omega, T) = |\mu_m|^2 \frac{2\Omega}{\Omega^2 - \omega^2}\tanh\left(\frac{\hbar\Omega}{2k_B T}\right)\,, \qquad |\mu_m|^2 = \frac{g_s^2\mu_B^2}{4\hbar}\,. \tag{3.16}$$

do not depend on the wave vector and can be separated from the trace, defining the trace of the Green's tensor (*trace-function* H) by

$$\beta_{ij}H^{ji} =: H(\omega, L)\beta^T(\omega, T)\,,$$

which depends on frequency and includes the $\mathbf{k}$-integral. How useful this is will turn out in section 3.2.3, where a more detailed analysis of the trace function will enable to see the physical origin of many effects much more clearly.

3.2 Atom near a metal surface

3.2.1 Length scales and asymptotics at $T = 0$

Fig. 3.2 and 3.2 show the numerical results for the free energy vs. distance of a magnetic anisotropic dipole placed in front of a metal half-space described by the Drude model or plasma model respectively (see the caption for parameters) at zero and finite temperature[1].

The energies are normalized to the L^{-3} power law of the non-retarded electric Casimir-Polder energy. Clearly there are at least three different regimes, in which the potential follows characteristic power laws. In this section, the power laws will be motivated and obtained from asymptotic expansions. The magnetic Casimir-Polder potential is *repulsive* at all distances. Nowhere is there a change of sign of the free energy or the Casimir-Polder force.

The asymptotics for the Drude model at $T = 0$ have been calculated in [Power *et al.* 2005b, Power *et al.* 2005a, Henkel 2005]. At zero temperature, the system is characterized by two characteristic length- or energy-scales. The first is the *penetration depth* $\delta(\Omega_m)$ evaluated at the transition wavelength. In the Drude model this is the skin depth (1.33) and in the case of the plasma model it coincides with the plasma wavelength λ_p. The second is the *transition wavelength* $\lambda_m = 2\pi c/\Omega_m$ connected to the dipole transition. Due to these length scales, there are three distinct distance regimes:

- *Sub-skin depth regime* $L \ll \delta(\Omega_m) \ll \lambda_m$: At distances smaller than the penetration depth depth $\delta(\omega)$, the asymptotic behavior is dominated by the $T = 0$-contribution. The zero-temperature limits for the Drude model reads [Power *et al.* 2005b, Power *et al.* 2005a, Henkel 2005]

$$U_m^{Dr}(L) \approx \frac{|\mu_m|^2\mu_0}{16\pi^2\delta^2(\Omega_m)}\frac{1}{L}\ln\left(\frac{\delta(\Omega_m)}{L}\right) \tag{3.17}$$

[1] In this work, atoms, fields and surfaces are always considered to be in a global thermal equilibrium.

The small distance calculation for the plasma model at $T = 0$ can be done analog to the Drude case. In the sub-skin-depth regime the wave vector is dominated by its transverse component ($\kappa \approx k$), and in the plasma model the Green's tensor becomes independent of ξ. Hence, the frequency-integral depends only on the polarizability and does not show the logarithmic behavior

$$H_{xx} = \frac{-\mu_0\omega_p^2}{8\pi c^2}\int_0^\infty dk \underbrace{\frac{k}{\kappa}}_{\approx 1} e^{-2\kappa z} \approx -\frac{\mu_0\omega_p^2}{16\pi c^2 z}. \tag{3.18}$$

$$U_m^{Pl}(L) \approx -\frac{\hbar}{2\pi}2H_{xx}\int_0^\infty d\xi\beta^0(i\xi) \tag{3.19}$$

$$= \frac{|\mu_m|^2\mu_0\omega_p^2}{64\pi^2c^2}\frac{1}{L} = \frac{|\mu_m|^2\mu_0}{16\lambda_p^2}\frac{1}{L}\,. \tag{3.20}$$

- *Non-retarded regime* $\delta(\Omega_m) \ll L \ll \lambda_m$: At intermediate distances the free energy for the Drude model obtained in [Power *et al.* 2005b, Power *et al.* 2005a, Henkel 2005] is

$$U_m^{Dr}(L) \approx \frac{|\mu_m|^2\mu_0}{64\pi}\frac{1}{L^3}\,, \tag{3.21}$$

  which shows just the trace function's power law stemming from the dipole field. The same power law holds for the plasma model, where it extends also to the large distance limit in the limit of very high temperatures covered below.

- *Retarded Casimir-Polder regime* $L \gg \delta, \lambda_m$: In the limit of large distances the power law is changed due to retardation effects. Wherever a model displays good conductivity at low frequencies and low values of k, the specific dielectric features of the model become irrelevant[2] and it can be assumed that $|\epsilon(\omega)| \gg 1$. No difference is therefore expected between the Drude and the plasma model at $T = 0$ and the energy follows a power law given by

$$U_m = \frac{3\mu_0|\mu_m|^2c}{16\pi^2L^4}\,. \tag{3.22}$$

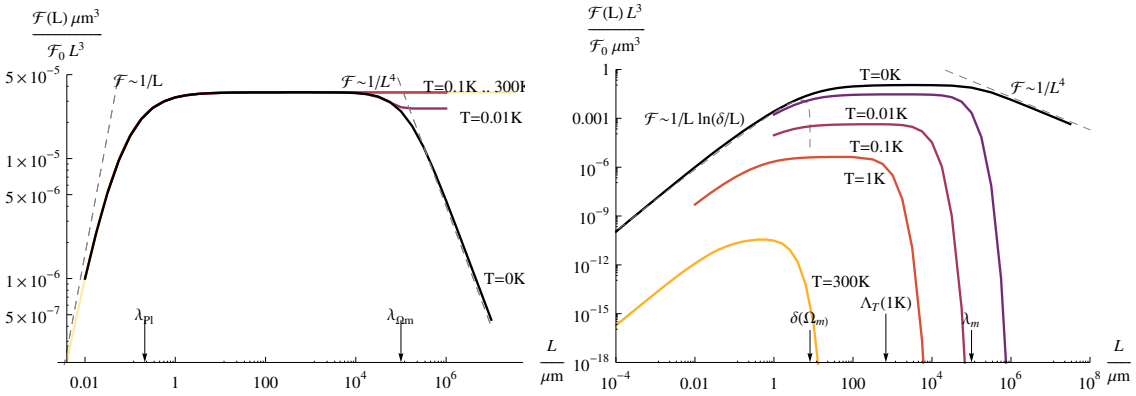

Figure 3.2: *Casimir-Polder free energy vs. distance for an anisotropic magnetic dipole. Plasma model (left) and Drude model (right), where* $\omega_p = 8.5 \cdot 10^{15}\,\mathrm{s}^{-1}$ *and* $\gamma = 0.01\omega_p$. *The transition frequency is* $\Omega_m = 3 \cdot 10^9\,\mathrm{s}^{-1}$. *The free energy scale* $\mathcal{F}_0$ *is the value at* $T = 0, L = 10^{-2}\,\mu\mathrm{m}$, *this value is* $\mathcal{F}_0 = 3.0 \cdot 10^{-32}\,\mathrm{J}$ *in the plasma model and* $9.6 \cdot 10^{-36}\,\mathrm{J}$ *in the Drude model.*

3.2.2 Casimir-Polder interaction at $T > 0$

Distance dependence and dissipative quenching

At finite temperature, the thermal wavelength λ_T introduces a characteristic *thermal regime* at large distances $L > \lambda_T$. As the temperature rises and λ_T gets eventually smaller than the other characteristic length scales

[2] This is true only in the $T = 0$ limit. At finite temperature things become more difficult as discussed in the following.

$\delta(\Omega_m), \lambda_m$, the thermal effects set in at smaller distances, so that the power laws calculated for $T = 0$ do not hold any longer.

Plots 3.2 and 3.2 show the Casimir-Polder free energies vs. distance calculated for the plasma and Drude-model at different temperatures. In both models the thermal corrections lead to big variations from the $T = 0$ values at large distances, i.e. in the thermal regime, but the impacts are much stronger in the Drude model.

In the dissipationless plasma model, the large distance limit of the Casimir-Polder free energy is finite. Even at low temperatures the system approaches very rapidly the limit of $T \to \infty$, where the non-retarded regime extends to large distances. At distances much smaller than the thermal wavelength, and specially in the range of temperatures and distances accessible to measurements, the thermal corrections to the plasma model are negligible ($\lambda_T(0.1\,\mathrm{K}) \approx 14\,\mathrm{cm}$, cf. (2.40).

A very remarkable effect occurs in the case of the Drude metal (fig. 3.2). Here, the magnetic Casimir-Polder free energy is exponentially suppressed at large distances and finite temperatures. This phenomenon will be called *dissipative quenching*, because it is due to the effects of dissipation on the low-frequency reflectivity for TE-modes known from section 1.7.3, as will be shown in the next section. It is very interesting, that the inset of the thermal effects occurs at a very similar length scale $L \approx \Lambda_T \approx 0.045\lambda_T$ as found in (2.48) for the Casimir-interaction between perfectly reflecting plates.

Nothing alike occurs for the electric dipole interacting (in any of the models) nor for the magnetic dipole in the plasma model. This can be seen immediately comparing figure 3.8 to 3.3), which show the thermal Casimir-Polder energy vs. temperature in the different models for an electric and magnetic dipole. Note that even at distances below the thermal wavelength, where the $T = 0$ power laws remain valid, the thermal effects result in an overall much smaller value of the free energy.

From an experimental point of view, the thermal quenching and the large deviations of the free energy vs. distance from the $T = 0$ curve might indicate a convenient way of distinguishing the two models in experimental data. The high sensitivity towards dissipation makes the magnetic dipole a very good detector for surface currents and their dynamics. Still, one should keep in mind that the magnetic contribution to the Casimir-Polder interaction is rather small and that it is not easy to separate the magnetic interaction from the electric one in an experiment.

This first discussion of the numerical results has shown that dissipation is of crucial significance for the thermal effects in the magnetic Casimir-Polder interaction. The next sections will investigate in more detail, how dissipation accounts for the thermal deviation from the $T = 0$ curve and also discuss the entropy corresponding to the atom surface interaction.

Limits of high and low temperatures

Fig. 3.3 shows the Casimir-Polder free energy and entropy vs. temperature at a fixed distance for the anisotropic magnetic dipole[3] in different models, including the two fluid model for a superconductor, covered in section 3.3. In the global equilibrium considered here, there is no ambiguity to define an entropy. The dissipative quenching leads to a very strong dependence on temperature in the Drude case, while only very small thermal corrections occur in the plasma model. The asymptotic values can be calculated in a analog way as in the analysis done for the Casimir effect between two plates using different expansions at low and high temperatures. The transition between the two regimes occurs approximately at the temperature $T = \frac{\hbar\Omega_m}{2k_B}$. Above this value, both states of the two level atoms are almost equally occupied and the polarizability $\beta^T(\omega)$ vanishes as T^{-1}.

- *High temperatures*: This limit is dominated by the zeroth term in the Matsubara expansion. In this regime the $\tanh\left(\frac{\hbar\Omega_m}{2k_BT}\right)$ can be replaced by its argument, so that

$$\mathcal{F}(T \to \infty) \approx -\frac{k_BT}{2}\beta^T(0)H(0) = -\frac{\hbar}{2}|\mu_m|^2H(0)\,. \tag{3.23}$$

  Thus, the factor T^{-1} from the polarizability at high temperatures is compensated by the prefactor, and the limit is independent of temperature. Of course the free energy depends still on distance.

  In the plasma model, the free energy saturates at a finite positive value ($H(0) < 0$) while $H(0) = 0$ in the Drude model and other related models, due to the transparency of a dissipative metal for TE-fields of

[3] The analysis holds equivalently for the isotropic dipole. The two cases are compared in section 3.2.4.

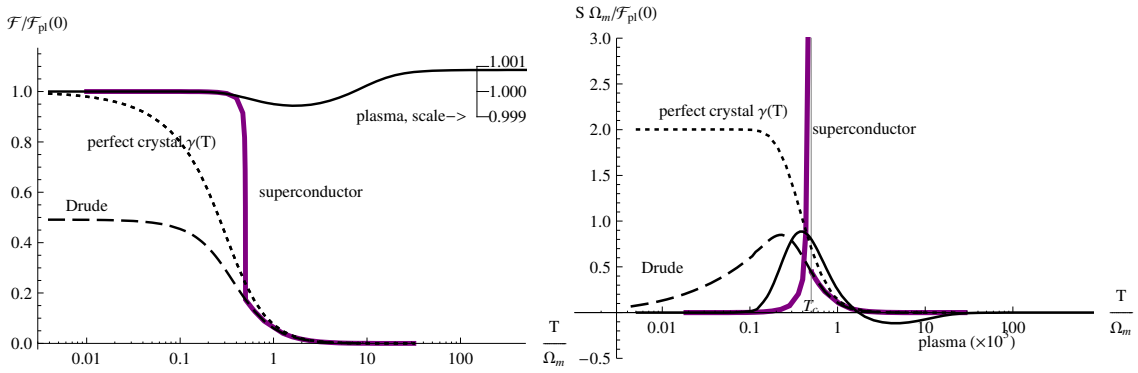

Figure 3.3: *Casimir-Polder free energy and entropy of a magnetic anisotropic dipole with a plasma (solid), Drude-metal (dashed), perfect crystal (dotted) and two fluid superconductor (gray).* $\omega_p = 10^{18}\,\mathrm{s}^{-1}$ *and the dipole is placed* $10^{-2}\,\mu\mathrm{m}$ *from the surface. The transition energy is* $\hbar\Omega_m = 1/3600\,\mathrm{K}k_B^*$. *In the temperature dependent plots,* $k_B^* = 3600k_B$ *for better visibility.*

low frequencies (section 1.7.3). Therefore, the origin of dissipative quenching of the thermal Casimir-Polder interaction is due to the same physical effect that has given rise to the large distance anomalies in the case of the interaction between two plates (section 2.2.2).

The saturation towards a temperature independent value of the free energy implies automatically a vanishing entropy in all models.

- *Low temperatures*: The limit is obtained by replacing the sum with its integral. In this limit, $\tanh\left(\frac{\hbar\Omega_m}{2k_BT}\right) \to 1$ and the zeroth and first Matsubara terms loose their special role so that any distributional effects at $\omega \equiv 0$ become irrelevant.

  The free energy in the plasma model at $T = 0$ is

$$\mathcal{F}(0) \;=\; -\frac{\hbar}{2\pi}\int_0^\infty \beta^T(i\xi)H(i\xi)d\xi \tag{3.24}$$

  In this mode, the trace function has a behavior close to a step-function and the support of the polarizability lies well inside the one of the (monotonous) trace function (see section 3.2.3 and fig. 3.5). Using these properties, the trace-function can be taken out of the integral by introducing a factor $C \leq 1$ that depends on Ω_m/T, and the remaining integral over the polarizability gives the area of a Lorentzian.

$$\begin{aligned}\mathcal{F}(0) &\approx -\frac{\hbar}{2\pi}H(0)C\int_0^\infty \beta^T(i\xi)d\xi \\ &= -\frac{\hbar}{2}|\mu_m|^2H(0)C = \mathcal{F}(\infty)C\,,\end{aligned} \tag{3.25}$$

  A value of C very close to one can be read off the numerical results in graph 3.3.

  The entropy at zero temperature can be estimated with help of the formalism from section 2.2.3. Since no non-interchanging limits nor any other temperature-dependences occur for the plasma model, the entropy at absolute zero must vanish, so that - as in the Casimir effect - no thermal anomalies appear in the plasma model.

  This calculation cannot be done identically for the Drude model. In this model the trace function decays at low frequencies $\omega \ll \gamma$, again due to the TE-transparency in the low frequency regime. Thus the integral over the polarizability and the trace function cannot be separated as before and only a part of the Lorentzian polarizability curve can contribute to the integral. This yields a much lower interaction energy as in the plasma model. The transparent regime for TE-modes covers a larger frequency interval as γ becomes larger and the dissipative quenching becomes stronger. Figure 3.4 shows the magnetic Casimir-Polder free energy at fixed distance and temperature over the dissipation rate γ and confirms this qualitative prediction.

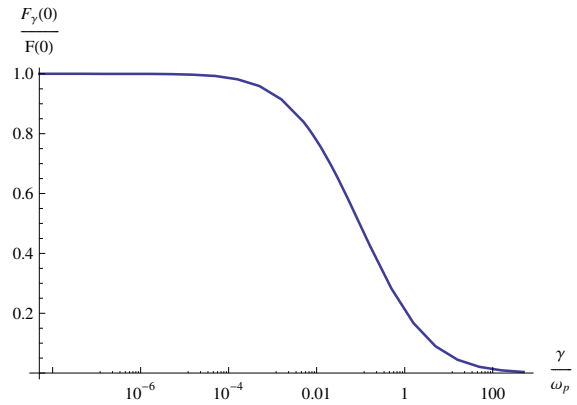

Figure 3.4: *Free energy of a magnetic anisotropic dipole in the Drude model scaled to the plasma limit ($\gamma = 0$). $\omega_p = 10^{18}\,\mathrm{s}^{-1}$ and the distance to the surface is $10^{-2}\,\mu$m. The transition energy is $\hbar\Omega_m = 1\,\mathrm{K}k_B^*$.*

Zero-point entropy in the perfect crystal

The phenomena arising in Casimir context if the rate of dissipation γ varies with temperature rapidly enough have been addressed before in section 2.2.3. The previous analysis and the numerical computations have shown, that a Drude metal or the plasma model satisfy Nernst's theorem. For the perfect crystal model, no such anomalies have been found in the investigation done on the entropy an electric dipole near a surface described by any model [Bezerra *et al.* 2008]. (Cf. section 3.2.5 and figure 3.8).

Yet, in the case of the magnetic dipole, a positive finite zero-point entropy appears for the perfect crystal shown in fig. 3.3. It is straight forward to apply the formalism exposed in section 2.2.3 to this case. The equivalent to the energy density used there is

$$g(0) - \tilde{g}(0) = \beta(0)(H_{Pl}(0) - H_{Dr}(0)) \,.$$

Remembering that due to the transparency of the Drude model for low frequency TE-modes $H_{Dr}(0) = 0$, the Casimir-Polder entropy at $T = 0$ is given by

$$\begin{aligned} \Delta S(T=0) &= \frac{k_B(g(0) - \tilde{g}(0))}{2} = \frac{k_B}{2}\beta^0(0)H_{Pl}(0) \\ &= \frac{k_B|\mu_m|^2}{\Omega_m}H(0) = \frac{2k_B}{\hbar\Omega_m}|F_{Pl}(\infty)| \,. \end{aligned} \tag{3.26}$$

This result fits perfectly with the entropy offset obtained numerically. In the units chosen, the value $2C$ can be read off the graph 3.3 directly.

Interestingly the zero-temperature entropy is positive in the Casimir-Polder configuration, while it has a negative value in the Casimir configuration with plates. The reason is the paramagnetic nature of the permanent dipole that favors a parallel alignment of the dipole to the field fluctuation. In contrast, the current response in the Casimir effect between plates must obey the Lenz rule. If these currents are interpreted as connected to a magnetic moment, the response would be diamagnetic, leading to an antiparallel alignment.

3.2.3 Analysis of the trace functions

Partial trace functions

So far the complete trace function H has been used in the analysis. It is possible to separate distinct contributions from the r^{TM}- and r^{TE}-polarizations separately. This offers a way of relating contributions to the energy to special sets of modes and will reveal the origins of some of the structure discovered earlier in the total free energy much more clearly and also understand better the differences between the interaction energies of the electric and magnetic dipole.

The four basic partial trace functions are given by

$$H_{p1} = \int_0^\infty dk\kappa^2 r^{TM} e^{-2\kappa L}, \qquad H_{p2} = \int_0^\infty dk(-)\frac{\xi^2}{c^2} r^{TM} e^{-2\kappa L} \tag{3.27}$$

$$H_{s1} = \int_0^\infty dk\kappa^2 r^{TE} e^{-2\kappa L}, \qquad H_{s2} = \int_0^\infty dk(-)\frac{\xi^2}{c^2} r^{TE} e^{-2\kappa L} \tag{3.28}$$

All relevant trace functions can be constructed by summing two or three of them. The magnetic trace function in the anisotropic and isotropic case are given by

$$H_{an} = H_{p2} + H_{s1}, \qquad 3H_{iso} = H_{p2} + H_{s2} + 2H_{s1}$$

and the electric ones can be obtained by interchanging $r^{TE} \leftrightarrow r^{TM}$, i.e. the indices $s \leftrightarrow p$ using the recipe given above:

$$G_{an} \sim H_{s2} + H_{p1}, \qquad 3G_{iso} \sim H_{s2} + H_{p2} + 2H_{p1}\ .$$

Figure 3.5 shows the polarizability and the trace functions for the plasma model over frequency in arbitrary units.

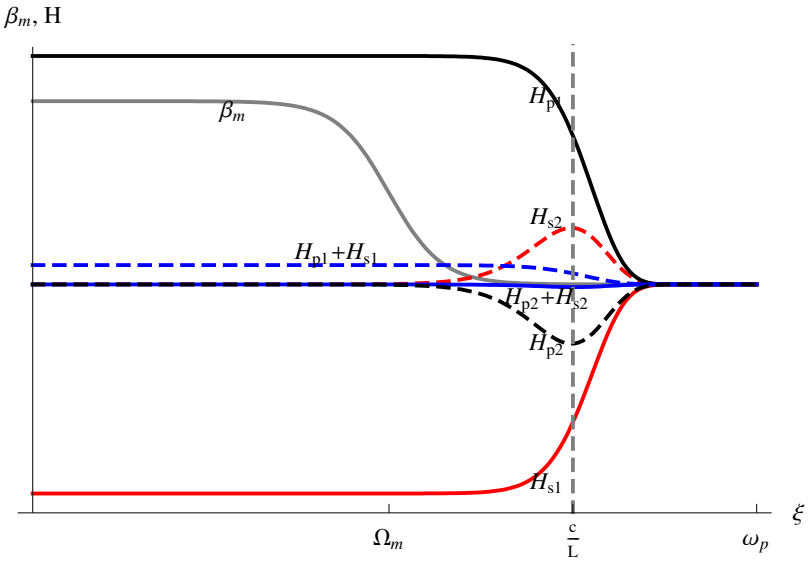

Figure 3.5: *Partial magnetic trace functions for the plasma model and the magnetic polarizability. As before, red lines indicate TE or s-polarization and black lines TM or p-polarization. Blue lines indicate sums of two partial trace functions. β_m is the magnetic polarizability.*

Monotony and the geometry of the system

The thermal Casimir-Polder free energies can be expressed in terms of the Matsubara sum

$$\mathcal{F}(T, L) = -\frac{k_B T}{2}{\sum_n}' \beta^T(i\xi_n) H(i\xi_n)\ . \tag{3.29}$$

Interesting effects occur, if $\beta^T(i\xi)H(i\xi)$ is not monotonous or locally peaked in an interval around a frequency Ξ. The Matsubara-sum produces a Riemann-partition of the integral (i.e. the limit $T = 0$), which becomes coarser and more sensitive to local structures as T rises. The strongest effects are expected when the first Matsubara summand $\xi_1 = 2\pi k_B T/\hbar$ crosses the local extremum Ξ, which will translate directly to an extremum in the free energy. In the two-level atom β^T is monotonous anyway, and it is sufficient to consider the monotony of the trace functions.

Examples for such non-monotonous partial trace functions are the functions H_{p2} and H_{s1} of the plasma model shown in figure 3.5. In fact, in the case of the magnetic anisotropic dipole's interaction with a plasma, the contribution from the trace function H_{p2} associated to the r^{TM}-polarization leads to a characteristic notch and produces the maximum of entropy shown in fig. 3.3. The notch in H_{p2} occurs generally close to the frequency $\Xi \approx \frac{c}{L}$

connected to the geometric scale of the system. The frequency can be calculated analytically in the two special cases of a plasma model at small distances and for a perfect reflector, where the angular integration inside the trace function can be performed explicitly.

- *The perfect reflector* trace function H_{p2} has a peak with its maximum at ξ_{max}, and its width Γ is measured as the distance between its turning points

$$G_{p2}^{perfect} \sim \int_{\xi/c}^{\infty} \xi^2 \exp(-2\kappa L) d\kappa = \frac{\xi^2}{2L} \exp(-2\frac{\xi}{c}L) \tag{3.30}$$

$$\Rightarrow \Xi = \frac{c}{L}, \qquad \Gamma = \frac{\sqrt{2}c}{L}. \tag{3.31}$$

  So the contribution comes from modes that "fit" between the cavity wall and the atom and has a geometric origin.

- In the *plasma model* in the limit of distances below the skin depth $L \ll \delta_0$, one can again use that $\kappa \gg \xi/c$ and approximate the reflectivity by

$$r^{TM} \approx \pm \frac{\epsilon(i\xi) - 1}{\epsilon(i\xi) + 1}.$$

  Therefore the trace function can be calculated explicitly and the maximum can be found

$$G \sim \int_{\xi/c}^{\infty} \xi^2 r_{TM}^2 \exp(-2\kappa L) d\kappa = \frac{\xi^2}{2L + 4L\xi^2} \exp(-2\frac{\xi}{c}L) \tag{3.32}$$

$$\Rightarrow \Xi \approx \frac{c}{L}\left[1 - \frac{2c^2}{L^2\omega_p^2} + \mathcal{O}((\frac{c}{L\omega_p})^4)\right], \tag{3.33}$$

  which recovers the perfect reflector limit, where $L \gg \lambda_p$.

3.2.4 Anisotropic and isotropic polarizability

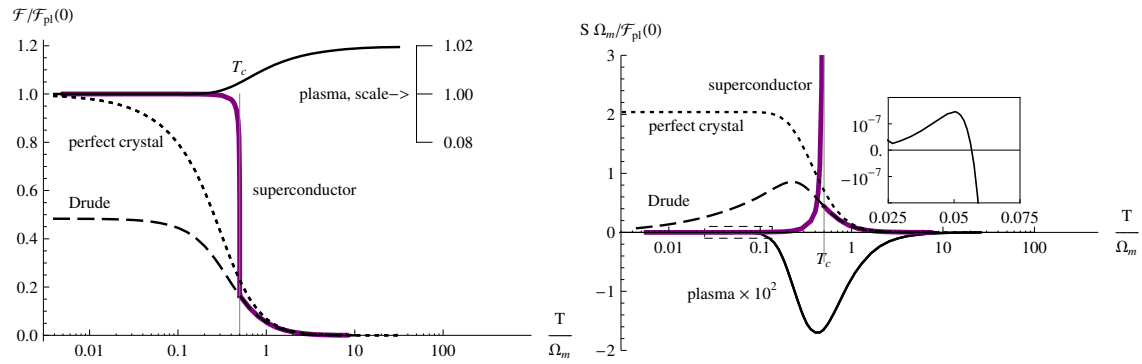

Figure 3.6: *Isotropic magnetic dipole, same parameters as above.*

Numerical calculations show that the energetic behavior of the Drude model, perfect crystal and two fluid model with an isotropic polarizability (fig. 3.6)) is almost identical to the anisotropic case shown in fig. 3.3.

An interesting feature occurs in the plasma model. Fig. 3.7 shows the comparison of the anisotropic and isotropic dipole interaction with a plasma. It was shown in the last section, how for in the anisotropic magnetic dipole the trace function H_{p2} creates the minimum of the free energy (or the entropy maximum respectively) due to the dependence of on the system geometry, clearly present in the graph. But in the isotropic case the minimum is strongly suppressed - by a factor 10^4 at this distance.

This effect can be understood immediately by looking at the partial trace functions (3.27, 3.28). In the isotropic case the contributions $H_{p2} + H_{s2}$ connected to TE and TM modes cancel each other out almost completely, so that the extremum found in the anisotropic case is much smaller. The dominating contribution in the isotropic case is H_{s1}, which is monotonous in ω.

Also the limit of the free energy at high temperatures is much higher in the isotropic case.

This result indicates that the magnetic dipole-transitions perpendicular to the surface (not included in the anisotropic case) give the most relevant contribution to the magnetic Casimir-Polder free energy. A very similar phenomenon is known from the case of electric dipoles covered below.

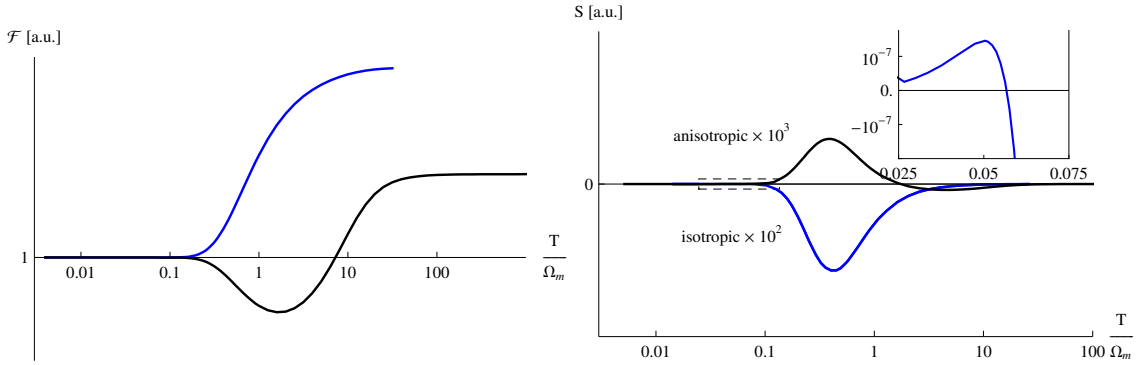

Figure 3.7: *Casimir-Polder free energy and entropy of a magnetic isotropic (blue) and anisotropic (black) dipole at* $10^{-2}\ \mu\mathrm{m}$ *from a surface described by the plasma model, where* $\omega_p = 10^{18}\,\mathrm{s}^{-1}$. *The transition energy is* $\hbar\Omega_m = 1\,\mathrm{K}k_B^*$.

3.2.5 Comparison to the electric dipole

Fig. 3.8 shows the numerical results of the interaction energy and entropy of an isotropic electric dipole with a surface described by different models. A comparison of the atom-surface interaction in the Drude model at $T = 0$ has been given in [Henkel 2005].

The values are very similar for all the materials to within $< 1\%$, which is below the precision reached in any of the recent experiments (mind the relative energy scale of the plot). The qualitative form of the curves resembles the case of the isotropic magnetic dipole in the plasma-case, but with an overall negative sign of the free energy. The high-temperature limit of the free energy is finite and nonvanishing in all models, which means that the electric dipole does not feature the strong dissipative quenching of the interaction at finite temperature found in the magnetic case.

When having a closer look at the entropy in the plasma model, there is a small local minimum at temperatures just below the value, where the maximum occurs (cf. the inset in fig. 3.8). Recently Bezerra *et al.* [Bezerra *et al.* 2008] have shown that the Casimir-Polder entropy takes negative values in the case of a dipole with a temperature-independent isotropic electric polarizability and assuming perfect reflection. The authors mentioned that analog behavior is to be expected in more realistic models as well, and pointed out that there is no finite zero-temperature entropy for an electric dipole in any of the models. The numerical results agree with all of these statements and show in fact a vanishing entropy at $T = 0$ even for the notorious perfect crystal model. The value can also be easily checked by an analog calculation as in the magnetic case.

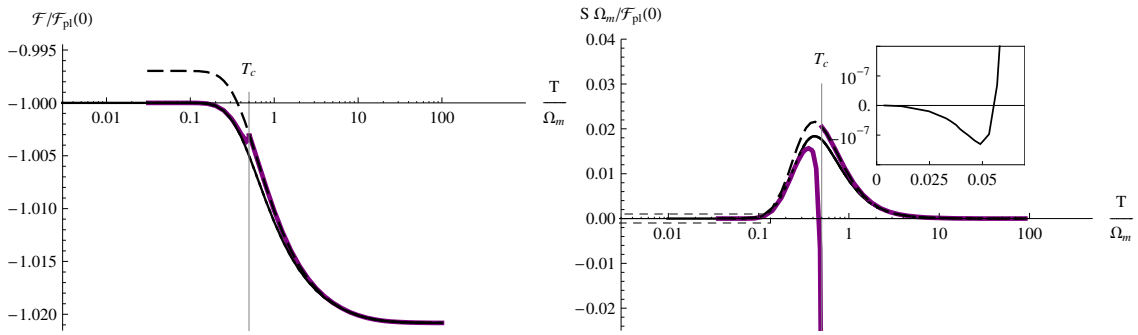

Figure 3.8: *Casimir-Polder free energy and entropy of an electric isotropic dipole with a plasma (solid), Drude-metal (dashed), perfect crystal (dotted) and two fluid superconductor (gray), where* $\omega_p = 10^{18}\,\mathrm{s}^{-1}$. *The distance to the surface is* $10^{-2}\ \mu\mathrm{m}$ *and the transition energy is* $\hbar\Omega_m = 1\,\mathrm{K}k_B^*$.

Keeping in mind that the role of the TE and TM reflectivities is interchanged in the electric case w.r.t to magnetic one, it becomes clear, why dissipation (and thus the model under consideration) plays a minor role: Since the dominating trace function is now G_{p2} connected to the r^{TM} reflectivity, the Casimir-Polder interaction of the electric dipole is sensitive mostly towards the surface charges, which are independent of dissipation as has been argued before (section 1.7.3). In other words: the image of the static dipole is the same in all models, due to perfect electrostatic screening at a metallic surface.

The near coincidence of all models is an advantage for experimental prediction. From another viewpoint, it makes the the electric dipole a bad detector for the current response of the surfaces, but a highly sensitive one for surface charges. In fact, the first data taken in a recent experiment by E. Cornell *et al.* were found to be dominated by random, static surface charges due to adsorbate atoms [McGuirk *et al.* 2004]. Thus, if atoms are to be used to probe the dissipative properties or decide on the correct model to describe a material, the magnetic contribution would give a much more decisive answer, if it was measurable separately.

3.3 Atom near a superconductor

During the investigation of the magnetic Casimir-Polder interaction of an atom with a metallic surface in the previous sections, it has become clear that the dissipative properties play a key role here. Very interesting effects can thus be expected in the interaction with a superconductor, where dissipation sets in suddenly at temperatures above the transition temperature.

Fig. 3.9 shows the dependence of the magnetic Casimir-Polder free energy for a two fluid superconductor on distance at different temperatures. It features significant differences to the plasma and Drude model at both small and large distances. At $T = 0$, the interaction energy coincides of course with the plasma model, but approximately in the interval $0.5T_c < T < T_c$ the low distance law approaches the Drude curve. On the other hand, at large distances $L \gg \lambda_m$ the free energy approaches the high-temperature-limit very rapidly. In this regime, no signature of the dissipative quenching encountered in the Drude model in section 3.2.2 can be found below T_c, even though a fraction of the charge carriers contributes to a dissipative current. Only above this value does the effect set in abruptly.

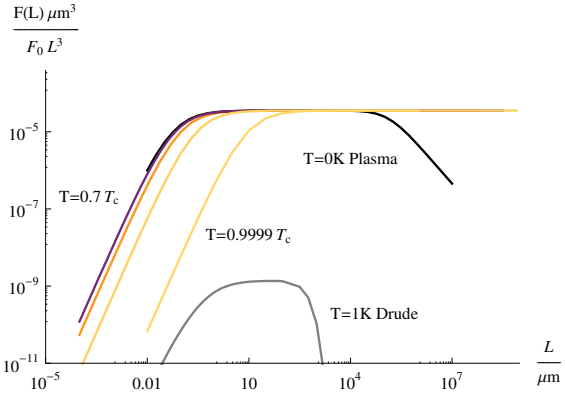

Figure 3.9: *Two fluid model, where* $\omega_p = 8.5 \cdot 10^{15}\,\mathrm{s}^{-1}, T_c = 0.5K, \gamma = 0.01\omega_p$. *Casimir-Polder free energy vs. distance for an anisotropic magnetic dipole. The transition frequency is* $\Omega_m = 3 \cdot 10^9\,\mathrm{s}^{-1}$. *The free energy scale* $\mathcal{F}_0 = 3.0 \cdot 10^{-32}$ J *is the value at* $T = 0, L = 10^{-2}\ \mu$m.

The temperature dependence of the Casimir-Polder free energy and entropy has already been shown along with the other models in figures 3.3, 3.6 and 3.8. Here, the transition between plasma and Drude-like can be seen clearly.

The discussion of entropy at $T = 0$ and the entropy discontinuity at T_c can be performed analogous to the case of the Casimir interaction, but the relative signs of the electric and magnetic dipole energies must be taken into account. For this reason, the entropy-discontinuity changes it sign in the magnetic atom-surface coupling, where the Drude model free energy is smaller than the plasma model one at zero temperature. Also, the entropy minimum found for superconducting plates translates to a maximum.

Comparing the effects found for the magnetic case to to the electric one, it is noticeable that the strong difference of the interaction energy below and above the superconducting transition is almost non-existing in the case of the electric dipole, because the plasma and Drude model behave very much alike (cf. plot 3.6 to 3.8), as was shown in the previous section.

Therefore, experiments similar to the ones proposed by Bimonte (see section 2.3.1) but measuring the change of the Casimir-Polder energies above and below T_c should be a promising way to isolate to the magnetic dipole contribution.

3.4 Towards experimental measurements

The main problem in measuring the magnetic dipole Casimir-Polder interaction is the very small value of the interaction energy as compared to the electric one. The typical orders of magnitudes given as an example in the first section of this chapter, assumed that the electric polarizability will depend frequencies in the order of electronic transitions while the magnetic one is due to Zeeman-splitting in an external field and connected to much smaller energies.

A comparison of the electric and magnetic interaction energy at zero temperature calculated in the Drude model has been performed in [Henkel 2005]. See also [Spagnolo and Intravaia 2008]. Due to the different interaction energies $\Omega_e \gg \Omega_m$ in the magnetic and electric case, the distance regimes set in at different length scales $\lambda_e \ll \lambda_m$. In the retarded regime one can compare the electric and magnetic dipole interaction energy

$$U_e(L) \approx A\alpha(0)L^{-4}, \qquad U_m(L) \approx \frac{A}{c^2}\beta(0)L^{-4}\,, \tag{3.34}$$

where $A \approx \frac{\hbar c}{\epsilon_0}$is the same constant, cf. Casimir's expression (3.1). Hence, the relation between the electric and magnetic interaction energies is

$$\frac{c^2\alpha(0)}{\beta(0)} \approx \frac{1}{\alpha^2}\,,$$

where $\alpha = 1/137$ is the fine-structure constant.

Due to the smallness of the effect, future measurements of the magnetic Casimir-Polder interaction will most probably involve high precision spectroscopic techniques making use of the level shift due to the surface interaction. The calculation of these energy shifts is a perspective for future work. So far numerical calculations have been performed for the two-level system, but a first step towards a realistic system could be the calculation of the effects in a hydrogen atom.

In any case it is interesting to find control parameters that have an effect only the magnetic but not on the electric coupling. One possibility to influence the magnetic dipole coupling, could come through variation of external fields. If the transition frequency Ω_m is due to Zeeman splitting, the level splitting is proportional to the external magnetic fields. Apart from the external field, the level splitting depends also on the static magnetic moments, i.e. the hyperfine state. Another possibility is the use of different isotopes or hyperfine states that differ in their magnetic dipole moment.

Atom chip experiments, which have successfully been used to measure the electric Casimir-Polder force with good precision, might not be the best setups for measurements of the magnetic Casimir-Polder interaction because today's normally conducting traps work at quite large distances in the order of μm, where the thermal quenching is highly relevant. The next generation of atom chips, using still smaller structures or superconducting elements [Dikovsky *et al.* 2009], might be better suited. Also, other kinds of trap setups could be a better choice for experiments involving spectroscopic techniques. These could be applied e.g. in optical traps involving evanescent fields, e.g. [Power *et al.* 1997, Grimm *et al.* 2000], where both hyperfine states are trapped at close distances from a surface ($\leq 1\,\mu$m).

3.5 Conclusions

This chapter has covered some aspects of the interaction of an atom with a metallic surface. The interaction was described through magnetic and electric dipole coupling, and a two-level system was considered in the numerical evaluations.

New effects were found in the magnetic contribution to the interaction, that were unknown from previous work dealing with the electric dipole coupling only. Among these was the strong dissipative quenching of the interaction at finite temperature and distance and the reappearing of thermal anomalies such as a finite entropy at zero temperature in the perfect crystal model. Interestingly the entropy defect takes a positive value in the Casimir-Polder case, while the one of the Casimir effect was negative. This is due to the overall negative sign of the interaction energy w.r.t the Casimir scenario. The asymptotic evaluations of the energies and entropies coincide well with the numerical results.

A decomposition of the Casimir-Polder free energy into the contributions from different partial trace functions allowed to consider the TM and TE effects separately and helped to understand all the above effects more clearly. It became clear how the sensitivity of an electric or magnetic dipoles to electric surface charges or surface currents respectively leads to the differences between anisotropic and isotropic polarizabilities and between the electric and magnetic surface interaction.

In the magnetic Casimir-Polder interaction between an atom and a superconductor, very similar effects as those encountered in the Casimir effect occur. They include a entropy discontinuity and extremum close to the critical temperature, connected to a strong change of the free energy due to the inset of dissipation. The corresponding effects occurring in the electric dipole coupling are very small, since the electric dipole is primarily sensitive to the surface charges but not to dissipation.

The Casimir-Polder interaction can be measured in atom chip experiments. The separation of the magnetic contribution remains a challenge, that can possibly be mastered by using optical spectroscopy on the hyperfine or Zeeman levels.

4 Conclusions and Outlooks

The aim of this work was the investigation of the surface interactions involving superconducting materials.

The optical response of normal metals has been described in the Drude model

$$\epsilon(\omega) = 1 - \frac{\omega_p^2}{\omega(\omega + i\gamma)} ,$$

in which the dissipation rate γ is constant if it depends on impurity scattering, or has a temperature dependence $\gamma(T)$, if it is dominated by electron-phonon scattering.

If the dissipation rate is set $\gamma \equiv 0$, one recovers the plasma model. The results of this work suggest to interpret the plasma model as the low temperature limit of a superconductor known as London theory, rather than a description of a normal metal. Also, the above form of the plasma model is not a causal response function. This problem can be solved formally by taking the limit $\gamma \to 0^+$, which leads to a transparency of the superconductor for *exactly* static magnetic fields $\omega \equiv 0$ in contradiction with the Meißner-Ochsenfeld effect. A possible solution to this conundrum is the commonly used recipe to just neglect the localized contribution in the optical description when calculating fluctuation induced interactions.

Optical reflectivities were calculated from the dielectric functions using the Fresnel formulas. It turned out that the TM-reflectivity of all metals and superconductors coincides closely, because surface charges can build up in a similar way, independent from the effects of dissipation. In contrast, the TE reflectivity is determined mostly by surface currents and is therefore very sensitive to dissipative effects, especially at low frequencies $\omega \ll \gamma$. In this regime, normal metals become transparent to magnetic fields ($r^{TE} \to 0$), which can be understood as the consequence of the Bohr-van-Leeuwen theorem and has a strong impact on the thermal Casimir and Casimir-Polder effect.

Knowing the optical reflectivities of a material, one can calculate Casimir energies and related quantities using the Lifshitz formula (2.24). Thermal effects become important, when the plate distances become larger than the thermal wavelength $\lambda_T = 2\pi\hbar c/k_B T$. More precisely, a crossover between distance power laws occurs, when $L \approx 0.045\lambda_T$. The numerical prefactor obtained in the case of perfectly reflecting plates holds very well generally, including in the Casimir-Polder interaction between an atom and a surface.

Another universal feature of the Casimir interaction between metals is a crossover of the energy-distance power law at small distances $L \ll \lambda_p$ below the plasma wavelength. This is due to the contribution from the surface plasmons. In this work, the thermal correction to the plasmonic Casimir energy was calculated numerically and asymptotically for the first time. The energy correction factor was found to scale as L/λ_p at small distances, where its slope depends on temperature.

The free energy and entropy of the Casimir effect, including the full mode spectrum of the plasma, Drude model and perfect crystal were reviewed. Arguments have been given, that negative values of the Casimir entropies at finite temperatures are not necessarily unphysical, since they are actually entropy differences, and how the apparent violation of Nernst's theorem at $T = 0$ featured by some models could be understood in terms of a *glassy state* of persistent currents.

One important original result of this work gives analytical expressions for the continuation of the BCS conductivity to purely imaginary frequencies $\omega = i\xi$, which are highly desirable for the calculation of the Casimir effect. The analytical continuation has been performed for both the expressions given by Mattis-Bardeen, valid in the extremely anomalous limit $\hbar\gamma \gg \Delta$, and by Berlinsky-Zimmermann, which hold for general values of γ. The results were confirmed by a check against a numerical analytical continuation obtained from Kramers-Kronig relations. The numerical results for the Casimir free energy obtained in this model were compared to the ones calculated in the two-fluid model. The results were found to great accuracy, at least in the reasonably realistic regime $\hbar\gamma \approx \Delta(0)$ encountered already in the comparison of the reflectivities. In this regime (future work may define the validity of the approximation more precisely) it is therefore sufficient to use the two fluid model for the

description of the optical response of a superconductor. This result is highly valuable for numerical work, because it reduces significantly the computational effort.

The Casimir entropy between superconducting plates features a characteristic jump of entropy at the transition temperature T_c and a minimum of entropy slightly below. These properties were shown to be universal in the Casimir effect between superconductors and it has been proven that Nernst's theorem holds for a general class of two fluid models.

The interaction of an atom with a metallic surface is dominated by electric and magnetic dipole coupling. The important quantities are the Green's tensor of the electromagnetic field and the electric or magnetic polarizability. In numerical calculations, atoms were described by two-level systems. The magnetic contribution to the Casimir-Polder interaction at finite temperatures has not been investigated before, because it is generally much smaller than its electric counterpart.

Furthermore, the magnetic Casimir-Polder interaction depends very sensitively on the dissipation in metals with finite conductivity and especially on the surface currents. Dissipation leads to a strong quenching in the thermal regime $L \gg \lambda_T$. This effect is closely related to the thermal Casimir-effect in the Drude model is due to the transparency of a dissipative metal for low frequency magnetic fields ($r^{TE}(0) \to 0$). Thermal anomalies including a non-vanishing zero-point entropy – very similar to the one occurring in the interaction between two surfaces but with a positive sign – were found to reappear in the case of the magnetic atom-surface interaction with a perfect crystal. None of the above effects occurs for the electric dipole coupling, which is highly sensitive to surface charges, but not to currents. Therefore the electrical coupling of an atom to a metal is almost independent of the dissipative properties.

The sensitivity of the magnetic Casimir-Polder interaction to dissipation leads to strong thermal effects in the atom-superconductor interaction, which occur in the temperature and distance regimes accessible in experimental setups. The magnetic Casimir-Polder entropy shows feature very similar to the ones encountered in the Casimir-interaction between plates, including an strong entropy discontinuity at the critical temperature. This is connected to a strong change of the Casimir-Polder free energy at the onset of dissipation, which might allow to identify the magnetic contribution in an experimental measurement, since the phase transition leaves the electric atom-surface coupling almost unchanged.

The opportunity to control the dissipation of surface currents to a great extent by switching them on and off through temperature makes superconductors a promising tool for an investigation of the low frequency response of metals, which has a strong effect on the thermal Casimir and Casimir-Polder interaction. In experimental setups measuring the Casimir-effect between macroscopic bodies, the experimental precision and the validity of theoretical predictions are usually limited by the alignment of plates or by the necessity to use the proximity force theorem if non-planar geometries are used. The atom-surface system could thus provide a better defined system, in which measurements of the Casimir-Polder forces can be done with a very high precision. Such measurements could also help to understand better the Casimir-effect between macroscopic bodies.

From another point of view, Casimir-Polder interactions are becoming important in atomic traps on microchips. In future work, the atom-surface interaction occurring in atom chip environments could be investigated more explicitly. Here, important topics are the physics of the trapped atom carrying a static magnetic moment, the excitation to trappable states and the level shift in an external field, which have strong effects on the polarizability. In this work, no external field was assumed and no static dipole moment has been considered. This could be done, since the static dipole moment does not contribute to the dynamical fluctuations and has therefore no influence on the Casimir effect. Anyway, if the transition frequency Ω_m that characterizes the Casimir-Polder interaction is connected to Zeeman-levels, the level splitting is connected to an external field $\hbar\Omega_m \sim B$, and could thus be used to control the relative magnitude of the magnetic dipole coupling with respect to the electric one.

Also, it has recently become interesting to use superconducting materials for the trapping wires, because it allows to reduce the magnetic noise [Dikovsky *et al.* 2009]. This noise induces spin-flips of the trapped atoms, leading to their loss from the trap [Henkel *et al.* 1999,Henkel 2005,Hohenester *et al.* 2007,Skagerstam *et al.* 2006]. Hence, another topic not directly connected to the Casimir-effects, might be the study of the electric and magnetic noise from these materials. In superconductors, the fluctuations of the order parameter close to the critical temperature [Tinkham 1974] can be expected to produce a strong noise. Another very interesting contribution to the noise should arise in type II superconductors (section 1.5) from the vortices in the mixed state, whose number can be controlled very precisely by tuning the magnetic field. Finally, should it turn out possible to measure Casimir-Polder interactions in a trap including superconducting elements to a good precision, some of the effects calculated in this thesis might become relevant.

The calculations in this work were based on the assumption made in section 1.1.1, that nonlocal effects can be neglected. For this reason, no distinction was made between longitudinal and transverse response. While this is a good description at high frequencies, nonlocal effects may become relevant at low frequencies [Dressel and Grüner 2002]. In the context of the Casimir effect nonlocal effects in normal conductors have been taken into account, e.g. in [Buhl 1976, Esquivel and Svetovoy 2004, Svetovoy and Esquivel 2005, Esquivel-Sirvent and Svetovoy 2005, Esquivel-Sirvent *et al.* 2006, Sernelius 2006b]. Overall, the corrections are rather small, because the geometric length scale L is much larger than the other scales involved, such as the Thomas-Fermi screening length v_F/ω_p or the inverse Fermi wave vector $1/k_F$.

In atom chips, these corrections might provoke a change of the noise-spectrum close to the surface and hence influence the spin-flip rate of trapped atoms. A step towards the calculation of these effects has been done by Horovitz and Henkel [Horovitz 2007, Henkel and Horovitz 2007], including carrier diffusion in either a sheet of surface charges or in the bulk medium.

For both fields, the Casimir-effect and atom-chips, it would be interesting to investigate further the nonlocal effects occurring in superconductors. In BCS-superconductors, the very approach of Mattis and Bardeen is nonlocal, but locality is introduced at an early stage in the calculations. Pöpel [Pöpel 1989] has given a more general description including effects of nonlocality and it would be very interesting to extract the physical effects arising from this description.

References

[Antezza *et al.*, 2004] M. Antezza, L. P. Pitaevskii, and S. Stringari. Effect of the casimir-polder force on the collective oscillations of a trapped bose-einstein condensate. *Phys. Rev. A*, 70:053619, 2004.

[Antezza *et al.*, 2005] M. Antezza, L. P. Pitaevskii, and S. Stringari. New asymptotic behavior of the surface-atom force out of thermal equilibrium. *Phys. Rev. Lett.*, 95:113202, 2005.

[Antezza *et al.*, 2008] M. Antezza, L. P. Pitaevskii, S. Stringari, and V. B. Svetovoy. Casimir-Lifshitz force out of thermal equilibrium. *Phys. Rev. A*, 77:022901, 2008.

[Antezza, 2008] M. Antezza. Atom-Superconductor force out of thermal equilibrium. Report, April 2008.

[Ashcroft and Mermin, 1987] N. W. Ashcroft and N. D. Mermin. *Solid state Physics* Holt, Rinehart and Winston, New York, 1987.

[Aspect and Dalibard, 2002] A. Aspect and J. Dalibard. Measurement of the atom-wall interaction: from London to Casimir-Polder. 2002.

[Bardasis and Schrieffer, 1961] A. Bardasis and J. R. Schrieffer. Excitons and plasmons in superconductors. *Phys. Rev.*, 121:1050–1062, 1961.

[Bardeen *et al.*, 1957] J. Bardeen, L. N. Cooper, and J. R. Schrieffer. Theory of superconductivity. *Phys. Rev.*, 108:1175–1204, 1957.

[Bardeen, 1958] J. Bardeen. Two-fluid model of superconductivity. *Phys. Rev. Lett.*, 1:399, 1958.

[Basov and Timusk, 2005] D. N. Basov and T. Timusk. Electrodynamics of high-T_c superconductors. *Rev. Mod. Phys.*, 77:721–779, 2005.

[Bednorz and Müller, 1986] J. G. Bednorz and K. A. Müller. Possible high T_c superconductivity in the Ba-La-Cu-O system. *Z. Phys. B*, 64:189–193, 1986.

[Beeby and Thomas, 1974] J. L. Beeby and E. G. Thomas. The long-range potential in the scattering of atoms from surfaces. *J. Phys. C*, 7:2157–2164, 1974.

[Beltrami and Wohlers, 1966] E. J. Beltrami and M. R. Wohlers. *Distributions and the Boundary Values of Analytic Functions*. Academic Press, 1966.

[Berlinsky *et al.*, 1993] A. J. Berlinsky, C. Kallin, G. Rose, and A.-C. Shi. Two-fluid interpretation of the conductivity of clean bcs superconductors. *Phys. Rev. B*, 48:4074–4079, 1993.

[Bezerra *et al.*, 2004] V. B. Bezerra, G. L. Klimchitskaya, V. M. Mostepanenko, and C. Romero. Violation of the Nernst heat theorem in the theory of the thermal Casimir force between Drude metals. *Phys. Rev. A*, 69:022119, Feb 2004.

[Bezerra *et al.*, 2006] V. B. Bezerra, R. S. Decca, E. Fischbach, B. Geyer, G. L. Klimchitskaya, D. E. Krause, D. López, V. M. Mostepanenko, and C. Romero. Comment on "temperature dependence of the casimir effect". *Phys. Rev. E*, 73:028101, 2006.

[Bezerra *et al.*, 2008] V. B. Bezerra, G. L. Klimchitskaya, V. M. Mostepanenko, and C. Romero. Lifshitz theory of atom-wall interaction with applications to quantum reflection. *Phys. Rev. A*, 78:042901, 2008.

[Bimonte *et al.*, 2005a] G. Bimonte, E. Calloni, G. Esposito, L. Milano, and L. Rosa. Towards Measuring Variations of Casimir Energy by a Superconducting Cavity. *Phys. Rev. Lett.*, 94:180402, 2005.

[Bimonte *et al.*, 2005b] G. Bimonte, E. Calloni, G. Esposito, and L. Rosa. Variations of Casimir energy from a superconducting transition. *Nuclear Phys. B*, 726:441–463, 2005.

[Bimonte *et al.*, 2006] G. Bimonte, E. Calloni, G. Esposito, and L. Rosa. Casimir energy and the superconducting phase transition. *J. Phys. A*, 39:6161–6171, 2006.

[Bimonte, 2008] G. Bimonte. The casimir effect in a superconducting cavity: a new tool to resolve an old controversy. *eprint arXiv: 0807.2950*, 2008.

[Bimonte, 2009] G. Bimonte. The bohr-van leeuwen theorem and the thermal casimir effect for conductors authors:. *eprint arXiv: quant-ph/0903.0951*, 2009.

[Bloch, 1930] F. Bloch. Zum elektrischen Widerstandsgesetz bei tiefen Temperaturen. *Z. Phys. A*, 59:208–214, 1930.

[Blokland and Overbeek, 1978] P. H. G. M. Blokland and J. T. G. Overbeek. van der Waals forces between objects covered with a chromium layer. *J. Chem. Soc.*, 74:2637–2651, 1978.

[Bordag *et al.*, 2000] M. Bordag, B. Geyer, G. L. Klimchitskaya, and V. M. Mostepanenko. Casimir force at both nonzero temperature and finite conductivity. *Phys. Rev. Lett.*, 85:503–506, 2000.

[Bordag *et al.*, 2001] M. Bordag, U. Mohideen, and V. M. Mostepanenko. New developments in the casimir effect. *Phys. Rep.*, 353:1, 2001.

[Boström and Sernelius, 2000] M. Boström and Bo E. Sernelius. Thermal effects on the casimir force in the $0.1...5\mu m$ range. *Phys. Rev. Lett.*, 84:4757–4760, 2000.

[Boström and Sernelius, 2004] M. Boström and B.E. Sernelius. Entropy of the Casimir effect between real metal plates. *Physica A*, 339:53–59, 2004.

[Boyer, 1974] T. H. Boyer. Van der Waals forces and zero-point energy for dielectric and permeable materials. *Phys. Rev. A*, 9:2078–2084, 1974.

[Bressi *et al.*, 2002] G. Bressi, G. Carugno, R. Onofrio, and G. Ruoso. Measurement of the casimir force between parallel metallic surfaces. *Phys. Rev. Lett.*, 88:041804, 2002.

[Brevik and Aarseth, 2006] I. Brevik and J. B. Aarseth. Temperature dependence of the casimir effect. *J. Phys. A*, 39:6187–6193, 2006.

[Brevik *et al.*, 2005] I. Brevik, J. B. Aarseth, J. S. Høye, and K. A. Milton. Temperature dependence of the casimir effect. *Phys. Rev. E*, 71:056101, 2005.

[Brevik *et al.*, 2006] I. Brevik, S. A Ellingsen, and K. A. Milton. Thermal corrections to the casimir effect. *New J. Phys.*, 8:236, 2006.

[Buckel, 1977] W. Buckel. *Supraleitung*. Phys.-Verlag, Weinheim, 1977.

[Buhl, 1976] W. Buhl. On the theory of Van der Waals interaction. *Z. Phys. B*, 23:221–232, June 1976.

[Buhmann and Scheel, 2008] S. Y. Buhmann and S. Scheel. Thermal casimir vs casimir-polder forces: Equilibrium and non-equilibrium forces. *Phys. Rev. Lett.*, 100:253201, 2008.

[Buks and Roukes, 2001] E. Buks and M. L. Roukes. Stiction, adhesion energy, and the casimir effect in micromechanical systems. *Phys. Rev. B*, 63:033402, 2001.

[Casimir and Polder, 1948] H. B. Casimir and D. Polder. The influence of retardation on the london-van der waals forces. *Phys. Rev.*, 73:360–372, February 1948.

[Casimir, 1948] H. B. G. Casimir. On the attraction between two perfectly conducting plates. *Indag. Math.*, 10:261–263, 1948.

[Chan *et al.*, 2001] H. B. Chan, V. A. Aksyuk, R. N. Kleiman, D. J. Bishop, and F. Capasso. Quantum mechanical actuation of microelectromechanical systems by the Casimir force, 2001.

[Chen *et al.*, 2005] F. Chen, U. Mohideen, G. L. Klimchitskaya, and V. M. Mostepanenko. Investigation of the casimir force between metal and semiconductor test bodies. *Phys. Rev. A*, 72:020101, 2005.

[Davies, 2005] P. C. W. Davies. Quantum vacuum friction. *J. Opt. B*, 7:40–46, 2005.

[Decca *et al.*, 2005] R. S. Decca, D. Lopez, E. Fischbach, G. L. Klimchitskaya, D. E. Krause, and V. M. Mostepanenko. Precise comparison of theory and new experiment for the Casimir force leads to stronger constraints on thermal quantum effects and long-range interactions. *Ann. Phys. (NY)*, 318:37–80, 2005.

[Derjaguin *et al.*, 1956] B. V. Derjaguin, N. V. Churaev, and V. M. Muller. The measurement of the Casimir force by using a curved surface. *Quarterly Rev.*, 10:295–302, 1956.

[Dikovsky *et al.*, 2009] V. Dikovsky, V. Sokolovsky, B. Zhang, C. Henkel, and R. Folman. Superconducting atom chips: advantages and challenges. *Europ. Phys. J. D*, 51:247–259, 2009.

[Dressel and Grüner, 2002] M. Dressel and G. Grüner. *Electrodynamics of solids : optical properties of electrons in matter*. Cambridge Univ. Pr., 2002.

[Dugdale, 1996] J. S. Dugdale. *Entropy and its physical meaning*. Taylor & Francis, London, 1996.

[Einstein, 1920] A. Einstein. Ether and the Theory of Relativity, *Sidelights on Relativity*, 1920.

[Ellingsen *et al.*, 2008] S. A. Adnoy Ellingsen, I. Brevik, J. S. Hoye, and K. A. Milton. Low temperature Casimir-Lifshitz free energy and entropy: the case of poor conductors, *J. Phys. Conf. Ser.*, 161, 2009.

[Esquivel and Svetovoy, 2004] R. Esquivel and V. B. Svetovoy. Correction to the casimir force due to the anomalous skin effect. *Phys. Rev. A*, 69:062102, 2004.

[Esquivel-Sirvent and Svetovoy, 2005] R. Esquivel-Sirvent and V. B. Svetovoy. Nonlocal thin films in calculations of the Casimir force. *Phys. Rev. B*, 72, 2005.

[Esquivel-Sirvent *et al.*, 2006] R. Esquivel-Sirvent, C. Villarreal, W. L. Mochán, A. M. Contreras-Reyes, and V. B. Svetovoy. Spatial dispersion in casimir forces: a brief rev. *J. Phys. A*, 39:6323–6331, 2006.

[Failache *et al.*, 1999] H. Failache, S. Saltiel, M. Fichet, D. Bloch, and M. Ducloy. Resonant van der waals repulsion between excited cs atoms and sapphire surface. *Phys. Rev. Lett.*, 83:5467–5470, 1999.

[Fermi, 1956] E. Fermi. *Thermodynamics*. Dover Publ., New York, 1956.

[Ferrell and Glover, 1958] R. A. Ferrell and R. E. Glover. Conductivity of superconducting films: A sum rule. *Phys. Rev.*, 109:1398–1399, 1958.

[Ford and Weber, 1984] G. W. Ford and W. H. Weber. Electromagnetic interactions of molecules with metal surfaces. *Phys. Rep.*, 113:195–287, 1984.

[Fortagh and Zimmermann, 2007] J. Fortagh and C. Zimmermann. Magnetic microtraps for ultracold atoms. *Rev. of Mod. Phys.*, 79:235–289, 2007.

[Gel'fand *et al.*, 1962] I. M. Gel'fand, G. E. Silov, and N. Ja. Vilenkin. *Verallgemeinerte Funktionen*. Dt. Verl. d. Wiss., Berlin, 1962.

[Genet *et al.*, 2003] C. Genet, A. Lambrecht, and S. Reynaud. Casimir force and the quantum theory of lossy optical cavities. *Phys. Rev. A*, 67:043811, 2003.

[Genet *et al.*, 2004] C. Genet, F. Intravaia, A. Lambrecht, and S. Reynaud. Electromagnetic vacuum fluctuations, casimir and van der waals forces. *Ann. Fond. L. de Broglie*, 29:311, 2004.

[Geyer *et al.*, 2007] B. Geyer, G. L. Klimchitskaya, and V. M. Mostepanenko. Generalized plasma-like permittivity and thermal Casimir force between real metals. *J. Phys. A*, 40:13485–13499, 2007.

[Ginzburg and Landau, 1950] V. L. Ginzburg and L. D. Landau. On the theory of superconductivity. *Soviet Phys. JETP*, 2, 1950.

[Ginzburg, 1955] V. Ginzburg. On the theory of superconductivity. *Il Nuovo Cimento*, 2:1234–1250, December 1955.

[Glover and Tinkham, 1957] R. E. Glover and M. Tinkham. Conductivity of superconducting films for photon energies between 0.3 and $4ktc$. *Phys. Rev.*, 108:243–256, 1957.

[Gorkov and Eliashberg, 1968] L. P. Gorkov and G. M. Eliashberg. *Soviet Phys. JETP*, 54:612, 1968.

[Gorkov, 1959] L. P. Gorkov. Microscopic derivation of the Ginzburg–Landau equations in the theory of superconductivity. *Sov. Phys. JETP*, 9, 1959.

[Gorter and Casimir, 1934] C. J. Gorter and H. B. G. Casimir. The thermodynamics of the superconducting state. *Phys. Z.*, 35:963, 1934.

[Gourdon and Sebah, 2002] X. Gourdon and P. Sebah. Introduction on Bernoulli's numbers. http://numbers.computation.free.fr, 2002.

[Grimm *et al.*, 2000] R. Grimm, M. Weidemuller, and Y. B. Ovchinnikov. Optical dipole traps for neutral atoms. *Adv. at. mol. opt. phys.*, 42:130, 2000.

[Grüneisen, 1933] E. Grüneisen. Die Abhängigkeit des elektrischen Widerstandes reiner Metalle von der Temperatur. *Ann. Phys.*, 408:530–540, 1933.

[Haakh *et al.*, 2009] H. Haakh, C. Henkel, F. Intravaia, and G. Bimonte. BCS conductivity at imaginary frequencies. in preparation, 2009.

[Harber *et al.*, 2005] D. M. Harber, J. M. Obrecht, J. M. McGuirk, and E. A. Cornell. Measurement of the Casimir-Polder force through center-of-mass oscillations of a Bose-Einstein condensate. *Phys. Rev. A*, 72:33610, 2005.

[Harris *et al.*, 2000] B. W. Harris, F. Chen, and U. Mohideen. Precision measurement of the casimir force using gold surfaces. *Phys. Rev. A*, 62:052109, 2000.

[Henkel and Horovitz, 2007] C. Henkel and B. Horovitz. Noise from metallic surfaces – effects of charge diffusion, *eprint arXiv: 0709.1242v2*, 2007.

[Henkel *et al.*, 1999] C. Henkel, S. Pötting, and M. Wilkens. Loss and heating of particles in small and noisy traps. *Applied Phys. B*, 69:379–387, 1999.

[Henkel, 2005] C. Henkel. Magnetostatic field noise near metallic surfaces. *Eur. Phys. J. D*, 35:59–67, 2005.

[Henkel, 2007] C. Henkel. Quantenmechanik 2. Lecture notes, 2007.

[Hohenester *et al.*, 2007] U. Hohenester, A. Eiguren, S. Scheel, and E. A. Hinds. Spin-flip lifetimes in superconducting atom chips: Bardeen-cooper-schrieffer versus eliashberg theory. *Phys. Rev. A*, 76:033618, 2007.

[Horovitz, 2007] B. Horovitz. Noise from metallic surfaces – effects of non-local electrodynamics. *eprint arXiv: 0709.1242*, 2007.

[Hoye *et al.*, 2007] J. S. Hoye, I. Brevik, S. A. Ellingsen, and J. B. Aarseth. Analytical and Numerical Verification of the Nernst Theorem for Metals. *Phys. Rev. E*, 75:051127, 2007.

[Hushwater, 1997] V. Hushwater. Repulsive Casimir force as a result of vacuum radiation pressure. *American J. Phys.*, 65:381, 1997.

[Iannuzzi *et al.*, 2004] D. Iannuzzi, M. Lisanti, and F. Capasso. Effect of hydrogen-switchable mirrors on the Casimir force. *Proc. National Acad. Sc. USA*, 101:4019–4023, 2004.

[Ibach and Lüth, 1981] H. Ibach and H. Lüth. *FestkörperPhys.* Springer, Berlin, 1981.

[Intravaia and Henkel, 2008] F. Intravaia and C. Henkel. Casimir energy and entropy between dissipative mirrors. *J. Phys. A*, Special Issue, 2008.

[Intravaia and Henkel, 2009] F. Intravaia and C. Henkel. Casimir interaction from magnetically coupled eddy currents. 2009.

[Intravaia and Lambrecht, 2005] F. Intravaia and A. Lambrecht. Surface plasmon modes and the casimir energy. *Phys. Rev. Lett.*, 94:110404, 2005.

[Intravaia *et al.*, 2007] F. Intravaia, C. Henkel, and A. Lambrecht. The role of surface plasmons in the casimir effect. *Phys. Rev. A*, 76:033820, 2007.

[Intravaia, 2005] F. Intravaia. *Effet Casimir et interaction entre plasmons de surface*. PhD thesis, Université Paris 6, 2005.

[Jackson, 2002] J. D. Jackson. *Klassische Elektrodynamik*. de Gruyter, Berlin, 2002.

[Jaekel and Reynaud, 1991] M. T. Jaekel and S. Reynaud. Casimir force between partially transmitting mirrors. *J. Phys. I France*, 1, 1991.

[Jones and March, 1973] W. Jones and N. H. March. *Theoretical solid state Phys.* Wiley, 1973.

[Joulain *et al.*, 2003] K. Joulain, R. Carminati, J. P. Mulet, and J. J. Greffet. Definition and measurement of the local density of electromagnetic states close to an interface. *Phys. Rev. B*, 68:245405, 2003.

[Kammerlingh-Onnes, 1911] H. Kammerlingh-Onnes. The dissapearance of the resistivity of mercury. *Comm. Leiden*, 122, 1911.

[Ketterson and Song, 1999] J. B. Ketterson and S. N. Song. *Superconductivity*. Cambridge Univ. Press, Cambridge, 1999.

[Kittel, 2002] C. Kittel. *Einführung in die FestkörperPhys.* Oldenbourg, München ; Wien, 2002.

[Klimchitskaya and Mostepanenko, 2008] G. L. Klimchitskaya and V. M. Mostepanenko. Comment on "Analytical and numerical verification of the Nernst heat theorem for metals". *Phys. Rev. E*, 77:023101, 2008.

[Klimchitskaya *et al.*, 2007] G. L. Klimchitskaya, U. Mohideen, and V. M. Mostepanenko. Kramers-Kronig relations for plasma-like permittivities and the Casimir force. *eprint arXiv: quant-ph/0703139*, 2007.

[Klimchitskaya *et al.*, 2009] G. L. Klimchitskaya, U. Mohideen, and V. M. Mostepanenko. The Casimir force between real materials: experiment and theory. *eprint arXiv:0902.4022*, 2009.

[Klimchitskaya, 2009] G. L. Klimchitskaya. Calculation of the Casimir force between Ge test bodies in different theoretical approaches. *eprint arXiv: 0902.4254*, 2009.

[Kramers, 1927] H. A. Kramers. La diffusion de la lumiere par les atomes. *Atti Congr. Int. Fis. Como*, 2:545–557, 1927.

[Kronig, 1926] R. Kronig. *J. Opt. Soc. Am*, 12:547, 1926.

[Laliotis *et al.*, 2007] A. Laliotis, I. Maurin, P. Todorov, I. Hamdi, G. Dutier, A. Yarovitski, S. Saltiel, M.-P. Gorza, M. Fichet, M. Ducloy, and D. Bloch. Testing the distance-dependence of the van der waals interaction between an atom and a surface through spectroscopy in a vapor nanocell, *eprint HAL: hal-00136244*, 2007.

[Lambrecht and Reynaud, 2000] A. Lambrecht and S. Reynaud. Casimir force between metallic mirrors. *Eur. Phys. J. D*, 8:309, 2000.

[Lambrecht *et al.*, 1998] A. Lambrecht, M. T. Jaekel, and S. Reynaud. Frequency up-converted radiation from a cavity moving in vacuum. *Eur. Phys. J. D*, 3:95–104, 1998.

[Lamoreaux, 1997] S. K. Lamoreaux. Demonstration of the Casimir force in the 0.6 to 6 mm range. *Phys. Rev. Lett.*, 78:5–8, 1997.

[Landau and Lifshitz, 1974] L. D. Landau and E. M. Lifshitz. *Lehrbuch der theoretischen Phys. VIII, Elektrodynamik der Kontinua*. Akad.-Verl., Berlin, 1974.

[Landau and Lifshitz, 1979] L. D. Landau and E. M. Lifshitz. *Lehrbuch der theoretischen Phys. V, Statistische Phys.* Akad.-Verl., Berlin, 1979.

[Landragin *et al.*, 1996] A. Landragin, J. Y. Courtois, G. Labeyrie, N. Vansteenkiste, C. I. Westbrook, and A. Aspect. Measurement of the van der Waals force in an atomic mirror. *Phys. Rev. Lett.*, 77:1464–1467, 1996.

[Lide, 1995] D. R. Lide. *CRC Handbook of Chemistry and Phys., 75th edit*. CRC Press Inc., Boca Raton, USA, 1995.

[Lifshitz *et al.*, 1984] E. M. Lifshitz, L. P. Pitaevskii, and L. D. Landau. *Lehrbuch der theoretischen Phys. IX, Theorie der kondensierten Materie*. Akad.-Verl., Berlin, 1984.

[Lifshitz, 1956] E. M. Lifshitz. The theory of molecular attractive forces between solids. *Sov. Phys. JETP*, 2, 1956.

[Lisanti *et al.*, 2005] M. Lisanti, D. Iannuzzi, and F. Capasso. Observation of the skin-depth effect on the Casimir force between metallic surfaces. *Proc. National Acad. Sc. USA*, 102:11989–11992, 2005.

[Loder *et al.*, 2008] F. Loder, A. P. Kampf, T. Kopp, J. Mannhart, C. W. Schneider, and Y. S. Barash. Magnetic flux periodicity of h/e in superconducting loops. *Nature Phys.*, 4:112–115, 2008.

[London and London, 1935] F. London and H. London. The Electromagnetic Equations of the Supraconductor. *Proc. R. Soc. London. Series A, Math. Phys. Sciences*, 149:71–88, 1935.

[London, 1930] F. London. Zur Theorie und Systematik der Molekularkräfte. *Z. Phys. A*, 63:245–279, 1930.

[London, 1937] F. London. The general theory of molecular forces. *Transactions of the Faraday Society*, 33:8–26, 1937.

[Mattis and Bardeen, 1958] D. C. Mattis and J. Bardeen. Theory of the anomalous skin effect in normal and superconducting metals. *Phys. Rev.*, 111:412–417, 1958.

[McGuirk *et al.*, 2004] J. McGuirk, D. Harber, J. Obrecht, and E. Cornell. *Phys. Rev. A*, 72:033610, 2004.

[Mehra, 1967] J. Mehra. Temperature correction to the casimir effect. *Physica*, 37:145–152, 1967.

[Meißner and Ochsenfeld, 1933] W. Meißner and R. Ochsenfeld. Ein neuer Effekt bei Eintritt der Supraleitfähigkeit. *Naturwissenschaften*, 21:787–788, 1933.

[Milonni and Shih, 1992] P. W. Milonni and M.-L. Shih. Source theory of the Casimir force. *Phys. Rev. A*, 45:4241–4253, 1992.

[Milonni *et al.*, 1969] P. W. Milonni, R. J. Cook, and M. E. Goggin. Radiation pressure from the vacuum: Physical interpretation of the Casimir force. *J. Math. Phys*, 38:1621, 1969.

[Milton, 2004] K. A. Milton. The casimir effect: Recent controversies and progress. *J. Phys. A*, 37:209, 2004.

[Mohideen and Roy, 1998] U. Mohideen and Anushree Roy. Precision measurement of the Casimir force from 0.1 to $0.9\mu m$. *Phys. Rev. Lett.*, 81:4549–4552, 1998.

[Mostepanenko and Trunov, 1997] V. M. Mostepanenko and N. N. Trunov. *The Casimir effect and its applications*. Clarendon, Oxford, 1997.

[Mostepanenko *et al.*, 2006] V. M. Mostepanenko, V. B. Bezerra, R. S. Decca, B. Geyer, E. Fischbach, G. L. Klimchitskaya, D. E. Krause, D. Lopez, and C. Romero Present status of controversies regarding the thermal Casimir force. *J. Phys. A*, 39:6589–6600, 2006.

[Nernst, 1906a] W. Nernst. Heft I. Sitz.-Ber. preuß. Akad. Wiss. 20.06.1906.

[Nernst, 1906b] W. Nernst. Nachr. Ges. Wiss. Göttingen, Math.-Phys. Kl. 1906.

[Nolting, 1990] W. Nolting. *Theoretische Physik 7: Vielteilchen-Theorie*. Vieweg, 1990.

[Novotny and Henkel, 2008] L. Novotny and C. Henkel. Van der waals versus optical interaction between metal nanoparticles. *Opt. Lett.*, 33:1029–1031, 2008.

[Nussenzveig, 1972] HM. Nussenzveig. *Causality and Dispersion Relations*. Academic Press, New York, 1972.

[Obrecht *et al.*, 2007] J. M. Obrecht, R. J. Wild, M. Antezza, L. P. Pitaevskii, S. Stringari, and E. A. Cornell. Measurement of the temperature dependence of the Casimir-Polder force. *Phys. Rev. Lett.*, 98:063201, 2007.

[Obrecht, 2007] J. M. Obrecht. *Measurement of the Temperature Dependence of the Casimir-Polder Force*. PhD thesis, University of Colorado, 2007.

[Petrov *et al.*, 2008] P. G. Petrov, S. Machluf, S. Younis, R. Macaluso, T. D. , B. Hadad, Y. Japha, M. Keil, E. Joselevich, and R. Folman. Trapping cold atoms using surface-grown carbon nanotubes. *arXiv:0812.3940v1*, 2008.

[Pitaevskii, 2008a] L. P. Pitaevskii. Private communication, 2008.

[Pitaevskii, 2008b] L. P. Pitaevskii. 1st network meeting, ESF RNP Casimir. 2008.

[Planck, 1927] M. Planck. *Vorlesungen über Thermodynamik*. de Gruyter, Berlin, 1927.

[Power *et al.*, 1997] W. L. Power, T. Pfau, and M. Wilkens. Loading atoms into a surface trap: simulations of an experimental scheme. *Optics Communications*, 143:125 – 132, 1997.

[Power *et al.*, 2005a] B. Power, C. Henkel, and F. Sols. Comparison of numerical and analytical evaluations of the energy shift due to the interaction of a magnetic dipole with a metal surface. Report, 2005.

[Power *et al.*, 2005b] B. Power, C. Henkel, and F. Sols. Magnetic energy shift. Report, 2005.

[Pöpel, 1989] R. Pöpel. Surface impedance and reflectivity of superconductors. *J. Applied Phys.*, 66:5950–5957, 1989.

[Rickayzen, 1959] G. Rickayzen. Collective excitations in the theory of superconductivity. *Phys. Rev.*, 115:795–808, 1959.

[Rickayzen, 1965] G. Rickayzen. *Theory of superconductivity*. Interscience, 1965.

[Ruvalds, 1987] J. Ruvalds. Plasmons and high-temperature superconductivity in alloys of copper oxides. *Phys. Rev. B*, 35:8869–8872, 1987.

[Sandoghdar *et al.*, 1992] V. Sandoghdar, C. I. Sukenik, E. A. Hinds, and S. Haroche. Direct measurement of the van der Waals interaction between an atom and its images in a micron-sized cavity. *Phys. Rev. Lett.*, 68:3432–3435, 1992.

[Scheel and Buhmann, 2008] S. Scheel and S. Y. Buhmann. Macroscopic quantum electrodynamics - concepts and applications. *acta physica slovaca*, 58:675–809, 2008.

[Schram, 1973] K. Schram. On the macroscopic theory of retarded Van der Waals forces. *Phys. Lett. A*, 43:282–284, 1973.

[Schrieffer, 1999] J. R. Schrieffer. *Theory of Superconductivity*. Perseus Books, 1999.

[Schwabl, 2002] F. Schwabl. *Statistical Mechanics*. Springer, 2002.

[Sernelius, 2006a] B. E. Sernelius. Casimir force and complications in the van Kampen theory for dissipative systems. *Phys. Rev. B*, 74:233103, 2006.

[Sernelius, 2006b] B. E. Sernelius. Finite-temperature Casimir force between metal plates: full inclusion of spatial dispersion resolves a long-standing controversy. *J. Phys. A*, 39:6741–6752, 2006.

[Shimizu, 2001] F. Shimizu. Specular reflection of very slow metastable neon atoms from a solid surface. *Phys. Rev. Lett.*, 86:987–990, 2001.

[Shoenberg, 1938] D. Shoenberg. *Superconductivity*. Univ. Pr., Cambridge, 1938.

[Skagerstam *et al.*, 2006] B. Skagerstam, U. Hohenester, A. Eiguren, and P. K. Rekdal. Spin Decoherence in Superconducting Atom Chips. *Phys. Rev. Lett.*, 97:70401, 2006.

[Soldati, 2003] R. Soldati. *Meccanica statistica*. http://www.robertosoldati.com, Bologna, 2003.

[Spagnolo and Intravaia, 2008] S. Spagnolo and F. Intravaia. Casimir-Polder poential between a magnetic dipole and a surface at temperature T. Report, July 2008.

[Spagnolo *et al.*, 2006] S. Spagnolo, R. Passante, and L. Rizzuto. Field fluctuations near a conducting plate and casimir-polder forces in the presence of boundary conditions. *Phys. Rev. A*, 73:062117, 2006.

[Spagnolo, 2009] S. Spagnolo. *Quantum Electrodynamics with Boundary Conditions and Casiir-Polder Forces*. PhD thesis, Università degli studi di Palermo, 2009.

[Sparnaay, 1957] M. J. Sparnaay. Attractive forces btween flat plates. *Nature*, 180:334–335, 1957.

[Sukenik *et al.*, 1993] C. I. Sukenik, M. G. Boshier, D. Cho, V. Sandoghdar, and E. A. Hinds. Measurement of the Casimir-Polder force. *Phys. Rev. Lett.*, 70:560–563, 1993.

[Svetovoy and Esquivel, 2005] V. B. Svetovoy and R. Esquivel. Nonlocal impedances and the Casimir entropy at low temperatures. *Phys. Rev. E*, 72:036113, 2005.

[Svetovoy, 2007] V. B. Svetovoy. Evanescent character of the repulsive thermal casimir force. *Phys. Rev. A*, 76:062102, 2007.

[Thouless, 1960] D. J. Thouless. Strong-coupling limit in the theory of superconductivity. *Phys. Rev.*, 117:1256–1260, 1960.

[Tinkham, 1974] M. Tinkham. The electromagnetic properties of superconductors. *Rev. Mod. Phys.*, 46:587–596, 1974.

[Tinkham, 2004] M. Tinkham. *Introduction to superconductivity*. Dover Publ., Mineola (NY), 2004.

[Townsend and Sutton, 1962] P. Townsend and J. Sutton. Investigation by electron tunneling of the superconducting energy gaps in nb, ta, sn, and pb. *Phys. Rev.*, 128:591–595, 1962.

[Van der Waals, 1873] J. D. Van der Waals. *Over de continuiteit van den gas-en vloeistoftoestand*. PhD thesis, Universiteit Leiden, 1873.

[Van Kampen *et al.*, 1968] N. G. Van Kampen, B. R. .A. Nijboer, and K. Schram. On the macroscopic theory of van der Waals forces. *Phys. Lett. A*, 26, 1968.

[Vladimirov, 1972] V. S. Vladimirov. *Gleichungen der mathematischen Physik* Hochschulbücher für Mathematik ; 74. Dt. Verl. d. Wiss., 1972.

[Wylie and Sipe, 1984] J. M. Wylie and J. E. Sipe. Quantum electrodynamics near an interface. *Phys. Rev. A*, 30:1185–1193, 1984.

[Wylie and Sipe, 1985] J. M. Wylie and J. E. Sipe. Quantum electrodynamics near an interface. ii. *Phys. Rev. A*, 32:2030–2043, 1985.

[Yuju *et al.*, 2004] L. Yuju, I. Teper, C. Cheng, and V. Vuletic. Impact of the Casimir-Polder potential and J. son noise on Bose-Einstein condensate stability near surfaces. *Phys. Rev. Lett.*, 92, 2004.

[Zhou, 1991] S. A. Zhou. *Electrodynamic theory of superconductors*. Peregrinus, London, 1991.

[Ziman, 1972] J. M. Ziman. *Electrons and phonons*. Clarendon Pr., Oxford, 1972.

[Zimmermann *et al.*, 1991] W. Zimmermann, E. H. Brandt, M. Bauer, E. Seider, and L. Genzel. Optical conductivity of BCS superconductors with arbitrary purity. *Physica C*, 183:99–104, 1991.

List of Figures

Symbols and constants

Constant	Value	Description
α	$1/137$	Fine-structure constant
a_0	$5.29 \cdot 10^{-11}\,\mathrm{m}$	Bohr's radius
c	$3.00 \cdot 10^{8}\,\mathrm{m/s}$	Speed of light
e	$1.06 \cdot 10^{-10}\,\mathrm{C}$	Electron charge
ϵ_0	$8.85 \cdot 10^{-12}\,\mathrm{F/m}$	Vacuum permittivity
g_s	2	e^- spin Landé g-factor
$\hbar = h/2\pi$	$1.05 \cdot 10^{-34}\,\mathrm{Js}$	Reduced Planck constant
k_B	$1.38 \cdot 10^{-23}\,\mathrm{J/K}$	Boltzmann constant
μ_0	$4\pi \cdot 10^{-7}\,\mathrm{H/m}$	Vacuum permeability
μ_B	$9.27 \cdot 10^{-24}\,\mathrm{J/T}$	Bohr's magneton
Z_0	$377\,\Omega$	Vacuum impedance

Symbol	Description
A	Plate area
$\mathbf{A}$	Vector potential
α_{ij}, β_{ij}	Electric and magnetic polarizability tensor
α^T, β^T	Scalar electric and magnetic thermal polarizability
$\mathbf{B}$	Magnetic inductance
$\chi = \epsilon - 1$	Linear electric susceptibility
$\delta(\omega)$	Skin depth
$\Delta(T)$	Superconducting gap energy
$\mathbf{D}$	Electric displacement
$\epsilon(\omega) = \epsilon' + i\epsilon''$	Dielectric function, real and imaginary part
$\mathbf{E}$	Electric field
E	(Internal) Casimir energy
$E_C = \frac{A\hbar c\pi^2}{720L^3}$	Casimir energy between perfect reflectors
E_F	Fermi energy
$\eta(T)$	Superconducting order parameter
$\mathcal{F} = E - TS$	Helmholtz' free energy
$\gamma = 1/\tau$	Dissipation rate
G_{ij}, H_{ij}	Electric and magnetic Green's tensor
$G(T), H(T)$	Electric and magnetic trace function
$\mathbf{H}$	Magnetic field
$\mathbf{j}$	Current density
$\mathbf{k}$	Perpendicular wave vector
$\kappa = \sqrt{k^2 - \omega^2/c^2}$	Longitudinal imaginary wave vector
$\lambda_p = c/\omega_p$	Plasma wavelength
$\lambda_T = 2\pi\hbar c/k_B T$	Thermal wave length
L	Distance between two objects
$\mu_m = \mu_B g_s/2$	Magnetic dipole moment
ω	Frequency
Ω_e, Ω_m	Electric and magnetic transition frequency
$\omega_p = \frac{ne^2}{\epsilon_0}$	Plasma frequency
$\rho = 1/\sigma$	Electrical resistivity
r^{TE}, r^{TM}	Field amplitude reflectivity in TE, TM polarization
$\sigma(\omega) = \sigma' + i\sigma''$	Complex conductivity, real and imaginary part
S	Entropy
$\tau = 1/\gamma$	Relaxation time
T	Temperature
T_c	Superconducting critical temperature
$T_p = \hbar\omega_p/k_B$	Plasma temperature
U	(Internal) Casimir-Polder energy
$\xi = -i\omega$	Purely imaginary frequency
$\xi_n = 2\pi n k_B T/\hbar$	nth Matsubara frequency
Z	Surface impedance
$\mathcal{Z}$	Partition function